

COVER:

Stable oxygen isotopes in the Belukha ice core were used to reconstruct temperatures over the past 750 years at a highly continental site (marked with the red dot). The photo shows the drilling tent on the Belukha glacier (photo by Susanne Olivier). In the period 1250-1850 temperatures (orange) follow closely the proxy records of solar activity derived from cosmogenic nuclides (^{10}Be in polar ice cores, blue, and ^{14}C in tree rings, green), suggesting that the sun was an important driver of preindustrial temperature changes in the Siberian Altai. The strong rise in the temperatures in the industrial period 1850–2000, however, is due to increased concentration of the greenhouse gas CO_2 in the atmosphere. For details see Eichler et al., page.

EDITORIAL

No doubt, there is some nostalgic feeling while writing the 25th, my last Editorial of the Annual Report of our Laboratory. The very first editions were still much influenced by the rather strict rules of the EIR, the reactor research center. Basic research was nearly forbidden, our work had to concentrate on applied R&D. Only the merging in 1988 of EIR and SIN to PSI changed this situation. Now it became possible indeed to pursue with full support of the directorate basic research in Radiochemistry and in Environmental chemistry, the two main foci of our unit in the past.

Being on the cusp of retirement it is a great pleasure to realize that the joint partnership between PSI and Bern University has developed to a full success. This encouraging statement, result of an audit performed in 2006 by international experts in our field, was the basis for the decision to continue this collaboration also in future. I am very pleased that after the official opening of my position to search for a successor and a careful evaluation procedure a renowned scientist has been found. He will start his new position as head of the laboratory and as a full professor at Bern University in summer 2009.

But also our connection to the famous Oeschger center of Bern University (a follow-up institution of the NCCR climate) could be strengthened. Margit Schwikowski will act as a liaison person and keep our long-standing collaboration ongoing.

Finally, Soenke Szidat submitted his habilitation thesis to the faculty of natural sciences of Bern University. I wish him all the necessary success in the procedure to become a privatdocent.

On 18 January 2008 we celebrated at a special seminar the retirement of Urs Krähenbühl, Titular Professor at Bern University. Since 1973 he was responsible for the supervision of the Bern laboratories, was much involved in the education of students and responsible for many lecture

courses at the Bachelor as well as the Master level including several practical courses. I owe him my greatest thanks for his continuous support of our laboratory.

This annual report summarizes - as in previous years - ongoing research of our groups, both at PSI and at Bern University. The contributions are to a large extent status reports of ongoing Ph.D. work. In this respect it is once more appropriate to mention that these contributions have to be referred to as "*unpublished*", if cited in manuscripts.

Our social event of this year was very patriotic! We visited the Rütli, this famous meadow on the lake of Lucerne where our nation was founded on August 1st 1291. Thorsten Bartels, who became Swiss citizen a few month before the excursion presented to us an impressive laudation at this very historic place!



Heinz W. Gäggeler

MIEDEMA PARAMETERS FOR ELEMENT 112

R. Eichler (Univ. Bern & PSI)

From the experimentally determined adsorption enthalpy of element 112 on gold and the deduced volatility (ΔH_{sub}) a new set of parameters for the semi-empirical adsorption model based on the Miedema approach is deduced and can be used to evaluate the interaction of element 112 with other metals for the design of new experiments.

Thermochromatography with chemically inert carrier gases allowed the assessment of the elements of the groups 12, 14, 17 and 18 in their elemental state. The trends in the corresponding groups of the periodic table expect: 1) an increase of chemical inertness and volatility along groups 12 and 14, a decrease of metallic properties in group 12 and an increase of metallic properties in groups 13-16; 2) an increase of “metallic properties”, decrease of volatility and chemical reactivity along group 17; and 3) an increasing chemical reactivity and decreasing volatility along group 18. Those trends represent an expression of increasing relativistic effects in the electronic shell structure of the lighter homologues [1,2]. Adsorption chromatographic experiments with quartz and noble metals as stationary surfaces have confirmed these trends for the elements of the 6-th row of the periodic table using carrier-free amounts of Hg, Pb, At, and Rn. For transactinide elements first experiments with element 112 [3,4] confirmed the expected trends in group 12. A strong stabilization of the elemental state leading to an enhanced volatility is observed in this group down to element 112. However, still metallic properties distinguished from the noble gas physisorption have been observed for element 112 in contact with gold surfaces. These experimental results can be used to improve the available prediction models. For e.g. the Eichler-Miedema model (EMM) [5] is one of the models that successfully describes the adsorption enthalpy of a metal A (e.g. element 112) in the surface of a metal B (e.g. Au). based on the following set of equations:

$$\Delta H_{\text{ads}} = -\Delta H_{\text{g}} + 0.9 \cdot \left(\Delta H_{\text{sol}} - \frac{V_{\text{Asol}}}{V_{\text{B}}} \cdot \Delta H_{\text{vff}} \right) + \frac{V_{\text{Asol}}}{V_{\text{B}}} \cdot \Delta H_{\text{svf}}$$

$$-\Delta H_{\text{sol}} = \frac{2 \cdot V_{\text{Asol}}^{2/3} \cdot P}{n_{\text{WSA}}^{-1/3} + n_{\text{WSB}}^{-1/3}} \cdot \left(9.4 \cdot (n_{\text{WSA}}^{-1/3} + n_{\text{WSB}}^{-1/3})^2 - (\Phi_{\text{A}}^* - \Phi_{\text{B}}^*)^2 - \frac{R_{\text{m}}}{P} \right)$$

$$V_{\text{Asol}} = V_{\text{A}} \cdot (1 + a \cdot (\Phi_{\text{A}}^* - \Phi_{\text{B}}^*))^{1/2}$$

$$\Delta H_{\text{svf}} = 0.0595 \cdot T_{\text{m}}$$

$$\Delta H_{\text{vff}} = 0.0833 \cdot T_{\text{m}}$$

with:

T_{m}	melting point of Au (1337.33 K);
ΔH_{svf}	enthalpy of surface vacancy formation of Au;
ΔH_{vff}	enthalpy of volume vacancy formation of Au;
ΔH_{g}	standard sublimation enthalpy of element 112;
ΔH_{ads}	standard adsorption enthalpy of element 112;
ΔH_{netto}	net adsorption enthalpy of element 112;
n_{ws}	electron density at Wigner-Seitz cell boundaries
V_{Asol}	atomic volume of A in solid solution in B
$V_{\text{A/B}}$	atomic volume of solid A and B
Φ^*	electronegativity Miedema scale
R_{m}/P	empirical hybridisation term

A new set of semi-empirical parameters (n_{ws} and Φ^*) has been deduced from the experimental results with element 112. A considerable involvement of the d-orbitals of element 112 in its interaction with gold was suggested in

[6]. Since the EMM model distinguishes between the various possible electron orbitals involved in the metal-metal interaction we derived the parameters for element 112 as s-element and as d-element. The results are compiled in table 1. For the typical group 12 elements the EMM includes a special parameter set (column 3).

Tab. 1: Miedema parameters for element 112 dependent on the electrons assumed to be involved in the adsorption interaction with the gold surface.

	2/4d	1s	Group 12	Pred [5]
$-\Delta H_{\text{ads}}$ kJ/mol	52	52	52	86 (65[6])
ΔH_{g} kJ/mol	38	38	38	39 (110[7])
$-\Delta H_{\text{netto}}$ kJ/mol	14	14	14	48
$-\Delta H_{\text{sol}}$ kJ/mol	28	19	23	19
$n_{\text{ws}}^{1/3}$	1.113	1.113	1.113	1.09
Φ_{112}	3.870	3.860	3.964	3.94
V [7] cm^3	15.52	15.52	15.52	13.6
$V_{\text{Asol}}^{2/3}$ cm^2	6.057	5.758	5.485	5.47
P $\text{V}^{-1} \text{cm}^{-2} \text{du}^{-1/3}$	0.147	0.128	0.128	0.128
A V^{-1}	0.04	0.14	0.1	0.1
R_{m}/P eV^2	0	0	0.42	0.42

The predictions for the interaction of element 112 with other metals appear to be feasible in preparation of more systematic experiments, where other metals than gold are used. For this purpose vacuum chromatographic systems are under development, in which stationary surfaces metals can be used more sensitive to oxidation.

REFERENCES

- [1] P. Pyykkö and J.-P. Desclaux, Acc. Chem. Res. **12**, 276 (1979).
- [2] P. Schwerdtfeger and M. Seth; Encyclopaedia of Computational Chemistry, Vol. 4, Wiley, New York, (1998), pp. 2480.
- [3] R. Eichler et al., Nature **447**, 72-75 (2007).
- [4] R. Eichler et al., Angew. Chem. Int. Ed. **47**(17), 3262 (2008).
- [5] B. Eichler, PSI Report 00-09, (2000) and PSI Report 03-01 (2002), ISSN 1019-0643.
- [6] V. Pershina and T. Bastug Chem. Phys. **311**, 139 (2005).
- [7] N. Gaston et al. Angew. Chem. Int. Ed. **46**, 1663 (2007).

ISOTHERMAL VACUUM CHROMATOGRAPHY (IVAC): GENERATION II

A. Serov, R. Eichler, H.W. Gäggeler (Univ. Bern & PSI), D. Piguet (PSI)

We present here the developed upgrade of the Isothermal Vacuum Chromatography (IVAC) setup to be used for the adsorption investigation of transactinides in their elemental state at clean chromatographic surface conditions.

INTRODUCTION

Since the discovery of isotopes of super heavy elements (SHE) 112-118 in ^{48}Ca -induced nuclear fusion reactions with actinide targets at the Flerov Laboratory of Nuclear Reactions (FLNR) Dubna, Russia [1] researchers endeavour to investigate their chemical properties. The first experiments were based on the well-known Insitu-Volatilization and On-line detection setup (IVO) with the Cryo-On-Line Detector (COLD) [2]. During these experiments a number of drawbacks were detected: 1) low spectroscopic resolution of detectors in the carrier gas atmosphere; 2. limitation to temperature ranges between 35 and -180°C ; 3. Deposition of ice layers on the stationary materials held at temperatures below -100°C . The new generation vacuum adsorption chromatographic method presented here may help overcoming these drawbacks. The present report summarizes technical data of the second generation IVAC system.

EXPERIMENTAL

For investigations of chemical properties of less volatile SHE with short half-lives we design an experimental set-up based upon the IVAC principle [3]. Generation I of IVAC was aimed to proof the principles of vacuum chromatographic methods. The design of this IVAC system revealed several problems: 1. Detection system, based on semiconductors cannot operate at isothermal oven temperature higher than 350°C ; 2. The electric connections in the system generated electronic noise; 3. The isothermal oven cooling was not efficient enough to continuously operate over days and months. Attempts to overcome these problems lead to the construction of a new version of IVAC. Problems with detection systems were solved by implementing new technique based on the coverage of detectors by thin metal layers [4]. As possible materials for protection of PIN diodes we have selected metals with relatively low Z: Al, Mg, Mn, Zn, Cu, and Ag. These metals were evaporated at vacuum conditions and deposited on the surface of the diodes. After establishing coverage parameters, technology was transferred to commercial company to obtain several diodes, covered by different materials with different thicknesses (Fig. 1).



Fig. 1: Diodes covered with different materials (Pd, Pt, Au and Al).

The newly covered detectors can be operated in IVAC II at significantly increased isothermal temperature. The new

Thermocoax® based oven provides temperatures up to $T=950^\circ\text{C}$. The semiconductor detector is operational up to temperatures of 700°C . The newly designed water cooling system and detector compartment held the diode surface temperature at 20°C . The electronic noise was fully suppressed by a new connector's scheme. At the highest temperatures a vacuum of $\sim 10^{-5}$ mbar was achieved.

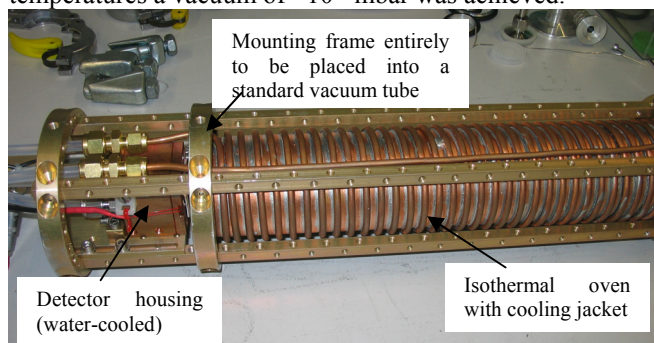


Fig. 2: IVAC (generation II) set-up.

RESULTS AND CONCLUSIONS

The Generation II IVAC system is available and designed for conditions sufficient for the investigation of the chemical behaviour of SHE elements. The system will be extensively tested in 2009 with lighter homologues of transactinides (I, At, Hg, Pb, Tl, and Po) produced in heavy ion induced reactions at the PSI Philips cyclotron and in neutron activation reactions at PSI-SINQ facility. Further efforts are needed to achieve an on-line coupling of IVAC to the production site of transactinides [5]. For this reason a new irradiation box was installed at the NeC area of PSI allowing for larger-scale setups to be installed in the vicinity of the heavy ion irradiation target.

ACKNOWLEDGEMENT

Authors kindly appreciate the financial support by the SNF.

REFERENCES

- [1] Yu. Ts. Oganessian et al., J. Phys. G **34**, R165 (2007).
- [2] R. Eichler et al., Nature **447**, 72-75 (2007).
- [3] R. Eichler et al., Ann. Rep. Lab. for Radio- & Environ. Chemistry, Uni Bern & PSI (2006), p. 7.
- [4] A. Serov et al., Ann. Rep. Lab. for Radio- & Environ. Chemistry, Uni Bern & PSI (2007), p. 6.
- [5] Qin Zhi et al., Ann. Rep. Lab. for Radio- & Environ. Chemistry, Uni Bern & PSI (2003), p. 9.

ADSORPTION INTERACTION OF ^{113m}In AND ^{212}Pb ISOTOPES WITH QUARTZ

A. Serov, R. Eichler, H.W. Gäggeler (Univ. Bern & PSI)

Indium-113m was prepared by epithermal neutron activation of tin. Lead-212 was prepared from a thorium-232 generator. Their adsorption properties on quartz were investigated by thermochromatography.

INTRODUCTION

Investigation of chemical properties of super heavy elements (SHE) produced in ^{48}Ca induced nuclear fusion reactions with actinide targets [1] is a challenging task for many research groups in the world. One of the main approaches to perform such an experiments is based on series of experiments involving lighter homologues of SHE. Recently, only a limited number of methods are available for studying the chemical behaviour of SHE and their lighter analogues: Liquid phase, gas-phase and electrochemical methods [2]. Recently, by using gas adsorption chromatography, based on the well-known In situ-Volatilization and On-line detection setup (IVO) with the Cryo-On-Line Detector (COLD), the chemical interaction of elements 112 was investigated [3]. In the present research an experimental determination of ΔH_{ads} of carrier-free ^{113m}In and ^{212}Pb isotopes on quartz surface was performed in preparation of experiments with the elements 113 and 114.

EXPERIMENTAL

Lighter homologues of SHE elements ^{113m}In ($T_{1/2}=99$ m) and ^{212}Pb ($T_{1/2}=10.65$ h) were prepared from home-made generator systems. For that purposes 0.5g of $^{\text{nat}}\text{Sn}$ were irradiated at the SINQ-NAA facility at PSI for 2hrs. The irradiated sample was dissolved in HCl_{conc} with a subsequent deposition onto an anion-exchange column. Using 1M HCl as an eluent separation of ^{113m}In isotope from parent ^{113}Sn was achieved (Fig. 1). ^{113m}In was transformed into oxide form and dried on a Ta surface. This sample was used as source for thermochromatographic investigations with quartz as stationary surface. ^{212}Pb was prepared from $^{\text{nat}}\text{Th}$ generator. $^{\text{nat}}\text{ThF}_2$ was dissolved under refluxing conditions in $\text{HNO}_3(\text{conc.})$ and deposited onto a cation-exchange column. Using 1M HCl/ CH_3OH (90:10 %) as eluent ^{212}Pb isotope was quantitatively separated from all by-products of the ^{232}Th decay.

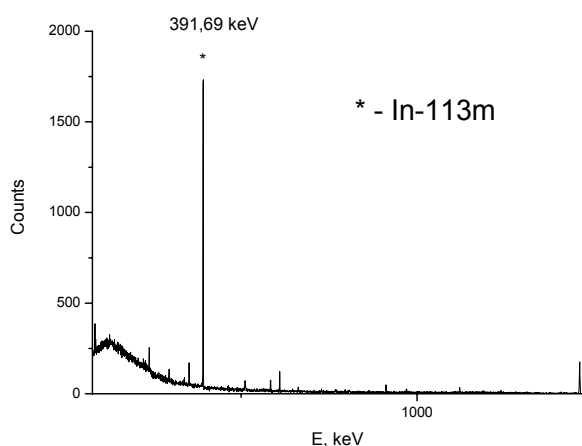


Fig. 1: Gamma spectrum of ^{113m}In eluted from a Sn isotope generator.

RESULTS AND CONCLUSIONS

The interaction of indium with quartz surface was investigated using a highly purified carrier gas to exclude trace amounts of water and oxygen. The entire thermochromatography column was encapsulated in a steel tube. The gas had to pass a Ta getter (1000°C) before hitting the In source deposited on Ta and heated up to 1000°C. Afterwards, the In was transported again over a hot Ta getter. This setup supposed to ensure the elemental state for the quite reactive indium. Reproducibility of obtained data was achieved by several repetition of experiment at the same conditions. After data collecting, Monte-Carlo simulation approach was applied to obtain ΔH_{ads} values (Fig. 2).

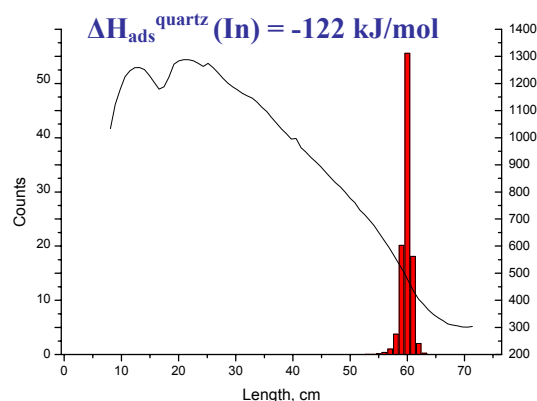


Fig. 2: Thermochromatogram of ^{113m}In on quartz surface.

The data obtained in this investigation show a remarkable discrepancy to previously obtained adsorption data. One possible explanation is the difficulties in the obtaining isotopes in a carrier-free form in those early researches and the uncertainty of the chemical states investigated previously.

Prepared generator systems allow to perform future experiments with indium and lead isotopes. Future studies will comprise the reinvestigation of the interaction of In and Pb with different metal surfaces using the thermochromatography method.

ACKNOWLEDGEMENT

Authors kindly appreciate the financial support by SNF.

REFERENCES

- [1] Yu. Ts. Oganessian et al., J. Phys. G **34**, R165-R242 (2007).
- [2] M. Schädel, Angew. Chem. Int. Ed. **45**, 368 (2006).
- [3] R. Eichler et al., Nature **447**, 72-75 (2007).

STOPPING FORCE MEASUREMENTS OF MERCURY, RADON AND NOBELIUM IN MYLAR AND ARGON

D. Wittwer, R. Dressler, R. Eichler, H.W. Gäggeler, A. Serov (Univ. Bern & PSI),
D. Piguet (PSI), V.K. Utyonkov (FLNR)

The stopping forces of Hg, Rn and No in Mylar and argon were investigated at energies of 20-50 MeV.

INTRODUCTION

Data for stopping forces of heavy ions at low velocities are still scarce. Stopping force calculation codes are known to deliver accurate results for light ions in solids but have difficulties to perform as accurate results for heavy ions. Even less accurate results are calculated for the stopping force in gaseous stopping media. This is especially true at low velocities (around and below the Bragg peak). In the field of transactinide investigations, the stopping of the produced evaporation residues produced in heavy ion induced nuclear fusion reactions is of essential importance. Here we report on the experimental determination of stopping force data and the deduced ranges for mercury, radon, and nobelium in Mylar (biaxial oriented PET) and gaseous argon.

EXPERIMENTAL

A 265 MeV $^{48}\text{Ca}^{18+}$ beam was delivered from the U-400 cyclotron from the *Joint Institute of Nuclear Research (JINR)* in Dubna, Russia. Three different target materials were irradiated, namely neodymium oxide (Nd_2O_3 , 300 $\mu\text{g}/\text{cm}^2$, on 1.6 μm Ti backing), dysprosium oxide (Dy_2O_3 , 330 $\mu\text{g}/\text{cm}^2$, on 1.6 μm Ti backing) and lead (^{208}Pb , 420 $\mu\text{g}/\text{cm}^2$, 1 μm Cu degrader and 1.6 μm Ti backing). The produced evaporation residues in the fusion of ^{48}Ca with target nuclei are either ^{185}Hg , ^{206}Rn (both at 244 MeV beam energy in the middle of the target) or ^{254}No (217 MeV). Beam intensities between 1.5 and $3 \cdot 10^{11}$ particles per seconds (0.3-0.6 μA current) were used. The *Dubna gas-filled recoil separator (DGFRS)* [1] separated the evaporation residues from the beam particles and the transfer products according to their different momentum leading to different m/q (mass over charge) ratio. The evaporation residues (EVR) were guided to the focal plane of the separator where an exchangeable Mylar foil of 2, 3 or 5 μm thickness separates the *reaction product collection chamber (RPC-chamber)* from the DGFRS. The RPC-chamber had a depth of 20 mm and was filled with argon gas of a pressure between 0.0 and 0.4 bar. At the back wall of the RPC-chamber a photo diode (PIN) was mounted and operated at a bias voltage of -40 V to spectroscopically resolve the energy of implanting EVR's and their α -decays. The Mylar foil thickness and the argon pressure were varied. Vacuum measurements were also performed with Mylar or without at 1 Torr H_2 .

RESULTS

From the implantation energy distribution of the measurements the remaining energy of the evaporation residue could be deduced by applying a pulse height defect (PHD) correction according to Ogihara, et al. [2]. The prefactor of Ogiharas' formula had to be adjusted to match

to the used PIN-diodes. By plotting the remaining energies versus the Mylar thickness or the surface density of argon, the stopping forces and the ranges of the evaporation residues could be determined as shown in Fig. 1.

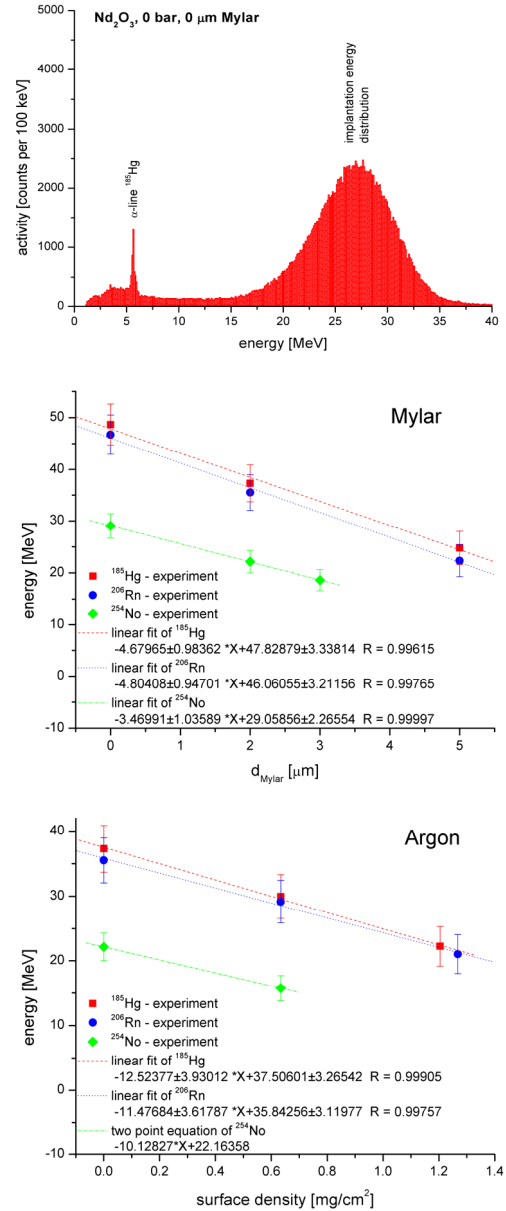


Fig. 1: Example spectrum of the implantation energy of mercury without Mylar and Argon (top). Remaining energies versus the Mylar thickness (middle) or the argon thickness (bottom). The slopes are the stopping forces.

REFERENCES

- [1] K. Subotic, et al., Nucl. Instr. And Meth. A **481**, 65 (2002).
- [2] M. Ogihara, et al., Nucl. Instr. And Meth. A **251**, 313 (1986).

STOPPING RANGE DETERMINATION OF $^{288}\text{114}$ IN MYLAR AND ARGON

D. Wittwer, R. Eichler, H.W. Gäggeler (Univ. Bern & PSI), R. Dressler (PSI)

The stopping range of element 114 ($^{288}\text{114}$) in Mylar and argon was determined by an extrapolation from experimental stopping force data.

INTRODUCTION

The stopping range of the eka-lead isotope $^{288}\text{114}$ is of significant importance for its chemical investigation by our group in the 2008 experimental setup. The produced isotopes must have a velocity that is high enough to pass a 3 μm thick Mylar foil and although low enough so that the isotopes can be stopped in a gaseous argon volume of 15 mm depth held at a pressure of 1.3 bar. Since there is no stopping range data available for this element an extrapolation from lighter elements had been made. This experimental data based extrapolation was compared with extrapolation results using the stopping force simulation program "SRIM-2008" [1].

THEORY

The extrapolation to deduce the stopping range was made by assuming the proportionality of the stopping force of a heavy ion to the effective charge and to the stopping force of a charge $q_{\text{eff}}=1$ particle [2]. This procedure demands that the heavy ion as well as the $q_{\text{eff}}=1$ particle have the same incident velocity.

$$-\left.\frac{dE}{dx}\right|_Z = q_{\text{eff}}^2(E_I, Z_1, A_1) \cdot \left[-\left.\frac{dE}{dx}\right|_{Z=1}\right] \quad (1)$$

$$q_{\text{eff}}^2(E_I, Z_1, A_1) = Z_1^2(1 - e^{-v/v_{\text{TF}}}) \quad (2)$$

$$v_{\text{TF}} = Z_1^{2/3} v_0 \quad \text{with} \quad v_0 = c/137.036 \text{ [m/s]} \quad (3)$$

In equation (1) q_{eff} is the velocity depending effective charge of the heavy ion and in equation (2) v_{TF} is the Thomas Fermi velocity that includes the Bohr velocity v_0 . From equation (1) a $q_{\text{eff}}=1$ particle stopping force can be derived. These stopping forces ($S_{\text{HI}}/q_{\text{eff}}^2$) were plotted against $1/\ln(Z_1)$ the dominant contribution of the atomic number Z_1 to the stopping number L [3].

RESULTS

The stopping force data used were either from our measurements [4] or from the data compilation of H. Paul [5]. The heavy ion data used are: mercury and radon. The light ion data used are: boron, carbon and oxygen. These were the only data available at the required velocity ($\pm 8\%$). This velocity, at which the extrapolation was made, was determined by the recoiling energy of the $^{288}\text{114}$ isotope from its production assuming momentum conservation at central inelastic collision (fusion) with the beam particles. The extrapolated range under these conditions for $^{288}\text{114}$ in Mylar is $4.4 \pm 0.4 \mu\text{m}$ and in argon is $2.4 \pm 0.6 \text{ mm}$. The cyan labeled data point (nobelium-254) in Fig. 1 was not included in the regression because it was measured at a too low velocity. For the comparison between the experimental data based extrapolation with SRIM-2008, all the used data points were simulated and processed as the experimental data. The results are shown in Fig. 1 where the black line is

the experimental extrapolation and the red line the simulated extrapolation. The simulated data extrapolation and the experimental data extrapolation are in good agreement in Mylar. In gaseous argon the extrapolation results differs considerably. This is because SRIM calculates stopping forces in a semi-empirical way and there are no heavy ion data at such low velocities in a gaseous stopping medium implemented.

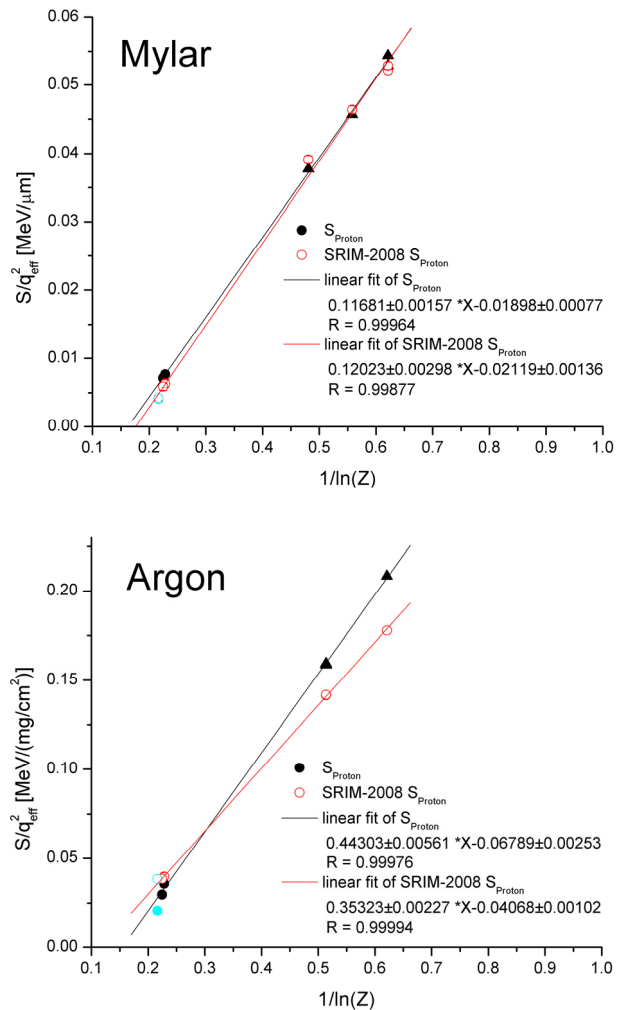


Fig. 1: Extrapolations of the stopping force from $^{288}\text{114}$ in Mylar (upper graph) and in argon (lower graph). The black lines are the extrapolation based on experimental data. The red lines are the extrapolations based on SRIM-2008 simulated values. The triangles are data from H. Paul [5] and the full circles from our measurements [4].

REFERENCES

- [1] J.F. Ziegler, et al., SRIM-2008, www.srim.org, 2008.
- [2] J.F. Ziegler, et al., *The stopping and range of ions in solids*, Pergamon Press, 1985.
- [3] J. Lindhard, et al., Phys. Rev. A **53**, 2443 (1996).
- [4] D. Wittwer, et al., see this report p.6.
- [5] H. Paul, www.exphys.uni-linz.ac.at/stopping, 2003.

SYSTEMATIC INVESTIGATION OF PREPARATION EFFICIENCY AND QUALITY OF LANTHANIDEOXIDE TARGETS

A. Serov, R. Eichler, H.W. Gäggeler (Univ. Bern & PSI)

The production of short-lived alpha-decaying tracers in heavy ion induced nuclear fusion reactions at the PSI Phillips cyclotron requires a secure lanthanide target preparation. The recently frequent use of ^{40}Ar beams demands a production of more stable target setups compared to irradiations with more light beams, such as ^{22}Ne , ^{18}O etc..

INTRODUCTION

During last decade development of experimental techniques allows scientist to synthesis new elements with $Z > 110$ (super heavy elements - SHE) [1]. It's challenging task for researchers to determine chemical properties of these elements and allocate their position in Periodic Table. Working hypothesis of investigations of their behavior can be based on comparison properties of SHE with ones of their lighter homologues. By selection of an appropriate target-projectile combination it's possible to synthesize different isotopes for both SHE and their light homologues. Quite often the reproducibility of the electrochemical plating procedure is low. The quality of the targets varies. Therefore, the present investigation comprises different parameters affecting the target quality and the efficiency of preparation. The main goal of investigation was the reproducible preparation of lanthanide targets with loading higher than $500 \mu\text{g}\cdot\text{cm}^{-2}$

EXPERIMENTAL

There are several experimental techniques for target preparation available: electrospraying, vacuum sublimation, cathode sputtering, electrodeposition etc. Electrodeposition (molecular plating) was selected for present research, because it allows for highest yields, produces high uniformed layers and can be tuned for preparation of targets with various thicknesses [2]. Starting material for target preparation was Tm_2O_3 . Thulium oxide was dissolved in $\text{HNO}_3(\text{conc.})$, solution was dried up to several micro liters. As prepared the $\text{Tm}(\text{NO}_3)_3$ was dissolved in i-PrOH and loaded into a home-made electrolysis cell. As target backing typically a $12 \mu\text{m}$ Be foil was used. After completing electrodeposition, as prepared target was baked in air at $T=450^\circ\text{C}$. The temperature was increased slowly ($5^\circ/\text{min}$). The loading was determined by weighing. Variable parameters affecting the Tm_2O_3 loading were: $\text{Tm}(\text{NO}_3)_3$ concentration, plating voltage, number of deposition steps, electrodeposition duration etc.

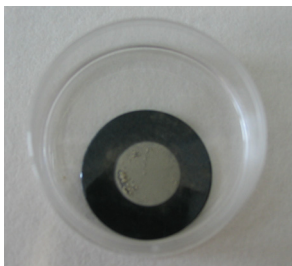


Fig. 1: Tm_2O_3 target prepared on $12 \mu\text{m}$ Be backing.

RESULTS AND CONCLUSIONS

Using the step-by-step method it was possible to achieve loading close to 1.1 mg of target material (**Fig. 2**) after 6

steps. Optimal duration of electrodeposition was found as 90 minutes with calculated yield of about 95 %. The voltage applied in the electrolysis was varied from 400 V up to 900 V. It was determined that at fixed electrodeposition time (90 minutes) loading increases linearly with increasing of voltage. Increase of $\text{Tm}(\text{NO}_3)_3$ concentration leads to increase of loading, with following plateau.

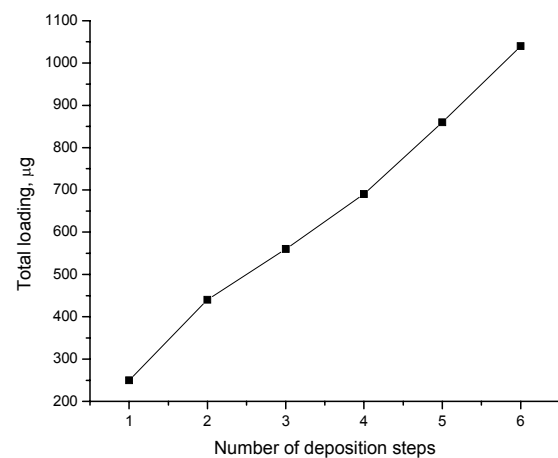


Fig. 2: Total loading of Tm_2O_3 on Be-foil after 6 deposition Steps.

After optimizing all experimental parameters, a Tm_2O_3 target with loading $\sim 500 \mu\text{g}$ was prepared and used for the production of short-lived astatine isotopes in nuclear fusion reactions with ^{40}Ar beams at the PSI Phillips cyclotron. It was found that under the beam conditions ($^{40}\text{Ar}^{11+}$, 303 MeV, 500 el.nA) the target is stable up to several days. Careful pre-treatment of backing material leads to increasing of Tm_2O_3 adhesion. Other optimal parameters are: increasing the baking temperature up to 500°C , increasing of baking time. The stability could be further increased by covering the target material with a $1.5 \mu\text{m}$ Rh foil, which is suggested also as a procedure against mechanical sputtering for actinide targets applied at higher beam doses of ^{48}Ca . The optimized parameters will be applied to production of other rare earth targets for the use at the PSI Phillips cyclotron.

ACKNOWLEDGEMENT

Authors kindly appreciated the financial support by SNF.

REFERENCES

- [1] Yu. Ts. Oganessian et al., J. Phys. G **34**, R165 (2007).
- [2] K. Eberhard et al., Nucl. Instr. Meth. A **590** 134 (2008).

KINETIC MODEL OF NO₂ UPTAKE TO AEROSOLS CONTAINING GENTISIC ACID CONSIDERING DEPLETION OF REACTIVE MOLECULES IN THE BULK

Yu. Sosedova (Univ. Bern & PSI), A. Rouvière, M. Ammann (PSI)

Data previously obtained for the reaction of gaseous NO₂ with gentisic acid sodium salt particles are compared to an explicit kinetic model including NO₂ bulk accommodation, and diffusion and reaction in the bulk.

Gentisic acid trisodium salt (Na₃GA), a proxy for biomass burning derived aromatic compounds, was used as a model compound to provide a fast aerosol phase sink for NO₂. The NO₂ uptake was investigated using the ¹³N tracer technique, by which the transfer of ¹³N labelled NO₂ to the particles is followed as function of time in an aerosol flow reactor [1].

For NO₂ uptake to the bulk of liquid Na₃GA particles a resistor model can be applied:

$$\frac{1}{\gamma_{net}} = \frac{1}{\alpha_b} + \frac{1}{\gamma_{brxn}} \quad (1)$$

where γ_{brxn} is a limiting uptake coefficient for the bulk reaction, and α_b is the bulk accommodation coefficient, which is the probability that a molecule colliding with the surface is entering the liquid phase [2]. For small droplets of radius r_p the concept of reacto-diffusive length l is important:

$$l = \sqrt{\frac{D_{b,NO_2}}{k_2[Na_3GA]_b}} \quad (2)$$

where D_{b,NO_2} is the NO₂ bulk diffusion coefficient. For particles used in our experiments l was between 1.7 and 21% of r_p depending on $[Na_3GA]_b$, the liquid phase concentration of Na₃GA. For this regime, we used the following corrected equation [2]:

$$\gamma_{brxn} = \frac{4HRT}{\omega} \sqrt{D_{b,NO_2} k_2 [Na_3GA]_b} \left[\coth\left(\frac{r_p}{l}\right) - \left(\frac{l}{r_p}\right) \right] \quad (3)$$

with H , R , T and ω being a Henry's law coefficient, the gas constant, temperature and mean thermal velocity, respectively. Considering that pseudo-first order loss from the gas to particle phase is equal to

$$k_p = \frac{4\gamma_{net}}{S\omega} \quad (4)$$

where S is the aerosol surface area, a system of differential equations can be written:

$$\begin{cases} \frac{d[NO_2]_g}{dt} = -\frac{0.25S\omega}{\frac{1}{\alpha_b} + \frac{1}{\gamma_{brxn}}} [NO_2]_g \\ \frac{d[Na_3GA]_g}{dt} = -\frac{0.25S\omega}{\frac{1}{\alpha_b} + \frac{1}{\gamma_{brxn}}} [NO_2]_g \\ [Na_3GA]_g = [Na_3GA]_b \frac{V_p}{V} \end{cases} \quad (5)$$

where V_p is the particle bulk volume per volume of aerosol.

The system (5) was solved numerically using ODE23 MATLAB® solver. All parameters are known from the experiments except for k_2 and α_b . The experimental data

cover cases, in which $[Na_3GA]_b$ was high, and cases, in which significant depletion of Na₃GA occurred during the residence time in the flow reactor. For the latter case, the loss of NO₂ from the gas phase is determined by the liquid phase rate constant k_2 and the depletion of liquid phase Na₃GA, i.e., for α between 10⁻² and 1, $1/\alpha \ll 1/\gamma_{brxn}$. The data shown in Fig. 1b then allow estimating k_2 to lie in the range (1-7)×10⁸ M⁻¹s⁻¹. In the case of large Na₃GA concentrations (Fig. 1a), the loss of gas phase NO₂ is strongly affected by the bulk accommodation coefficient, constraining its value to the range of 0.01 to 1. Running the simulations for all available experimental data leads to a best estimate for α_b of 0.025 and for k_2 of 3.6×10⁸ M⁻¹s⁻¹.

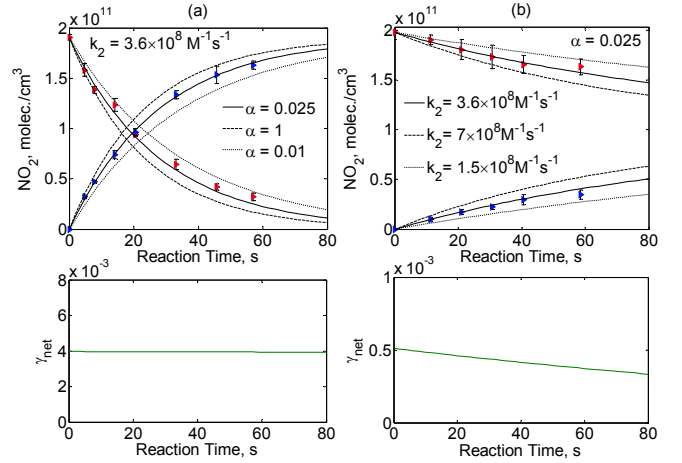


Fig. 1: Experimental data points (red for gas-phase NO₂ and blue for NO₂ on particles) and simulations (lines). $[Na_3GA]_g$ is (a) 365 ppb \gg initial $[NO_2]_g = 7.7$ ppb and (b) 3.5 ppb $<$ initial $[NO_2]_g = 8$ ppb.

It is also seen from the Fig. 1b that in this experiment with relatively low $[Na_3GA]_g$ γ_{net} (obtained from the simulation) decreases with time, which is due to depletion of Na₃GA in bulk particle phase. In this case one can not use a simple pseudo-first order approach any more and should use an explicit kinetic model instead as shown here.

ACKNOWLEDGEMENT

This work is supported the Swiss National Science Foundation.

REFERENCES

- [1] Yu. Sosedova et al., Ann. Rep. Lab. for Radio- & Environ. Chemistry, Uni Bern & PSI (2007).
- [2] U. Pöschl et al., Atmos. Chem. Phys., 7, 5989 (2007).

OZONE UPTAKE TO DELIQUESCED IODIDE PARTICLES: MEASUREMENTS AND MODELING

A. Rouvière, Yu. Sosedova, S. Brütsch, M. Birrer, M. Ammann (PSI)

A comparison between modeling and experimental data of ozone uptake to deliquesced iodide particles is shown and discussed.

It is well established that iodine chemistry has an active role in stratospheric and tropospheric chemistry, including the influence of iodine oxides on the oxidizing capacity, the formation of new particles, and the enrichment of iodine in marine aerosols. O_3 is a very important oxidant, and several details of its transfer to the aqueous phase are not well known. The aim of the present work is to investigate the reaction of deliquesced KI particles with gas phase O_3 using a combination of aerosol experiments and a chemical kinetics model in order to determine the bulk accommodation coefficient.

In the experiments, described in [1], the loss of O_3 in presence of deliquesced KI particles is followed as a function of the interaction time in a flow reactor. The measured uptake coefficient is close to $\gamma=10^{-2}$, independent of the pH of the solution.

Comparisons between measurements and modeling have been made. The model is driven by a system of two differential equations where the loss of ozone and iodide, in the gas and aqueous phase, respectively, can be described as:

$$\begin{aligned} \frac{d[O_3]}{dt} &= -\frac{a}{b+c[I^-]^{1/2}}[O_3] \\ \frac{d[I^-]}{dt} &= -\frac{a}{V_p(b+c[I^-]^{1/2})}[O_3] \end{aligned}$$

$$\text{with } a = S\omega/4; \quad b = \frac{1}{\alpha_b} \quad \text{and } c = \frac{\omega}{4HRT\sqrt{D_{b,O}k_b}}$$

S is the aerosol surface area, ω the mean molecular velocity of O_3 , α_b is the bulk accommodation coefficient, T is the temperature, H is the Henry's law coefficient of O_3 , D_{b,O_3} is the diffusion coefficient of O_3 in the liquid phase, R is the universal gas constant, k_{aq} the first order loss rate constant of O_3 in the liquid phase and V_p the volume of the particles. We are using Matlab to solve these equations with the solver ODE 45.

Fig. 1 shows the temporal evolution of the ozone and iodide concentration. The red plain circles represent measured data. The lines indicate the evolution of the concentrations predicted by our model with different values of the bulk accommodation coefficient. We assume that the second order rate constant between iodide and ozone is $k_b=1.2 \times 10^9 \text{ M}^{-1}\text{s}^{-1}$ [2]. Different values of α_b are chosen in the range of 0.01 to 1 to obtain different profiles of iodide and ozone concentrations. We observed that for $\alpha_b=1$ the model fit well with the data from the experiment, validating also the value of the second order rate constant k_b .

The reactive uptake coefficient of ozone on solid potassium iodide was recently estimated as $1.4 \pm 0.7 \times 10^{-4}$ [3]. We obtained a larger uptake indicating that aqueous phase iodide is more reactive than solid KI.

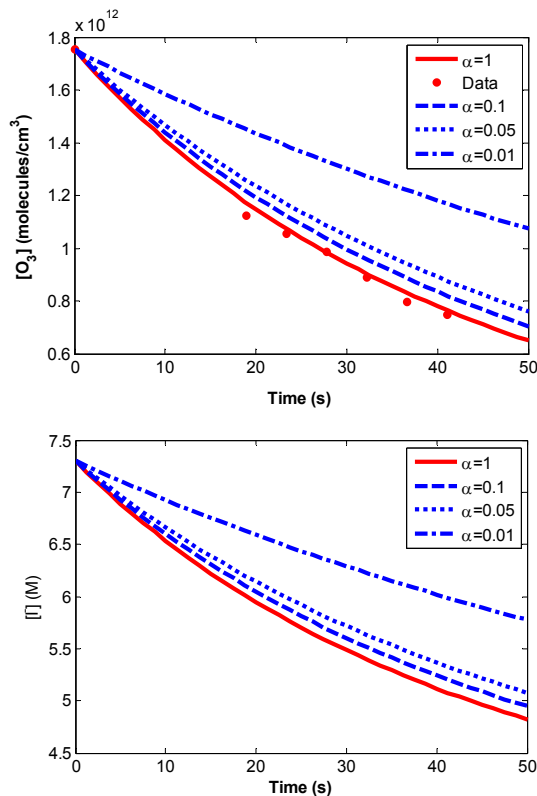


Fig. 1: Temporal evolution of the ozone concentration in the gas phase (upper panel) and the iodide concentration in the aqueous particle phase.

In the past the uptake of ozone to aqueous solutions has been carried out using different methods. Previous studies indicate that α_b for O_3 on iodide solutions is in the range of 2×10^{-3} to 1, and that bulk accommodation could be a rate limiting step [4]. Considering the uncertainties we consider our result to be in good agreement with the value of α_b in the past, and accepting some uncertainty in the liquid phase rate constant, we can constrain α_b to be closer to 1 than previously estimated.

ACKNOWLEDGEMENT

This work is supported by the Swiss National Science Foundation.

REFERENCES

- [1] A. Rouvière et al., Ann. Rep. Lab. for Radio- & Environ. Chemistry, Uni Bern & PSI (2007), p. 13.
- [2] Q. Liu et al., Inorg Chem., **40**, 4436 (2001).
- [3] M. Brown et al., J. Phys. Chem. C, **112**, 5520 (2008).
- [4] J.H. Hu et al., J. Phys. Chem., **99**, 8768 (1995).

INFLUENCE OF FATTY ACIDS ON THE UPTAKE OF OZONE TO DELIQUESCED POTASSIUM IODIDE PARTICLES

A. Rouvière, M. Birrer, M. Ammann (PSI)

The effect of fatty acids on the uptake of ozone to deliquesced iodide particles was investigated. It is shown that the fatty acids in monolayer quantities may substantially inhibit the phase transfer of ozone to deliquesced particles.

INTRODUCTION

Iodide provides a substantial aqueous phase sink to drive uptake of ozone. This reaction is also important in halogen activation processes of the marine boundary layer. The aim of this study was to determine the effect of (C_9 - C_{20}) fatty acid surfactants on the phase transfer of ozone to the underlying condensed phase. We have shown earlier that surfactants inhibit the phase transfer of HNO_3 [1] and that they may affect the interfacial halide enhancement [2].

EXPERIMENTAL

The experimental set-up is similar to that described in [1] (Fig. 1). The aerosol flow passes over a heated reservoir containing a given fatty acid (FA). The amount of the fatty acid condensed on the particles was controlled by changing the evaporator temperature. This amount was evaluated by comparing the diameters of the particles with and without fatty acid present, by using a first DMA to select monodisperse aerosol and the SMPS to measure the size changes due to condensing the fatty acid. The difference in diameter was used to estimate the fatty acid mass fraction. We don't know whether the organics form a homogeneous coating on the dry particles or condense as a separate droplet attached to the particle. However, once deliquesced, we assume, that FA spontaneously form a monolayer with the excess accumulating as a "lens" at the aqueous surface.

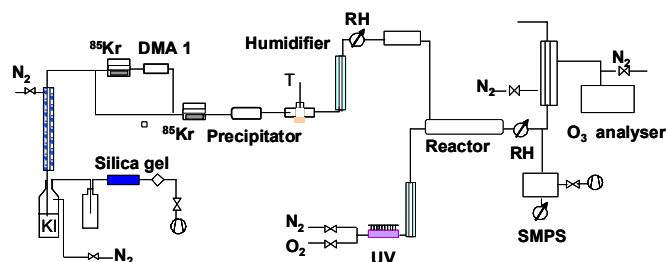


Fig. 1: Experimental set-up

RESULTS

An organic coating can reduce the mass transfer between the gas and the aerosol phases. The effectiveness of fatty acids films as barriers to the mass transfer is determined by the properties of the organic films, which depend on the carbon chain length, the nature of the head group (polarity), the pH and the temperature [2].

As shown in Fig. 2, we observed that C_9 and C_{12} both reduced the rate of uptake by about a factor of two, with only a small influence of the organic mass fraction. It seems that the permeability is not reduced much further for larger mass fractions. In contrast, for C_{15} , we observed a much

stronger decrease already at the lowest mass fraction, but again with only little effect by increasing mass fractions. For C_{18} and C_{20} , the organic mass fraction has a substantial effect on the reactive uptake coefficient. The observed behavior can be related to the structure and density of the FA monolayers at the equilibrium spreading pressure [3]. The behavior observed for O_3 in this study can also be compared to that observed previously for HNO_3 on deliquesced NaCl aerosol [1].

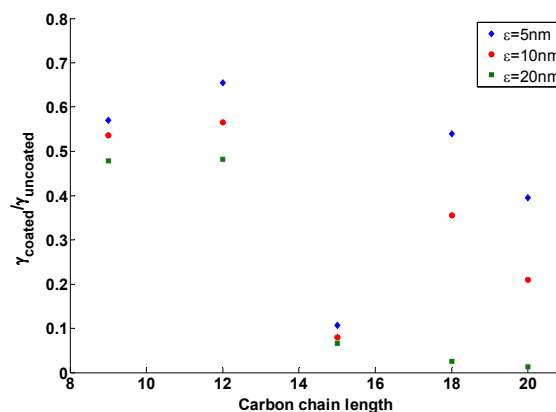


Fig. 2: The ratio of the reactive uptake coefficient in presence of an organic monolayer to the uptake coefficient of the uncoated particles as a function of the carbon chain length for three different mass fractions.

CONCLUSION

The effects of the fatty acids on the ozone uptake onto deliquesced potassium iodide particles were investigated. The results showed that especially for the C_{15} - C_{20} , the presence of FA limits the mass transfer of ozone to the aqueous phase.

ACKNOWLEDGEMENT

This work is supported by the Swiss National Science Foundation.

REFERENCES

- [1] K. Stemmler et al., Atmos. Chem. Phys. **8**, 5127 (2008).
- [2] M. Krisch et al., J. Phys. Chem. C **111**, 13497 (2007).
- [3] M. Latif and P. Brimblecombe, Environ. Sci. Technol., **38**, 6501 (2004).
- [4] W. Seidl, Atmos. Environ, **34**, 4917 (2000).

LIGHT INDUCED POLYMERIZATION OF ORGANIC AEROSOL COMPONENTS

M. Ammann, A. Schlierf, A. Rouviere (PSI), B. D'Anna, A. Jammoul, M. Brigante, C. George (IRCELYON)
P. DeCarlo (PSI/LAC)

We report evidence that the presence of an aromatic ketone as a photosensitizer is inducing oligomerisation of simple dicarboxylic acids in atmospheric aerosol particles.

INTRODUCTION

Ultraviolet or visible light absorbing organic constituents of atmospheric aerosols may act as photosensitizers for a number of processes [1]. Photosensitizers may be primary organics from combustion sources or be formed in situ during oxidation in the atmosphere [2]. The significance of photosensitized processes has been demonstrated by showing enhanced uptake of atmospheric oxidants to organic films or aerosol particles [3]. After our previous year's experiments with UV/VIS spectroscopy in aqueous solutions with different combinations of a photosensitizer with aromatic reductants, we have in a next step checked the reactivity of mixtures of a photosensitizer with dicarboxylic acids, using adipic acid and succinic acid as examples.

EXPERIMENTAL

For the bulk solution UV-VIS experiments, adipic acid or succinic acid and benzophenone were dissolved and irradiated using 6 sunlight lamps (Phillips Effect, 70W, diffuse). Similar solutions were investigated by laser flash photolysis. This technique allows monitoring transient species produced by a pulsed laser beam by means of time resolved absorption spectroscopy. Finally, preliminary experiments were performed with an Aerodyne HR-TOF Aerosol Mass Spectrometer (AMS), for which ammonium sulfate solutions containing in addition benzophenone and adipic or succinic acid as described above were nebulized, and the resulting aerosol passed through a photoreactor with about 5 min. residence time, which was coupled to the AMS and an SMPS.

RESULTS

First, we have looked at changes in the UV/VIS spectra of the bulk solutions as a function of irradiation (Fig. 1), indicating a significant build up of absorption in the range of 350 to 500nm, which could have resulted from polymerization reactions. More detailed information was obtained from the laser flash photolysis experiments in aqueous solutions. These experiments were carried out under pseudo-first order conditions, with the quencher concentration (i.e., the organic acid) in large excess over the initial concentrations of benzophenone used as photosensitizer. The decay of the triplet state of benzophenone was followed at 525nm (Fig. 2). In the presence of an organic acid, the triplet is quenched, and a new species is formed.

In an attempt to observe the initial products of the chemistry monitored in bulk aqueous solutions, we exposed an aerosol consisting of ammonium sulphate, benzophenone and adipic or succinic acid to light in a irradiated aerosol flow reactor. Using the AMS, we

observed changes to the ratio of m/z 44 to 43, with the changes being more pronounced in the case of succinic acid than in the case of adipic acid. Overall, the results are a strong indication that the presence of a photosensitizer leads to light induced oligomerization of simple dicarboxylic acids.

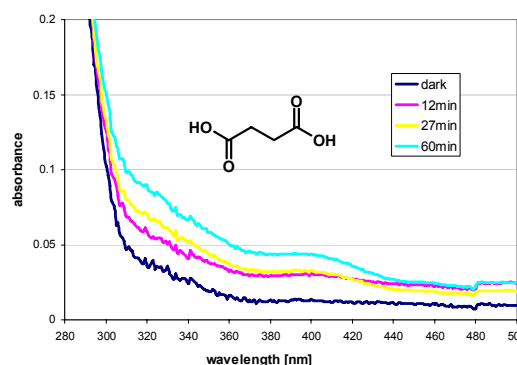


Fig. 1: Changes in UV/VIS spectra of adipic acid / benzophenone solutions following irradiation with 60W Xe lamp.

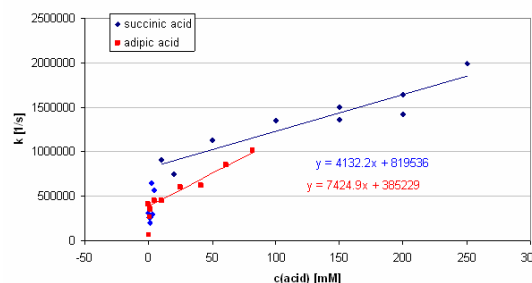


Fig. 2: Benzophenone triplet quenching kinetics in succinic and adipic acid solutions.

ACKNOWLEDGEMENT

This project is supported by the EU FP 6 project EUCAARI (European Integrated project on Aerosol Cloud Climate and Air Quality interactions) No 036833-2. We appreciate the technical support by M. Birrer.

REFERENCES

- [1] Canonica, S. et al., J. Phys. Chem. A, 104, 1226, (2000).
- [2] Gelencser, A. et al., J. Atmos. Chem., 45, 25, (2003).
- [3] George, C. et al., Faraday Discussions, 130, 195, (2005).
- [4] Stemmler, K. et al., Atmos. Chem. Phys., 7, 4237, (2007).

IN SITU STUDIES OF PHASE STATE AND MORPHOLOGY OF AEROSOL PARTICLES USING X-RAY MICROSPECTROSCOPY

V. Zelenay, A. Křepelová, M. Birrer, M. Ammann (PSI), J. Raabe, T. Huthwelker (SLS/PSI),
G. Tzvetkov (SLS/PSI & Univ. Erlangen-Nürnberg)

Transmission X-ray microscopy at the PolLux beamline at the Swiss Light Source (SLS) was used to observe morphological changes in internally mixed aerosol particles (adipic acid/ammonium sulfate) as a function of the relative humidity and to map the spectroscopic changes during water uptake and release.

INTRODUCTION

The phase state and morphology of ambient aerosol particles are important parameters determining the climate effect of atmospheric aerosols. Therefore it is desirable to look at individual particles microscopically and spectroscopically to track their morphological and chemical changes during processing by atmospheric gases e.g. during water uptake. We introduced last year [1] a new method to monitor water uptake in single nanometer sized particles. Using ammonium sulfate, the hygroscopic properties of which are well known, we demonstrated that even small amounts of water taken up by individual aerosol particles can be monitored by Near Edge X-ray Absorption Fine Structure (NEXAFS) spectroscopy. To perform such water uptake/release experiments a small aerosol chamber was developed, the so-called environmental cell, which fits into the Scanning Transmission X-ray Microscope (STXM) at the PolLux beamline at SLS. Here, we report morphological changes as a function of the relative humidity for a mixture of adipic acid and ammonium sulfate.

EXPERIMENTAL

The cell consists of a sample holder and a second part, which comprises the gas flow inlet and outlet. The reliability of the cell was tested last year. For further description the reader is referred to the last annual report [1].

RESULTS

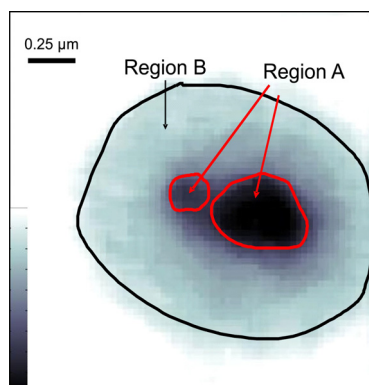


Fig. 1: Carbon distribution in an aerosol particle containing adipic acid and ammonium sulphate measured at 288.5 eV at 89 % relative humidity.

We used carbon absorption maps to image the carbon distribution in the aerosol particles at different relative

humidity, as shown in Fig. 1 for an example at high humidity. This image was obtained as the difference between an image taken at 288.5 eV and one taken at 282 eV representing background absorption. At the carbon edge the ammonium sulfate does not contribute to the absorption, therefore these maps show the distribution of adipic acid. As is evident from Fig 1, the map of these particles shows a large intensity originating from carbon in the middle of the particle. The spectra taken from these regions confirm the idea that adipic acid forms a precipitate in the ammonium sulfate solution (Fig. 2). Our finding is consistent with hygroscopic growth measurements performed with suspended aerosol particles [2]. The latter experiments also suspected a complex, spongelike morphology of adipic acid occurring in these particles. Our results reported here confirm that adipic acid is inhomogeneously distributed within the concentrated ammonium sulfate solution.

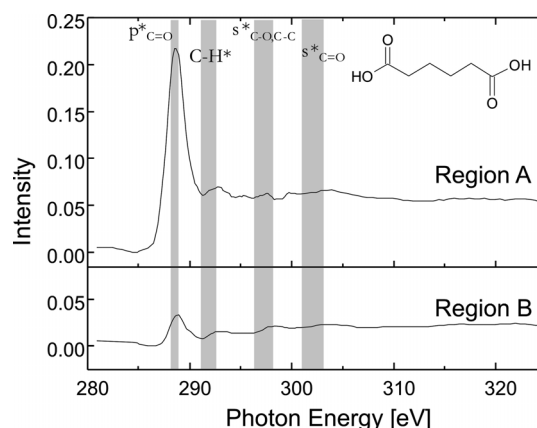


Fig. 2: Carbon NEXAFS spectra of adipic acid at different regions in the aerosol particle (region A and B, indicated in Fig. 1). The two spectra indicate a high concentration of adipic acid in region A and a lower one in region B.

ACKNOWLEDGEMENT

This work is supported by the NEADS project within the Center of Excellence in Energy and Mobility (CEM-CH).

REFERENCES

- [1] V. Zelenay et al., Ann. Rep. Lab. for Radio- & Environ. Chemistry, Uni Bern & PSI (2007).
- [2] Zardini et al., Atmos. Chem. Phys. Discuss., **8**, 5235 (2008).

WATER UPTAKE EXPERIMENTS WITH SOOT PARTICLES USING SYNCHROTRON LIGHT

V. Zelenay, A. Křepelová, M. Birrer, M. Ammann (PSI), J. Raabe, T. Huthwelker (PSI/SLS), G. Tzvetkov (PSI/SLS & Univ. Erlangen-Nürnberg), R. Chirico, T. Tritscher (PSI/LAC), M.G.C. Vernooij (EMPA)

In this work, we monitor water uptake in individual micrometer-sized soot particles from a EURO III diesel passenger car using X-ray microspectroscopy at the transmission microscope at the PolLux beamline at the Swiss light source.

INTRODUCTION

Soot can have an impact on human health by increasing the mortality rate (particle with diameter $< 2.5 \mu\text{m}$), and it plays a crucial role in the radiation balance of the Earth by absorbing short wave radiation. However, depending on their hygroscopic properties, particles containing soot can also act as cloud condensation nuclei. Therefore it is an important issue to understand the relationship between particle chemistry and their capability to interact with major (e.g. water) and trace gases (e.g. oxidants) under atmospheric conditions. In this work, we studied water uptake to soot particles from a diesel passenger car in our environmental cell [1], which allows in situ X-ray microscopy studies of micrometer sized aerosol particles under a controlled gas phase.

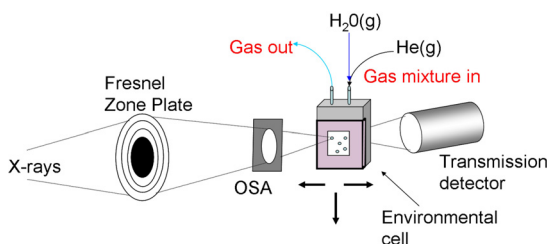


Fig. 1: Schematic view of the environmental cell placed in the Scanning Transmission Microscope, with only key components and the ordering sorting aperture (OSA) shown. The sample holder with the deposited aerosol particles is coloured in pink.

EXPERIMENTAL

The measurements were performed at the Swiss Light Source (SLS) (PolLux beamline) located at the PSI. Due to the excellent resolution of 30 nm of the microscope (Fig. 1) we have the possibility to map functional groups with very high spatial resolution (“microspectroscopy”). The soot particles stemmed from a diesel passenger car and were sampled at the smog chamber at the Paul Scherrer Institut after photo-oxidation during several hours. The aim of the sm chamber experiments was to follow the soot particle properties during simulated atmospheric aging, in which also secondary organic material from photo-oxidation of primary organic diesel exhaust gases condensed onto the particles.

RESULTS

Fig. 2 shows an individual soot particle at three different relative humidities. We obtained a set of images at different

energies and a data set of spectroscopic information about soot interacting with water. The pictures were taken at 541.2 eV, where oxygen associated with both, oxygenated organics in soot and with water absorbs due to a resonant transition. The increasing absorption is a direct and in situ probe of the increasing amount of water adsorbing to the soot particle with increasing humidity.

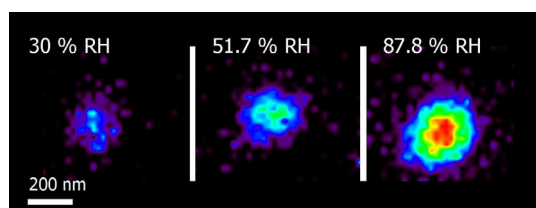


Fig. 2: Single soot particle at different relative humidity

Detailed spectral analysis at the O K-edge allows differentiating strongly bound water to hydrophilic functional groups at low humidity from liquid, potentially capillary water at high humidity.

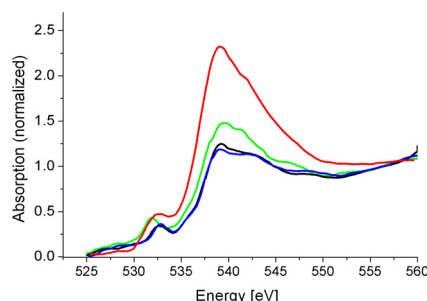


Fig. 3: Oxygen absorption of four different individual soot particles at the oxygen K-edge at different relative humidity (red: 30 %, black 51 %, blue 90 %, green: 30 %, after exposure to 90 % RH).

ACKNOWLEDGEMENT

This work is supported by the NEADS project within the Center of Excellence in Energy and Mobility (CEM-CH).

REFERENCE

- [1] V. Zelenay et al., Ann. Rep. Lab. for Radio- & Environ. Chemistry, Uni Bern & PSI (2007), p. 17.

THE IMPACT OF HNO₃ ON ICE SURFACE MELTING STUDIED BY AMBIENT PRESSURE XPS AND ELECTRON YIELD NEXAFS

A. Křepelová, T. Huthwelker, M. Ammann (PSI), J.T. Newberg, H. Bluhm (LBNL)

X-ray photoelectron spectroscopy (XPS) and electron yield near edge X-ray absorption spectroscopy (NEXAFS) performed at beamline 11.0.2 at the Advanced Light Source (ALS) were used to determine the impact of HNO₃ adsorption on the surface premelting of ice. Here, updated NEXAFS results and XPS probing depth measurements are described.

INTRODUCTION

In this report, we continue our study of the impact of HNO₃ on surface ice premelting [1]. Indications for the existence of surface melting on clean ice surfaces have been reported for temperatures above about -20 °C. It has been suggested that the thickness of the disordered layer increases in the presence of adsorbates.

EXPERIMENTAL

The principle of the ambient pressure photoemission spectrometer is described elsewhere [2]. The incident X-ray beam is admitted to the cell through a silicon nitride window. A 1 mm thick ice film was grown on a Peltier cooled gold substrate from water vapor and then equilibrated at -43.2°C. NO₂ was then added to the chamber to reach partial pressures up to 0.1 Torr. HNO₃ was formed by the hydrolysis of NO₂. The gas phase composition was monitored by a differentially-pumped mass spectrometer. The spectra were recorded at constant temperature.

RESULTS

Fig. 1 compares the Auger electron yield NEXAFS O K-edge spectra of clean ice, of ice with HNO₃ and of a HNO₃ solution. The most visible difference is that with increasing HNO₃ concentration a peak at 532 eV occurs. This is assigned to an O(1s) – π* transition of adsorbed nitrate. The more nitrate is present on the ice surface, the more significant is this peak. The main edge part of the spectrum of ice with adsorbed HNO₃ exhibits features of both, ice and solution (water). The broad band around 543 eV due to 4-fold coordinated water molecules has a different shape in ice and in solution. Observed changes in the magnitude and width of this feature with increased HNO₃ present on the ice resemble those obtained by Bluhm, et al. [3] at high temperatures. Overall, from the comparison of the main and post edge of all three spectra, it is evident that the nitrate on ice spectrum represents an intermediate between the ice spectrum and the concentrated solution spectrum. It can be represented as linear combination of the clean ice spectrum (80%) and that of the nitrate solution (20%). This can indicate that the ice surface consists of clean ice and nitrate ions that are coordinated as in a concentrated solution.

In the next experiment, the O1s and N1s XPS spectra at different photon energies (200-800 eV) were measured to obtain a depth profile of O and N, relying on the fact that the surface sensitivity in XPS arises from the inelastic mean free path (which is kinetic energy dependent) of the ejected photoelectrons. By tuning the incoming X-ray energy, the photoelectron kinetic energy can be varied. To directly compare elemental ratios, the sets of spectra corresponding to a single probing depth were taken on one spot on the

sample. The ratios of peak areas were calculated from the spectra of each element taken at the same kinetic energy to avoid using problematic sensitivity factors. The results, given as diamond points, are depicted in Fig. 2.

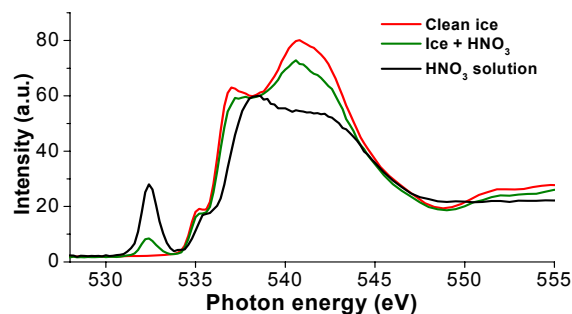


Fig. 1: Oxygen K-edge Auger electron yield NEXAFS spectra of clean ice, ice with HNO₃ and HNO₃ solution.

It is obvious that with increasing kinetic energy the ratio of N/O decreases slightly. This means that the amount of nitrate decreases with depth. Nevertheless, the N/O ratio dependence with probing depth indicates that most of HNO₃ was adsorbed at the surface but that a still significant part penetrates into the bulk of polycrystalline ice, possibly along grain boundaries.

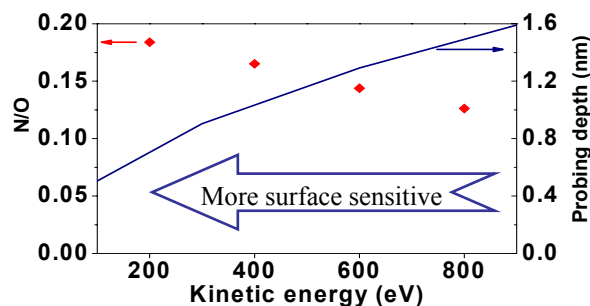


Fig. 2: Depth profiling: N/O (points, left y scale) and electrons probing depth (solid curve, right y scale) as a function of electrons kinetic energy.

ACKNOWLEDGEMENT

This work is part of our contribution to the EU FP6 project SCOUT-O3.

REFERENCES

- [1] A. Křepelová et al., Ann. Rep. Lab. for Radio- & Environ. Chemistry, Uni Bern & PSI (2007), p. 20.
- [2] D.F. Ogletree et al., Rev. Sci. Instrum., **73**, 3872 (2002).
- [3] H. Bluhm et al., J. Phys.: Condens. Matter, **14**, L227 (2002).

THE ADSORPTION OF HCl ON ICE STUDIED BY X-RAY PHOTOELECTRON SPECTROSCOPY

A. Křepelová, T. Huthwelker, M. Ammann (PSI), J.T. Newberg, H. Bluhm (LBNL)

X-ray photoelectron spectroscopy (XPS) and electron yield near edge X-ray absorption spectroscopy (NEXAFS) performed at beamline 11.0.2 at the Advanced Light Source (ALS) were used to determine the impact of HCl adsorption on the surface premelting of ice. First results are reported.

INTRODUCTION

HCl is a key species in stratospheric ozone depletion through its reaction with chlorine nitrate on ice or within liquid particles. In this study we use photoelectron spectroscopy to obtain local information of HCl adsorbed to ice. It has been suggested that impurities such as HCl affect the thickness of its disordered surface layer [1].

EXPERIMENTAL

The principle of the ambient pressure photoemission spectrometer is described elsewhere [2]. The incident X-ray beam was admitted to the ambient pressure cell through a 100 nm thick silicon nitride window. An about 1 mm thick ice film was grown on a Peltier cooled gold substrate from water vapor and then equilibrated at -54°C . HCl was dosed directly as a mixture HCl/N₂. The gas phase composition was monitored by a differentially-pumped mass spectrometer (MS). O 1s and Cl 2p XPS spectra were recorded at constant temperature. Additionally, O K-edge NEXAFS spectra were measured.

RESULTS

Fig. 1 shows O1s and Cl 2p XPS spectra obtained at -54°C . The incident photon energies were 350 eV for the Cl and 680 eV for the O spectrum, *i.e.*, at photoelectron kinetic energies of 150 eV. The Cl 2p spectrum is consistent with literature [3]. The typical 2p spin-orbit splitting is observable; the peak maxima were identified at binding energies of 203.5 and 202 eV for 2p_{1/2} and 2p_{3/2}, respectively. The low signal to noise ratio is due to the low pressures of HCl, which could not be directly measured by MS, but were estimated to be below 10^{-7} mbar. The Cl to O ratio was calculated to be at maximum 1 %.

Auger electron yield O K-edge NEXAFS spectra were measured using a kinetic energy window of 440-460 eV. Fig. 2 shows the comparison of NEXAFS spectra of clean ice and ice with HNO₃ and HCl. In contrast to measurements with HNO₃, no changes in O K-edge NEXAFS of ice were observed in presence of HCl. This may be due to the lower coverage and pressure in the HCl measurements compared to those with HNO₃. Further measurements at higher HCl concentrations are therefore required for a better comparison with the HNO₃ case. The results show that the ice surface is not changing its structure at very low HCl coverages.

ACKNOWLEDGEMENT

This work is part of our contribution to the EU FP6 project SCOUT-O3.

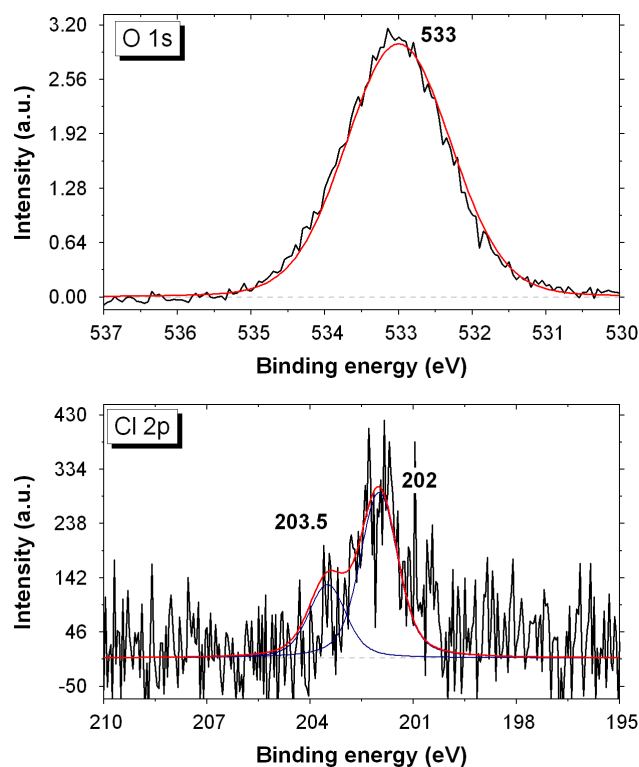


Fig. 1: Typical photoelectron spectra of O 1s (top) and Cl 2p (bottom) regions as a function of binding energy.

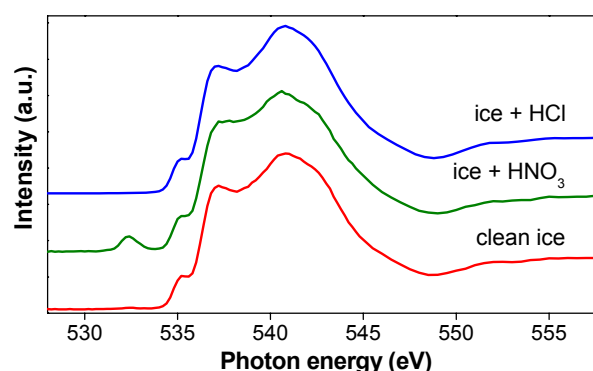


Fig. 2: Oxygen K-edge NEXAFS spectra of clean ice and ice in the presence of HNO₃ and HCl.

REFERENCES

- [1] X. Wei et al., Phys. Rev. Letters., **86**, 1554 (2001).
- [2] D.F. Ogletree et al., Rev. Sci. Instrum., **73**, 3872 (2002).
- [3] B. Winter et al., J. Am. Chem. Soc., **130**, 7130 (2008).

CAN LANGMUIR DESCRIBE PHOTO-ENHANCED CONVERSIONS IN ICE?

T. Bartels-Rausch, M. Ammann (PSI), J. Kleffmann, Y. Elshorbany (Univ. Wuppertal),
M. Brigante, B. D'Anna, C. George (IRCELYON)

A kinetic model framework, commonly used in surface chemistry research, is applied to analyze experiments on the light-driven reduction of nitrogen dioxide on ice films doped with humic acids. It turns out that this heterogeneous model can describe the results as good as previously used photo-chemical model.

INTRODUCTION

The photochemistry of humic substances is currently of great interest to the atmospheric research community. It is now well known that absorption of light by this class of compounds present on atmospheric surfaces leads to reduction of atmospheric trace gases such as NO_2 [1]. This is of importance as the product of this reaction, HONO, impacts the oxidative capacity of the atmosphere, *i.e.* the air quality. Recently, we have shown that this reaction also takes place, when the humic acid is diluted in an ice film [2]. Here, we compare the analysis of these data based on two different model frameworks.

ANALYSIS

Fig. 1 shows the production rate of HONO from VIS - irradiated ice films at different concentrations of nitrogen dioxide. The ice films had been doped with $30 \mu\text{g}$ humic acid.

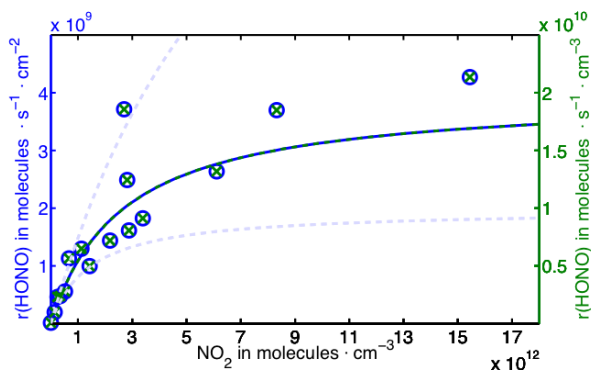


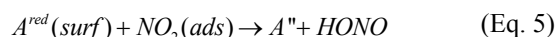
Fig. 1: HONO production rate versus the NO_2 concentration. The production rate is referred to the surface area (blue circles, left axis) and to the gas phase volume (green crosses, right axis) of the flow tube. The blue solid and green dashed lines are results of fits to the data using different model frameworks. The dashed light blue line denotes the 95 % confidence interval of both fits.

In previous studies the observed saturation behaviour was described by a photo-chemical model where in a first step humic acid is excited by VIS radiation (Eq. 1). This might, in a consequent step, lead to an electron transfer to an electron acceptor, NO_2 in this case (Eq. 2). The observed saturation of the HONO production rate at high NO_2 concentrations is explained by a deactivation reaction of photo-activated humic acid (Eq. 3).



Fig. 1 shows that this model framework can describe the data quite well (green dashed line, green crosses, right axis). The fit was derived based on a linear regression of $1/r(\text{HONO})$ versus $1/[\text{NO}_2]$ giving the pseudo first-order rate coefficient for low NO_2 concentration (k_{eff}) and a maximum production rate at high NO_2 concentrations (k_{max}).

Fig. 1 also illustrates that a similar analysis of the data using a heterogeneous kinetic model framework, the Langmuir-Hinshelwood approach, leads to indistinguishable results (blue solid line, blue circles, left axis). The key difference to the previous model is that within the Langmuir-Hinshelwood framework, the saturation derives from a rate-limiting adsorption step of NO_2 from the gas phase to a finite number of adsorption sites on the surface (Eq. 4). Only after adsorption the NO_2 reacts with photo-excited humic acid in a surface reaction step (Eq. 5).



Also, the dependency of the HONO production rate as well as of the two rate constants on the amount of humic acid can be well described by either models. For example, at the low humic acid content of $30 \mu\text{g}$ in the ice film the analysis presented here gives values for k_{eff} of $0.008 \pm 0.001 \text{ s}^{-1}$ for the photo-chemical model and $0.002 \pm 0.0001 \text{ s}^{-1} \text{ cm s}^{-1}$ for the Langmuir Model. Previous studies on 1 mg of pure humic acid films gave a k_{eff} of $0.6 \pm 0.09 \text{ s}^{-1}$ [1]. Normalizing this rate to the available surface area and extrapolating linearly to a humic acid amount of $30 \mu\text{g}$, gives $0.003 \pm 0.001 \text{ cm s}^{-1}$, corresponding to $0.015 \pm 0.005 \text{ s}^{-1}$, in agreement with the finding of this study.

Analysis of the HONO production rate in dependency of the NO_2 concentration and of the rate constants derived in experiments with two different amounts of humic acids reveals that the Langmuir model is as well suited to describe the data as the photo-chemical model.

ACKNOWLEDGEMENT

This work was supported by the European Science Foundation (INTROP) and EU FP6 ACCENT.

REFERENCES

- [1] C. Stemmler et al., Nature, **440**, 195 (2006).
- [2] T. Bartels-Rausch et al., Ann. Rep. Lab. for Radio- & Environ. Chemistry, Uni Bern & PSI (2007).
- [3] Pöschl et al., Atmos Chem Phys, **7**, 5989 (2007), p. 22.

HUMIC SUBSTANCES IN ICE: PHOTOLYTICAL MERCURY RELEASE

A. Bernhard (Univ. Bern), T. Bartels-Rausch, M. Schläppi, M. Schwikowski, M. Ammann (PSI)

The goal of this project is to investigate the influence of humic substances on the light-driven release of mercury from ice and snow. For this a method was optimized and implemented in our laboratory.

INTRODUCTION

The fate of the toxic mercury in the environment strongly depends on its oxidation state: elemental mercury is mainly found in the gas phase, where it can be transported over long distances. Ionic mercury species, such as divalent mercury, on the other hand, have a high affinity to aqueous phases from where they can enter the food web [1].

This study aims to investigate the light-driven reduction of divalent mercury observed in surface snow with focus on the influence of humic substances. It is well known that humic substances significantly enhance the yield of reduction of divalent mercury in liquid water [2] and of other atmospheric traces in surface snow [3].

The importance of such a conversion to elemental mercury lies in the subsequent removal of mercury from the snow to the atmosphere. This transfer might thus reduce the amount of mercury captured in the snow that will enter the aquatic system and the food web during snowmelt. Also, better knowledge of this loss process is important for paleoclimate research, e.g. for interpreting mercury profiles in ice cores.

METHOD DEVELOPMENT

For this study an analytical method was developed. The set-up basically consists of an ice coated flow tube and of a wash bottle filled with absorbing solution (Fig. 1). The flow tube can be irradiated by light in the UV- or VIS- range and the ice film can be doped with known amounts of divalent mercury and humic substances. Any mercury released to the gas phase during irradiation is transported with a carrier gas to a KMnO_4 absorbing solution and its amount is determined offline with atomic fluorescence spectrometry.

The characteristics of this method are (i) a quantitative absorption of elemental mercury from the gas phase in 80 ml 320 ppm KMnO_4 solution and with a carrier gas flow of 500 ml/min; (ii) a detection limit of $4.0 \times 10^6 \text{ atoms} \times \text{s}^{-1} \times \text{cm}^{-2}$; and (iii) a high reproducibility. The standard deviation of 3 experiments with similar settings was 5 %.

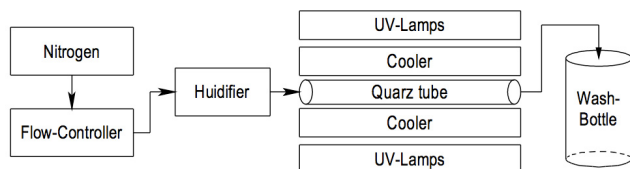


Fig. 1: Experimental Set-up.

FIRST RESULTS

Figure 2 shows the measured emission from ice films that contained 300 ppb divalent mercury. In the absence of irradiation, the mercury flux was well below the detection limit. Irradiation in the 300–420 nm spectral region induced

the release of 40 mercury atoms per second and per cm^2 . This observation is in qualitative agreement with previous studies that investigated the release of mercury from snow induced by UV-radiation [1]. The presence of humic substances in the ice film significantly enhanced the light-induced release of mercury by a factor of 4. This release of mercury corresponds to a loss of roughly 30 % of the divalent mercury in the ice film.

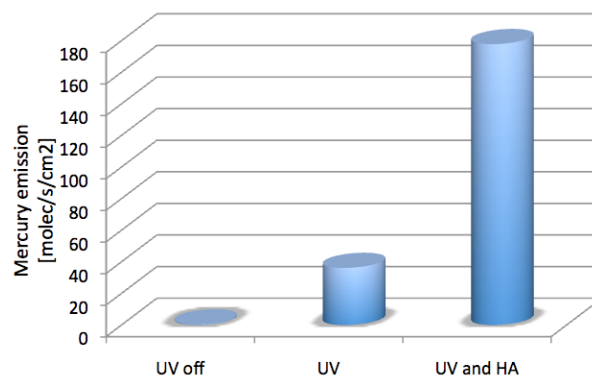


Fig. 2: Measured flux of Mercury from three ice films doped with 300 ppb $\text{Hg}(\text{NO}_3)_2$. The ice of the third sample (UV and HA) also contained 2 ppm humic substances.

This example shows that the method is well suited to study the photolysis reactions of divalent mercury in the presence of humic substances.

An open question that can be tackled with this approach is the mechanism by which the presence of humic substances enhances the photolytic release of mercury. In the literature focusing on the aqueous phase both, the direct photolysis of complexes between mercury and humic substances, and the secondary reaction of mercury with photolyzed humic substances or via additional intermediates are discussed. Also, the effect of the counter ion of the divalent mercury is not yet known. First experiments indicate that photolysis in the absence of humic substances is significantly enhanced if HgO solutions are used instead of the $\text{Hg}(\text{NO}_3)_2$ solutions (Fig. 2).

REFERENCES

- [1] Steffen et al., *Atmos. Chem. Phys.*, **8**, 1445 (2008).
- [2] Ravichandran, *Chemosphere*, **55**, 319 (2004).
- [3] T. Bartels-Rausch et al., *Ann. Rep. Lab. for Radio- & Environ. Chemistry, Uni Bern & PSI* (2007), p. 22.

THE SNOW DIFFUSION CHAMBER

M. Kerbrat, M. Birrer, M. Ammann (PSI), T. Huthwelker (PSI/SLS), H.W. Gäggeler (Univ. Bern & PSI), M. Schneebeli, B. Pinzer (SLF)

The experimental setup presented here was developed to investigate the diffusivity of trace gases in snow under low wind-pumping conditions.

INTRODUCTION

Up to now interactions of traces gases with ice or snow have been investigated mainly in flow tube or Knudsen reactors to address adsorption to ice. However, adsorption is not the only process taking place [1]. The newly developed set up presented here is meant to mimic low wind air/snow interactions with or without temperature. In experiments using this set-up, processes such as adsorption, bulk diffusion and gas phase diffusion in the interstitial air of snow are considered.

CHARACTERISTICS AND EXPERIMENTS

The key entity of the the set up is the sample holder. It is made of two cylindric aluminium cans having diameters of 65.4 and 53.0 mm. These are assembled concentrically, whereby open porous Porextherm WDS Ultra foam is filled into the annular space in between. Aluminium was chosen, because it does not significantly absorb hard X-Rays. Hence, the sample holder could be used in a μ CT (micro Computed Tomograph) to measure the microstructure of the snow sample used. For the diffusion experiments, a Teflon gas inlet can be mounted on the top of the aluminium cylinder, whereas the bottom is closed by an aluminium bloc coupled to a Peltier element. Two pictures of the sample holder are shown in Fig. 1.

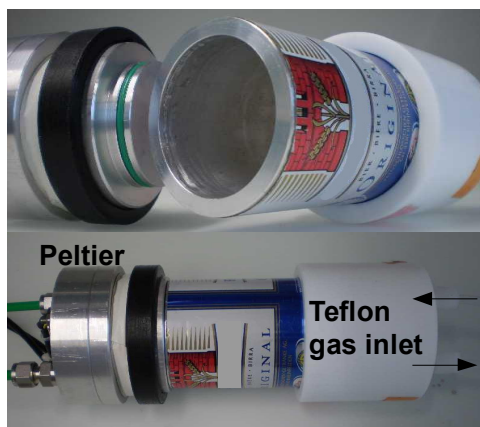


Fig. 1: The sample holder with its Teflon gas inlet and heater/cooler Peltier element.

The Peltier element can be used to apply a temperature gradient on the snow sample similar to the one found in alpine snowpacks i.e. typically on the order of 100 K m^{-1} . As shown in Fig. 2, during an experiment, the sample holder assembly is introduced into a cooling jacket whose temperature can be regulated down to -50°C .

A snow diffusion experiment starts by monitoring the gas phase concentration of the investigated compound without being exposed to the snow sample. The sample can

subsequently be opened and a drop in the gas phase concentration of the investigated compound can be observed. This drop, which is first due to convection and later due to diffusion, can be analyzed to retrieve the effective diffusivity.

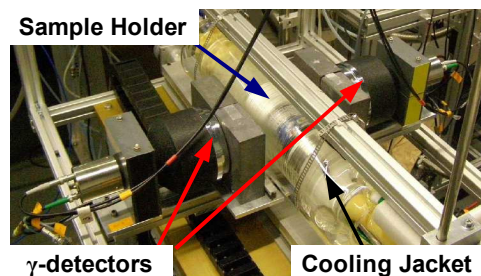


Fig. 2: The sample in its cooling jacket and the γ -detectors.

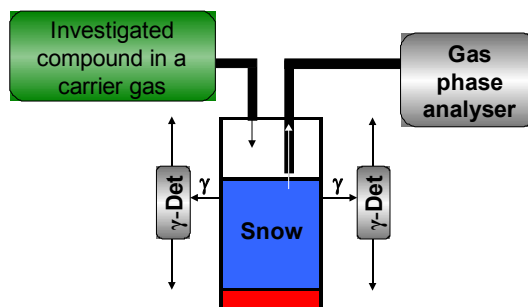


Fig. 3: Schematic representation of the snow diffusion chamber.

Another way of investigation can be made through the use of molecules synthesised from radioactive isotopes. In the case of positron emitters such as ^{13}N or ^{11}C , the migration of the labelled molecules can be followed in the sample by a coincident γ -counter composed of two γ -detectors moving along the sample (see figure 2 and 3).

ACKNOWLEDGEMENT

This project is supported by the Swiss National Science Foundation. This work is also part of our contribution to the EU FP6 project SCOUT-O3. We appreciate the stable beams from the PSI accelerator facilities and the service by IP-2.

REFERENCE

- [1] Grannas, A. M. et al., *Atmos. Chem. Phys.* **7**, 4329 (2007).

LABORATORY STUDY OF THE DIFFUSIVITY OF HONO IN SNOW

M. Kerbrat, M. Ammann (PSI), T. Huthwelker (PSI/SLS), H.W. Gäggeler (Univ. Bern & PSI),
B. Pinzer, M. Schneebeli (SLF)

The diffusion of HONO through a snow sample is investigated using a unique combination of techniques, namely, X-ray micro-tomography and nitrogen oxides labeled with the short-lived radioactive tracer ^{13}N in a snow diffusion chamber.

INTRODUCTION

The diffusivity D_g of a gas is the rate of transfer of the gas in a given matrix. When processes in addition to gas phase diffusion, D_g is referred to as the effective diffusivity and is denoted as $D_{g,\text{eff}}$. Diffusivity is one of the quantities needed to model mixing and exchange of gases between the interstitial air of snow and the atmosphere [1]. Nitrous acid (HONO) is a particularly important species in this context.

EXPERIMENTAL

We have used a snow diffusion chamber described overleaf [2] for the case of HO^{13}NO . An example of the steady-state distribution of HO^{13}NO along the snow is shown in Fig. 1.

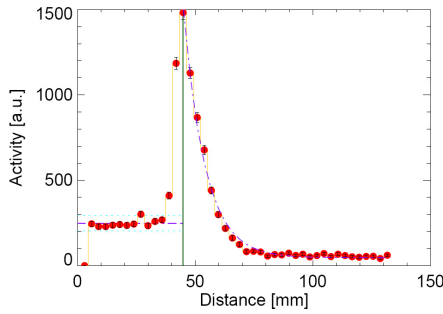


Fig. 1: Activity in the sample holder as measured by the coincident γ -counter. The solid line at 45 mm represents the interface gas/snow. The blue short-long dashed curve represents the fit of the diffusion profile using equation (1).

The micro structure of the artificially produced snow used in the experiment was measured and visualized by μCT and is identical to natural snow (Fig. 2).

RESULTS

The use of the short lived isotope ^{13}N ($t_{1/2} = 9.96$ min) allows measuring the speed of migration, v_{HONO} [m s^{-1}], of a species through a medium. This is achieved by using equation (1),

$$C_{\text{HONO}}(x) = C_{0,\text{HONO}} \exp\left(\frac{-\lambda}{v_{\text{HONO}}} x\right) \quad (1)$$

where x [m] is the depth in the sample, $C_{\text{HONO}}(x)$ [molecules m^{-3}] is the concentration of HO^{13}NO at the position x , and λ [s^{-1}] is the rate of decay of ^{13}N .

By combining the Fick's first Law of diffusion with eq. (1), one finds,

$$D_{g,\text{eff}} = \frac{(v_{\text{HONO}})^2}{\lambda}. \quad (2)$$

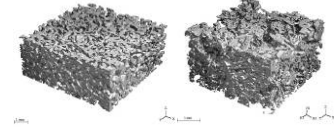


Fig. 2: Reconstructed X-Ray images of the old (left) and fresh (right) snow samples used.

As it can be seen in Fig. 3, $D_{g,\text{eff}}$ does not feature a significant temperature dependence and is equal to $\sim 7 \times 10^{-8} \text{ m}^2 \text{ s}^{-1}$ for the two samples. This is somehow surprising as HONO interacts strongly with ice surfaces [3] and $D_{g,\text{eff}}$ should therefore decrease with the temperature. The independence of $D_{g,\text{eff}}$ with temperature suggest that other mechanisms than adsorption only are involved in the diffusivity of HONO in snow. For comparison, the effective diffusivity of NO, considered an inert tracer, in the same snow samples, was $\sim 10^{-5} \text{ m}^2 \text{ s}^{-1}$.

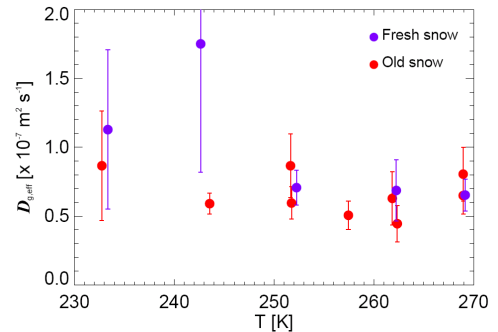


Fig. 3: Temperature dependence of the effective diffusivity $D_{g,\text{eff}}$ of HO^{13}NO , in fresh and old snow.

ACKNOWLEDGEMENT

This project is supported by the Swiss National Science Foundation. We appreciate the stable beams from the PSI accelerator facilities and the service by IP-2.

REFERENCES

- [1] F. Dominé et al., Atmos. Chem. Phys., **8**, 171, (2008).
- [2] M. Kerbrat et al., Ann. Rep. Lab. for Radio- & Environ. Chemistry, Uni Bern & PSI (2008), p. 19.
- [3] T. Huthwelker et al., Ann. Rep. Lab. for Radio- & Environ. Chemistry, Uni Bern & PSI (2005), p. 12.

TEMPERATURE RESPONSE IN THE ALTAI REGION LAGS SOLAR FORCING

A. Eichler, A. Laube, K. Henderson, M. Schwikowski (PSI), S. Olivier, H.W. Gaggeler (Univ. Bern & PSI), J. Beer (EAWAG), T. Papina (IWEF)

Solar forcing was found to be a main driver for temperature variations in the Altai region during the preindustrial time period 1250-1850. A mean lag of 20 years between the solar forcing and the temperature response underlines the importance of indirect sun-climate mechanisms involving ocean-induced changes in atmospheric circulation. Solar contribution to temperature change became less important during the industrial period 1850-2000.

The direct radiative forcing due to increases in total solar irradiance since 1750 is estimated to be only $+0.12$ (-0.06 , $+0.18$) W/m^2 [1]. Nevertheless, a number of climate records show a significant response to variations in solar activity [2-4], providing evidence for a solar forcing effect in spite of the fact that the underlying physical processes are still not yet understood. In this study we report on a 10-30 years lag between solar forcing and the temperature response in the Altai, pointing to an indirect sun-climate mechanism in this region.

We directly compared a temperature record from a Siberian Altai ice core (period 1250-2001, [5]) with a reconstruction of the total solar modulation derived from ^{10}Be measurements in polar ice cores and ^{14}C records from tree rings [6]. Our temperature record is significantly correlated with the solar activity proxies in the period 1250-1850 (Fig. 1a), suggesting that the sun was a main driving force for the temperature variation during the preindustrial period. This is corroborated by a spectral analysis of the temperature reconstruction showing significant periods at 205, 86, and 10.8 years [5], which can be related to the solar Suess, Gleissberg, and Schwabe cycles, respectively.

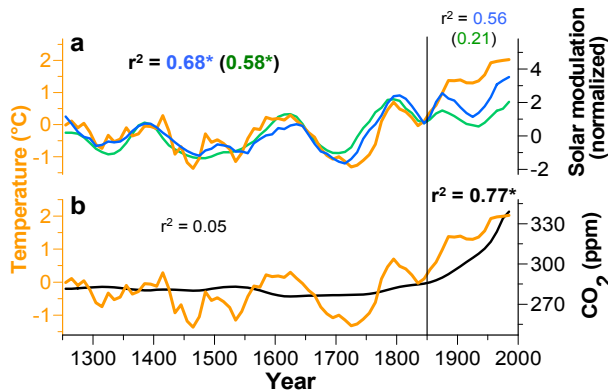


Fig. 1: Correlation between Altai temperature (orange) and ^{10}Be (blue), ^{14}C (green) based solar modulation (SM, a) and CO_2 concentration (black) (b). The SM curves were shifted by 20 years. Significant r^2 ($p < 0.05$) are marked (*, bold).

The highest correlation between our data and the solar activity reconstructions was obtained by introducing a lag of 20 years. However, this lag is not constant, but varies between 10 and 30 years (Fig. 2). The observed lag is indicative of a variable response time between the initial solar signal and the regional temperature and thus, an indirect effect of solar variability on the temperature evolution at our study site. Potential justifications for decadal lags are changes in ocean and atmospheric circulations triggered by solar activity changes. Perry [7] proposed that increasing solar radiation leads to a warming of the tropical and subtropical oceans. This temperature anomaly is transported within the ocean conveyor belt to the particular ocean area that affects regional climate with

varying lag times due to the heat capacity of the ocean and varying fluctuations in the velocity of the ocean currents. Furthermore, temperature gradients in the ocean influence the atmospheric pressure pattern. Indeed, models calculate that the lower Northern Hemispheric temperatures in the period 1650-1850 are due to a decreased solar activity in this time forcing a shift towards a low index state of the NAO/Arctic Oscillation (AO) with a lag of 20 years [8]. Temperatures in Central Siberia are influenced by the NAO [9,10]. This is corroborated by the spectral analysis of the reconstructed temperatures revealing significantly NAO specific periodicities at 8.3 and 2.3 years [5]. Thus, the above mentioned mechanism is one possible solar-temperature coupling for this region.

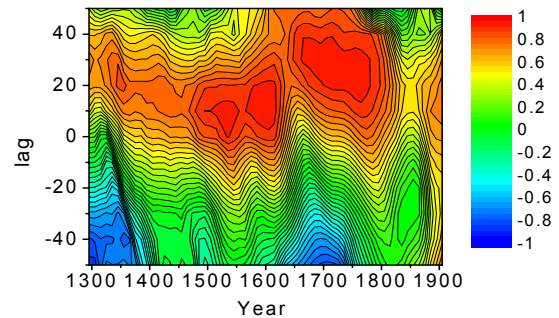


Fig. 2: Cross correlation (r) between Altai temperature reconstruction and ^{10}Be based solar activity.

Our reconstructed temperatures are significantly correlated with the ^{10}Be and ^{14}C based solar activity reconstructions in the period 1250-1850, but not with the greenhouse gas CO_2 (Fig. 1). This indicates that solar activity changes are a main driver for the temperature variation in the Altai region during the pre-industrial time. However, during the industrial period (1850-2000) solar forcing became less important and only the CO_2 concentrations show a significant correlation with the temperature record.

REFERENCES

- [1] P. Forster et al., IPCC report (2007).
- [2] G.J.M. Versteegh, *Space Sci. Rev.*, **120**, 243 (2005).
- [3] A. Mangini et al., *E. Plan. Sci. Lett.* **235**, 741 (2005).
- [4] N. Scafetta and B.J. West, *J. Geophys. Res.*, **112**, doi: 10.1029/2007JD008437 (2007).
- [5] A. Eichler et al., *Geophys. Res. Lett.* (2009), in press.
- [6] R. Muscheler et al., *Quart. Sci. Rev.*, **26**, 82 (2007).
- [7] C.A. Perry, *Adv. Space Res.*, **40**, 353 (2007).
- [8] D.T. Shindell et al., *Science*, **294**, 2149 (2001).
- [9] J. Marshall et al., *Int. J. Climatology*, **21**, 1863 (2001).
- [10] M. Ogi et al., *Geophys. Res. Lett.*, **30**, 1704, doi: 10.1029/2003GL017280 (2003).

ACKNOWLEDGEMENT

This work was supported by the SNF, Marie Heim-Vögtlin program, Grant no. PMPD2-110174.

HISTORY OF BIOGENIC EMISSIONS FROM A SIBERIAN ALTAI ICE CORE

A. Eichler, S. Brütisch, M. Schwikowski (PSI), S. Olivier (Univ. Bern & PSI), T. Papina (IWEF)

NH_4^+ and $HCOO^-$ concentration records from a Siberian Altai ice core are found to represent a history of temperature driven direct biogenic emissions from Siberian forests in the period 1250-1940. Strongly increased NH_4^+ concentrations as well as decreased $HCOO^-$ concentrations during the last 60 years are due to anthropogenic NH_3 emissions and the enhanced acidity in the atmosphere, respectively.

While comprehensive emission inventories for NH_3 and other air pollutants have been established for the last about 100 years, uncertainties about preindustrial times are particularly large [1]. In this work 750 years ice core NH_4^+ and $HCOO^-$ concentration records from Belukha glacier in the Siberian Altai are shown to reflect the history of direct biogenic emissions from Siberian forests and an impact of anthropogenic emissions in the last 60 years.

Correlation analysis and Principal Component Analyses (PCA) was performed to obtain the main sources of the trace species in the preindustrial time in Siberia 1250-1940 (see e.g. Table 1). We retained three PCs, explaining 83% of the data variance. PC1 with the highest loadings of Ca^{2+} , Mg^{2+} , Na^+ , Cl^- , and SO_4^{2-} explains 60% of the variance. These ions are typically dust-related [2]. The characteristics of PC3, explaining 10% of the data variance, is high loadings of K^+ and NO_3^- pointing to forest fires as main sources (see e.g. [3]). High loadings of NH_4^+ , $HCOO^-$, and $\delta^{18}O$ are observed in PC2, which explains 13% of the total variance. $\delta^{18}O$ was shown to be a good proxy of atmospheric temperature [4]. This result indicates that the main source of NH_4^+ and $HCOO^-$ is direct biogenic emissions from Siberian forests, but not forest fires as proposed by other studies [2]. Direct vegetation emissions of NH_3 are strongly temperature dependent (see e.g. [5]).

Tab. 1: Loadings of the PCA of 9 major ions and $\delta^{18}O$ (period 1250-1940) and the explained variance. Species exhibiting the highest loadings in the three PCs are marked.

	PC1	PC2	PC3
Ca^{2+}	0.89	-0.03	-0.30
Mg^{2+}	0.92	-0.18	-0.16
Na^+	0.82	-0.19	-0.41
Cl^-	0.85	-0.28	-0.06
SO_4^{2-}	0.84	-0.03	-0.19
NH_4^+	0.72	0.55	0.17
$HCOO^-$	0.73	0.48	-0.28
$\delta^{18}O$	0.31	0.78	0.16
K^+	0.71	-0.25	0.53
NO_3^-	0.79	0.01	0.46
variance (%)	60	13	10
	dust	direct biogenic emissions	forest fires

The Belukha $\delta^{18}O$ record is presented in Figure 1. We derived a strong correlation between the temperature proxy $\delta^{18}O$ and solar activity during the period 1250-1850 suggesting solar forcing as a main driver for preindustrial temperature change in the Altai region [4]. The records of PC2 and species with high loadings in PC2 (NH_4^+ and $HCOO^-$) show similar pattern compared to the temperature proxy in the period 1250-1940. They reveal low values during periods of low solar activity and an increasing trend since the Maunder minimum. This very interesting result points to solar-induced temperature changes as a main driver for preindustrial direct biogenic emissions from the vast forested areas in Siberia.

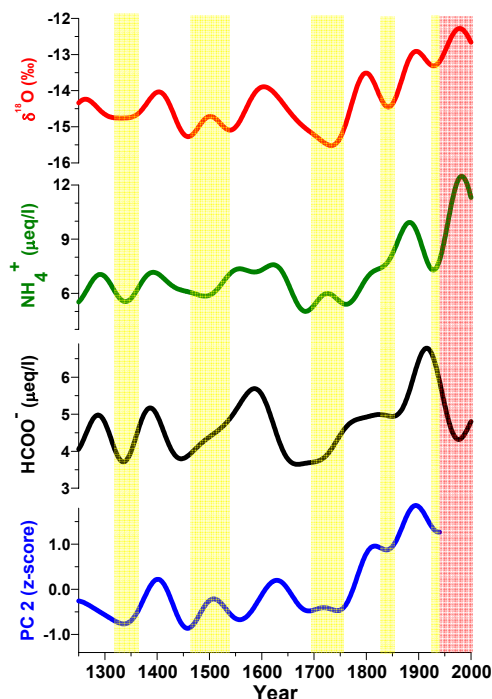


Fig. 1: Records of $\delta^{18}O$, NH_4^+ , $HCOO^-$, and PC2. Solar activity minima are marked in yellow (Wolf, Spörer, Maunder, Dalton, Gleissberg minima). The industrial period in Siberia 1940-2000 is marked in red. Data shown are smoothed with an 80-years lowpass filter.

The industrial period in Siberia (1940-2000) shows a stronger rise of the NH_4^+ concentrations than one would expect from the temperature increase. This is due to enhanced anthropogenic NH_3 emissions mainly from agriculture and a stronger acidification of the atmosphere caused by increased SO_4^{2-} and NO_3^- levels [2]. The latter is also responsible for the strong decrease of $HCOO^-$ concentrations at the same time. A stronger acidification of the atmosphere and precipitation leads to a less efficient scavenging of the weak acid $HCOOH$. Thus, anthropogenic emissions were responsible for the development of NH_4^+ and $HCOO^-$ concentrations in precipitation in the industrial era.

REFERENCES

- [1] M.A. Sutton et al., Environ. Poll., **156**, 583 (2008).
- [2] S. Olivier et al., J. Geophys. Res. **111**, D05309, doi: 10.1029/2005JD005830 (2006).
- [3] C.H. Song et al., J. Atmos. Chem., **51**, 43 (2005).
- [4] A. Eichler et al., Geophys. Res. Lett., doi:10.1029/2008GL035930 (2009), in press.
- [5] F.J. Dentener et al., J. Atmos. Chem., **19**, 331 (1994).

ACKNOWLEDGEMENT

This work was supported by the SNF, Marie Heim-Vögtlin program, Grant no. PMPD2-110174.

PAST CLIMATE VARIABILITY IN THE ALTAI

M. Schwikowski, A. Eichler (PSI), I. Kalugin (IGM SB RAS), D. Ovchinnikov (IF SB RAS), T. Papina (IWEF)

A Russian-Swiss workshop was held in Barnaul, Russia, in order to get together scientists working with the different kinds of natural climate archives in Siberia such as ice cores, lake sediments, peat bogs, and tree rings.

The Altai mountain range in Central Asia has a Northwest to Southeast extension of about 2100 km and is located on the boundary between Russia, Kazakhstan, China, and Mongolia. It forms a climate divide between vast Siberian forests in the North and arid regions of Central Asia in the South. The considerable remoteness from the oceans causes an extremely continental climate with cold winters and warm summers. This region of central Asia is characterized by the highest degree of continentality in the world. In winter, due to the prevailing stable Siberian High, cold and dry arctic air masses are predominant. In summer, humid air masses from the Atlantic Ocean as well as recycled moisture are the main sources of precipitation. The Altai mountain range has a great potential for a high-resolution, well-dated multiproxy reconstruction of past climate, since high-elevation glaciers, lakes with laminated sediments, and living trees as well as relict wood material can be found in close vicinity. Long meteorological records from Barnaul (1840-present) and glacier mass balance data from Malii Aktru (1961 to present) are available. These facts together with the geographical setting make the Altai particularly attractive in the context of climate change research.

In order to discuss the actual status as well as prospects and limitations in obtaining high-resolution millennial scale paleo records from natural archives in the Altai, a Russian-Swiss workshop was conducted at the Institute for Water and Environmental Problems, Siberian Branch of the Russian Academy of Sciences, in Barnaul, Russia.

One outcome of the workshop is a compilation of three annually resolved, millennial scale temperature records from Belukha ice core, Teletskoye Lake sediments, and tree-ring width chronologies for *Larix Sibirica* from the south-eastern part of the Altai (Fig. 1). Although the common proxy is temperature, different seasons are represented by the three archives (ice core: March-November, lake sediment: annual, tree ring width: June-July). This might explain to a certain extent why individual differences of the reconstructions exist. Nevertheless, a general feature of the three reconstructions is the pronounced long-term variation, along with a strong temperature increase of 2-3°C from the Little Ice Age minimum to the present. This is consistent with instrumental data and model simulations suggesting that warming is strongest at highly continental sites. Furthermore, it is in agreement with reconstructions of the recent mass-balance history of the Sofiyskiy glacier [1]. As indicated in Fig. 1 there is a strong correlation between ice core based temperature reconstruction and solar activity, suggesting solar forcing as an important driving force for temperature variations during the last 750 years in this region.

At the workshop there was a general consensus about the high potential of the Altai region for multiproxy climate reconstructions. Suggestions for future work include

extending the existing records further back in time, combining results from different proxies, and incorporating reconstructions from other archives like archeological data (e.g. from Plateau Ukok), documentary data, phonological data from Katun National Park as well as geomorphologic studies for reconstructing glacier history.

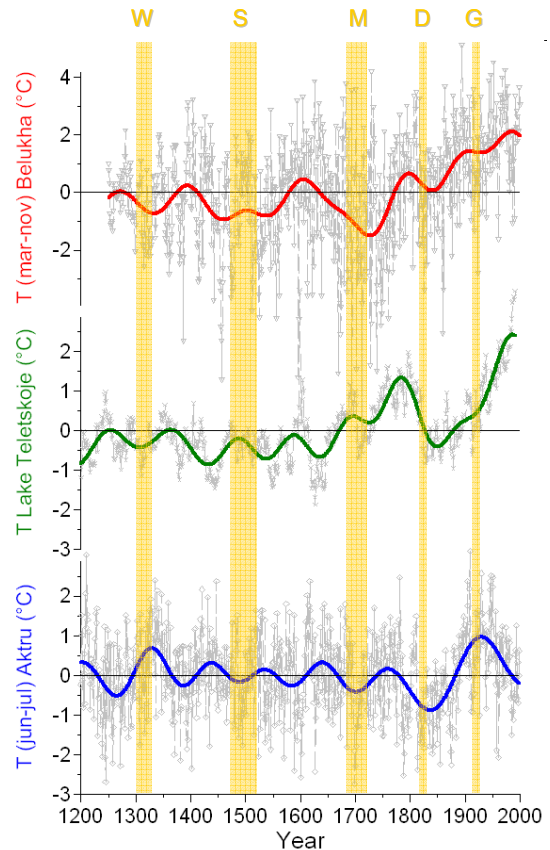


Fig. 1: Annual values and 100-year lowpass filtered temperature anomalies from the Belukha ice core $\delta^{18}\text{O}$ record (Mar-Nov T, [2]), the Lake Teletskoye sediment geochemistry (annual T, [3]), and the tree-ring width chronology for *Larix sibirica* Ldb at upper timberline in the south-eastern part of the Altai (Jun-Jul T, [4]). Periods of low solar activity are indicated by yellow bars (Wolf, Spörer, Maunder, Dalton, and Gleissberg minima).

REFERENCES

- [1] De Smedt, B. & F. Pattyn, *Ann. Glac.*, **37**, 143 (2003).
- [2] A. Eichler et al., *Geophys. Res. Lett.*, doi:10.1029/2008GL035930 (2009), in press.
- [3] I. Kalugin et al., *Quat. Res.*, **67**, 400 (2007).
- [4] D. Ovchinnikov et al., *Geolines*, **11**, 121 (2000).

ACKNOWLEDGEMENT

This meeting of 12 delegates from Russia and 8 from Switzerland was funded by the Russian Foundation for Basic Research and the Swiss National Science Foundation.

DETERMINATION OF CARBONACEOUS PARTICLE CONCENTRATIONS IN A TIBETAN PLATEAU ICE CORE

S. Kaspari, M. Schwikowski, M. Gysel (PSI), S. Kang (ITP, China), P. Mayewski, B. Grigholm (Univ. Maine)

Carbonaceous particles (CP) in the atmosphere can significantly contribute to climate change, however there are few historical measurements of CP. We use two methods to analyze a Tibetan Plateau ice core for CP.

Carbonaceous particles (CP) produced by the incomplete combustion of biomass, coal and diesel fuels can significantly contribute to climate change by altering the Earth's radiative balance. CP consist of organic carbon (OC), elemental carbon (EC; thermally defined), and black (BC) or light absorbing carbon (LAC; BC and LAC are optically defined). In the atmosphere, CP absorb and scatter light and can act as cloud condensation nuclei. BC deposited on snow and ice can significantly reduce the surface albedo, resulting in rapid melting of snow and ice. BC may have 60% of the global warming effect of CO₂ [1], but remains one of the largest sources of uncertainty in analyses of climate change during the Industrial Era. Assessing CP concentrations in snow and ice from the Himalayas and Tibetan Plateau is key to understanding the climatic impacts of CP, as the atmospheric composition in this region is influenced by the largest sources of CP globally, and it is estimated that the largest climate forcing from BC in snow occurs over the Tibetan Plateau [1, 2]. To date, there is little information regarding the CP composition of Tibetan Plateau snow and ice. Here preliminary CP results from a Mt. Nyainqentanglha ice core (5806 m asl; 30.24 N, 90.34 E) are summarized.

CP concentrations were determined by two different methods: EC using a thermo-optical device (RT 3080, Sunset Laboratory Inc.) [3], and BC via laser induced incandescence with a Single Particle Soot Photometer (SP2) [4]. In both methods the ice samples are rinsed with MQ to remove potentially contaminated ice, melted and sonicated. The thermal analysis indicates variable EC concentrations through time, but no trend is evident (Fig. 1). If valid, this suggests that the recent retreat of glaciers in the region is not due to changing EC concentrations.

There is large disagreement between EC and BC concentrations and trends between the two methods (Fig. 2). Both identify the same periods as having high concentrations, but there is greater variability in trends at lower concentrations. The atmosphere in this region can be heavily dust laden, further affecting the energy balance of the atmosphere and cryosphere. High dust concentrations in the ice core complicate determination of CP in both methods. Preliminary results from the thermal method indicate that dust and EC concentrations are highly correlated (not shown). Causes for this may be: joint transport; the dust has an EC component; melting in the surface snowpack results in trapping of the dust and EC in the same layers; or an analytical artefact.

Future work will focus on continued method development and comparison of the two methods, and analysis and interpretation of two ice cores from the Tibetan Plateau and one ice core from the northeast ridge of Mt. Everest. Aims of this research are to determine variations in the CP loading of the atmosphere since the pre-industrial era, the

relative importance of dust and CP on the snow albedo in this region, and the role of CP in recent and projected climate change.

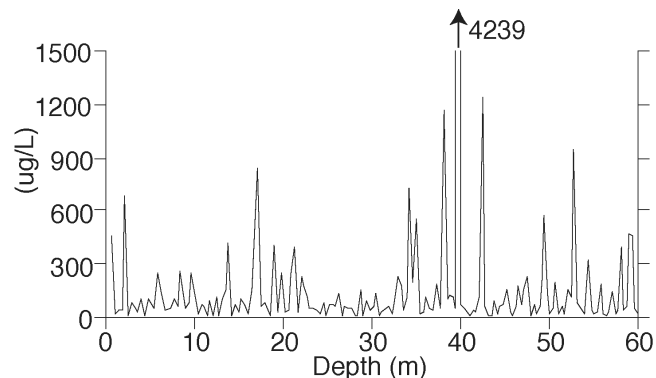


Fig. 1: EC concentration in the Nyainqentanglha ice core. This core is not yet dated.

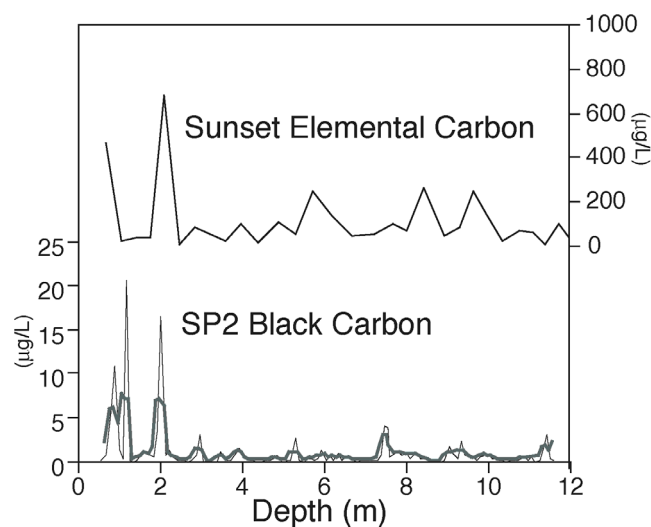


Fig. 2: Comparison of preliminary results of EC and BC concentrations using the thermal (Sunset) and laser induced incandescence (SP2) methods. The gray line in the SP2 plot is a 3-point running mean. Errors have not yet been estimated.

ACKNOWLEDGEMENT

S. Kaspari is supported by the US NSF International Research Fellowship Program.

REFERENCES

- [1] V. Ramanathan & G. Carmichael, *Nature Geoscience* **1**, 221-227 (2008).
- [2] M. Flanner et al., *J. Geophysical Research*, **112**, doi:10.1029/2006JD008003 (2007).
- [3] V. Lavanchy et al., *J. Geophysical Research*, **104**, 21227-21236 (1999).
- [4] J. P. Schwarz et al., *J. Geophysical Research*, **111**, doi:10.1029/2006JD007076 (2006).

RADIOCARBON DATING OF ICE CORES - VALIDATION OF A NEW METHOD

M. Sigl, T. Kellerhals, M. Ruff, H.W. Gaggeler (Univ. Bern & PSI), J.P. Steffenson, T.M. Jenk (CIC),
S. Szidat (Univ. Bern), L. Wacker (ETHZ), M. Schwikowski (PSI)

Carbonaceous aerosols extracted from glacier ice have been dated with the Mini Radiocarbon Dating System (MICADAS). The accuracy of this newly developed method is evaluated on a tropical ice core (Illimani, Bolivia, 6300m). Cross-validation against independent dating constraints reveals high agreement, demonstrating that the ^{14}C derived ages are indicative for the age of the ice samples.

INTRODUCTION

A method has been developed using the insoluble organic carbon (OC) fraction of aerosols incorporated in past precipitation to determine ^{14}C concentrations in ice core samples at a microgram level [1,2]. This method is used to establish additional dating constraints for various ice core archives [3,4]. Here we give a short overview of measures that were taken to assure the accuracy of the analysis.

METHODS

Validating the method by dating ice core samples from Greenland (GRIP) with a good independent age control was a first step to tackle the task. 8 Samples with masses of ~ 2 kg spanning the Holocene were processed and their $^{14}\text{C}/^{12}\text{C}$ ratios determined. Only in two samples, the OC concentrations significantly exceeded the procedural blank of $1.5 \mu\text{g}$. This samples with $>20 \mu\text{g}$ carbon match fairly well to the proposed ages, but it can not totally be ruled out that the high concentrations are caused by contamination.

As a second approach, we used cross-validation of the radiocarbon dates against independent dating constraints throughout the Illimani (6300 m asl., Bolivia) ice core. As time markers we chose the AD 1258 volcanic horizon, well identified in the excess-sulfate, fluoride and thallium records [3] and a pronounced isotopic ($\delta^{18}\text{O}$) depletion, indicating the Pleistocene-Holocene transition, which can be matched to various ice core archives [5,6,7].

Two samples bracketing the volcanic horizon with carbon masses $>70 \mu\text{g}$ were analysed and a weighted mean was calculated of the two values that were equal within their errors. A complete sequence of samples was measured for the last 10 meters down to bedrock.

All conventional ^{14}C ages were calibrated using OxCal v4.0 software with the IntCal04 [8] respectively the Southern Hemispheric calibration curve [9] for ^{14}C ages $<11,000$ years and presented as years AD or cal BP together with their accordingly 1σ uncertainty ranges. A continuous timescale was set up by interpolating between the single ^{14}C dating points.

RESULTS

With a calibrated age of $\text{AD } 1050 \pm 70$ the age of AD 1258 for the volcanic horizon is only slightly overestimated. The Last Glacial Termination is represented with a good temporal agreement, compared to other archives (Fig. 1). In contrary to the Huascarán and Sajama timescales our chronology is not fitted to other archives and therefore completely independent. There are strong evidences that ice core samples are measured precisely and accurately with

the proposed method, and that the obtained ^{14}C ages are indicative for the age of the ice segments. A small age offset towards too old ages may exist, indicated by the result of the well dated volcanic reference horizon. Small positive age artefacts may be explained through fossil carbon sources or long residence times of the organic carbon within other media prior to the final deposition.

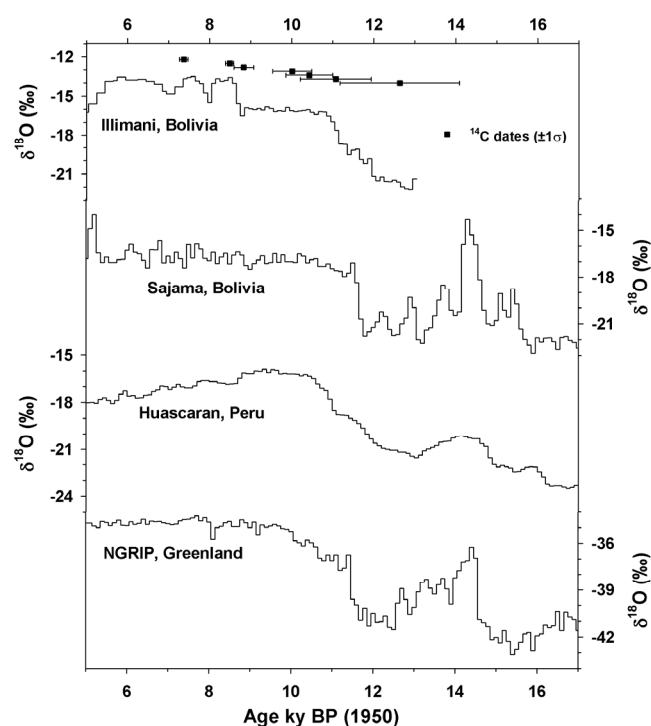


Fig. 1: 100-year averages of $\delta^{18}\text{O}$ revealing the presence of Last Glacial Termination ice at Illimani compared to $\delta^{18}\text{O}$ records from other ice core archives [5,6,7].

REFERENCES

- [1] T.M. Jenk et al., Nucl. Instrum. Meth. B, **259** (2007).
- [2] M. Ruff et al., Radiocarbon **49**(2) (2007).
- [3] T. Kellerhals, PhD thesis. Univ. of Bern (2008).
- [4] M. Sigl et al., to be submitted to J. Glac..
- [5] L.G. Thompson et al., Science **282**, 5395 (1998).
- [6] L.G. Thompson et al., Science **269**, 5220 (1995).
- [7] K.K. Andersen et al., Nature **431**, 7005 (2004).
- [8] P.J. Reimer et al., Radiocarbon **46**, 3 (2004).
- [9] F.G. McCormack et al., Radiocarbon **46**, 3 (2004).

COLLE GNIFETTI 2008 – TWO SHALLOW FIRN CORES OF AN EXCEPTIONAL WARM DECADE

M. Sigl, H.W. Gaggeler (Univ. Bern & PSI), A. König, B. Rufibach, S. Brütsch, M. Schwikowski (PSI)

Two shallow firn cores of 10 m length were drilled on Colle Gnifetti (Swiss Alps) in July 2008. A chronology based on annual layer counting combined with wigglematching to the Colle Gnifetti 2003 ice core is presented.

INTRODUCTION

Two shallow firn cores (CG08A and B) were drilled on Colle Gnifetti (4454m, 45°55'50.41"N 7°52'33.50"E) to update existing records of climate proxies and atmospheric pollution. CG08B will be shipped to Univ. Venice (Group C. Barbante) for analysis of polycyclic aromatic hydrocarbons. CG08A was analyzed at PSI. The motivation for drilling this core was:

- (1) to extend the time period of overlap between the proxy series ($\delta^{18}\text{O}$) and climate station data to improve skills of linear regression over time,
- (2) to study if the last decade, that was among the warmest since begin of measurements, is well reproduced by the temperature-sensitive $\delta^{18}\text{O}$ proxy and
- (3) to evaluate possible effects (e.g. increased melting) of exceptional warm mean conditions on the quality of the ice core archive.

Field work was done on July 24, 2008. Samples were decontaminated using standard procedures [1]. Cutting resolution was set to 4 cm and 240 resulting discrete samples were analyzed for major ions (Ca^{2+} , Mg^{2+} , Na^+ , K^+ , NH_4^+ , SO_4^{2-} , Cl^- , NO_3^-) using ionchromatography. Determination of $\delta^{18}\text{O}$ was done with isotope ratio mass spectrometry.

FIRST RESULTS

The drilling location at Colle Gnifetti is subject to strong wind erosion of predominantly winter snow [2], resulting in low net accumulation rates. For this reason, the oldest ice of the Alps is suspected near bedrock at this site. A nearby ice core record drilled on Grenzgletscher (4200 m asl.) offers an unbiased high-resolution $\delta^{18}\text{O}$ record spanning 1936-1994 [3]. This record, with a mean yearly net accumulation of 2.7 m waterequivalent (weq.), shows a clear seasonality in $\delta^{18}\text{O}$ with mean values of -21.2‰ for winter and -13.9‰ for summer months respectively, leading to a mean value of -16.5‰.

For CG08A the $\delta^{18}\text{O}$ signal is visibly biased. Maxima of around -8‰ marking summer conditions can be recognized, while typical winter values of lower than -20‰ occur only occasionally, resulting in a mean value of -13.9‰. However, although the full amplitude is disturbed, there seems to be enough seasonality preserved to identify annual cycles, as proposed in Figure 1. This dating approach is corroborated by several Saharan dust horizons with independent age control [4]. Given this timescale, a mean yearly net accumulation of 0.47 ± 0.12 weq. can be deduced for the time period 1997-2007. This is well in line with previous estimations and measurements at this site. To

match this new record to the existing record from the deep ice core (CG03) drilled in 2003, five matching points common to both time series were identified in the period of overlap. Minima close to -20‰ occur in both $\delta^{18}\text{O}$ records, probably reflecting higher fraction of non-summer snow being preserved between the accumulation seasons 1997 and 1998, respectively 2002 and 2003. Three pronounced Ca^{2+} signals were ascribed to Saharan dust events occurring in 1997, 2000 and 2001. In general there is a strong agreement between the $\delta^{18}\text{O}$ and calcium records of the two ice cores drilled in 2003 and 2008. Strong influences of prevailing warm summer conditions over the last decade on the quality of the ice core are not supported by the data. A more detailed survey will be the focus of future work.

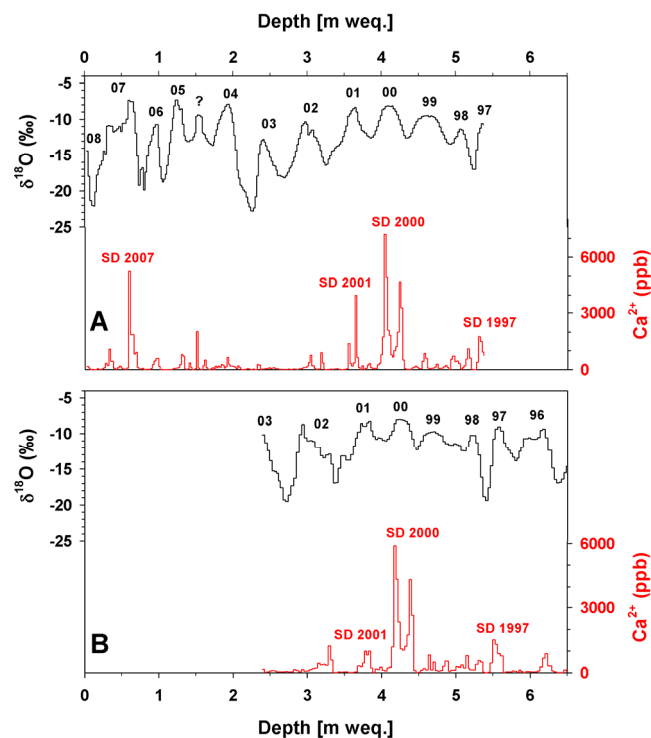


Fig. 1: Time series of $\delta^{18}\text{O}$ and Ca^{2+} concentrations for Colle Gnifetti ice cores CG08A (A) and for CG03 (B). To match the depth scales 2.37 m weq. were added to CG03 sample depths.

Emissions of climate active GHG related to the field campaign were offset by ‘myclimate’.

REFERENCES

- [1] D. Bolius, PhD thesis, University of Bern, (2006).
- [2] F. Maupetit et al., *Atm. Env.*, **29**(1), 1-9 (1995).
- [3] A. Eichler et al., *J. Glaciol.*, **46**(154), 507-515 (2000).
- [4] M. Collaud Coen et al., *Atm. Chem. Phys.*, **4**, 2465-2480 (2004).

THALLIUM AS TRACER FOR PRE-INDUSTRIAL VOLCANIC ERUPTIONS IN AN ICE CORE RECORD FROM ILLIMANI, BOLIVIA

T. Kellerhals, M. Sigl, H.W. Gäggeler (Univ. Bern & PSI), S. Brütsch, L. Tobler, M. Schwikowski (PSI)

Using an improved setup for the continuous analysis of trace elements in ice, a highly resolved thallium (Tl) record was obtained from the Illimani ice core. For the first time, it could be demonstrated that Tl is a suitable tracer for massive, explosive volcanic eruptions.

INTRODUCTION

Trace element records from glacier and ice sheet archives provide insights into biogeochemical cycles, atmospheric circulation changes and anthropogenic pollution history. Most investigations on heavy metals in snow and ice have been focused until recently on the anthropogenic contribution. Only few studies aimed at the characterization of natural emissions of trace elements to the atmosphere.

Here we present a high-resolution Tl record (no firm data 1964–1998 A.D.) from an accurately dated ice core from Nevado Illimani in the eastern Bolivian Andes (16°37'S, 67°46'W, 6300 m a.s.l.) and use it, for the first time, as a tracer for massive volcanic eruptions. Due to the extremely low concentrations of Tl in environmental samples, highly sensitive analytical methods and rigorous decontamination procedures are needed. We used an improved set-up for the continuous analysis of trace elements in ice cores with inductively coupled plasma sector field mass spectrometry (ICP-SFMS) [1].

The Illimani timescale (Fig. 1) was established by applying a multi-parameter approach, including annual layer counting (ALC), identification of reference horizons from nuclear weapon tests (tritium) and from volcanic eruptions, and radiocarbon dating of the lowermost part of the ice core. The volcanic horizons were, with the exception of the 'unknown 1258' eruption, identified prior to any chemical analysis with electrical conductivity measurements (ECM) [2] and thus assigned independently of the chemical signatures presented in Fig. 2.

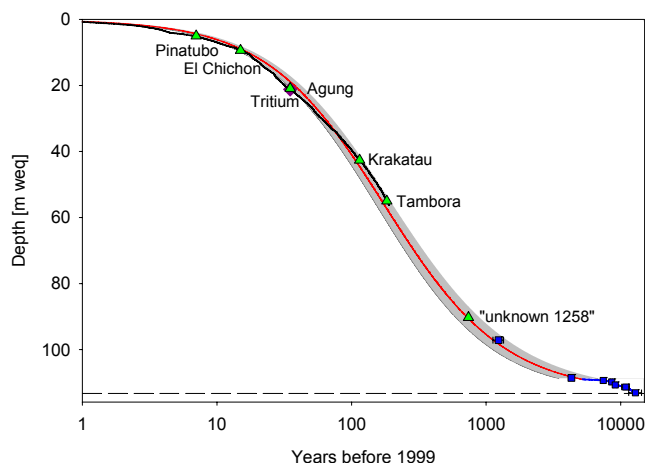


Fig. 1: Illimani timescale derived from ALC (black line), reference horizons from tritium (purple diamond) and volcanic eruptions (green triangles) and ^{14}C dating (blue squares). A two parameter model (red, grey shading envelops 2σ uncertainty) was fitted to the volcanic horizons and the two youngest ^{14}C time markers. Bedrock at a depth of 113.2 m weq is indicated by the dashed horizontal line.

RESULTS AND DISCUSSION

In the Tl record, four prominent Tl concentration peaks stand out at ~1260, ~1430, 1816 and 1884 A.D. (Fig. 2), representing signals from the massive volcanic eruptions of the 'unknown 1258' volcano, of Kuwae (~1450 A.D.), Tambora (1815 A.D.), and Krakatau (1883 A.D.). Tl is enriched in the volcanic horizons relative to its abundance in the continental crust by factors between 6 and 30. The enrichment factors (EF) were calculated as:

$$\text{EF Tl} = ([\text{Tl}]/[\text{U}]_{\text{ice core}}) / ([\text{Tl}]/[\text{U}]_{\text{Earth's crust}})$$

where the values for Tl and U in the Earth's crust (0.52 and $1.7 \mu\text{g g}^{-1}$, respectively) were taken from [3]. The conventionally used tracers for volcanic eruptions, excess sulphate and fluoride, confirm the volcanic character of the identified horizons. Tl is thought to be attached to sulphate aerosols, which can be transported in the stratosphere over long distances. Since Tl is less susceptible to contamination than e.g. Cu, Zn, or Pb, it may represent an especially suited volcanic eruption tracer.

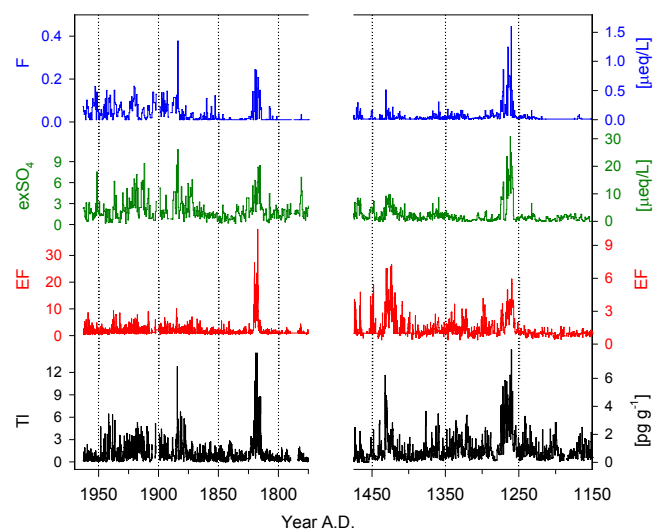


Fig. 2: Tl concentrations (black), Tl enrichment factors (red) as well as excess sulphate (green) and fluoride (blue) concentrations for the time periods 1150–1475 A.D. and 1750–1963 A.D., revealing the volcanic eruption horizons from the 'unknown 1258', Kuwae ~1450, Tambora 1815, and Krakatau 1883 A.D.

REFERENCES

- [1] T. Kellerhals, PhD thesis, University of Bern (2008).
- [2] S. Knüsel et al., *J. Geophys. Res.*, **108** (D6), 4181 (2003).
- [3] K.H. Wedepohl, *Geochimica et Cosmochimica Acta*, **59** (7), 1217-1232 (1995).

SOURCE APPORTIONMENT OF TRACE SPECIES IN THE MERCEDARIO ICE CORE

A. Ciric, H.W. Gäggeler (Univ. Bern & PSI), L. Tobler, M. Schwikowski (PSI)

A principal component analysis revealed the ocean and mineral dust as main sources of trace species in the Mercedario ice core. For the first time, Ammonium was found to originate from a marine source.

The ice core drilled at the La Ollada glacier on Cerro Mercedario (31°58.S, 70°07.W, 6100 m a.s.l.) in the Central Argentinean Andes [1] was analyzed for major ions by ion chromatography (IC) as well as $\delta^{18}\text{O}$ and δD using isotope mass spectrometry. In order to investigate sources of impurities a principal component analysis (PCA) was applied to the major ion records. Ten variables (concentrations of trace species, normalized values) were used as input and 5 factors retained explaining 90% of the variance (Table 1). Factor 1 and 2 are each explaining 28% of the variance, while factors 3 to 5 make only smaller contributions (14, 11 and 9%).

The first factor showed the highest loadings for Na^+ , NH_4^+ and Cl^- (0.80, 0.87 and 0.92 respectively). Na^+ and Cl^- are the major ionic components in seawater and are therefore normally used as tracers for sea salt. NH_4^+ , on the other hand, is usually an indicator for land-based biogenic emissions [2]. The high correlation with Na^+ and Cl^- suggests a marine source of NH_4^+ . Bouwman et al. showed in a global emission inventory for ammonia that the tropical Pacific can be a source of ammonia [3] and the Humboldt Current is known to be a biological active system [4, 5].

In the Mercedario ice core NH_4^+ is in a similar concentration range like the sea salt species (Fig. 1). However, much lower concentrations of NH_4^+ in comparison to Na^+ and Cl^- are found in marine aerosols from the marine boundary layer (e.g. 82 ppt in contrast to 588 and 732 ppt, median values, [6]). NH_4^+ is usually attached to small particles ($<0.56\ \mu\text{m}$), whereas Na^+ and Cl^- are most abundant in coarse particles (diameters between 3.2 and 5.6 μm [6]). A possible explanation for the observed similar concentration range might be a fractionation towards smaller particles during air mass transport to the high-elevation glacier (6100 m a.s.l.).

The abundance of methane sulfonic acid (MSA) is another indication for a nearby marine source. Its precursor is dimethylsulfide (DMS) which is produced by phytoplankton and then released to the atmosphere. In the atmosphere it is oxidized to MSA and further sulfur species. Its lifetime is around one day in the atmosphere. Due to the different pathways and production of the marine species, MSA and the sea salt species are not found in the same factor (factor 1 and 3).

Factor 2 has highest loadings in mineral dust related ions (Ca^{2+} , SO_4^{2-} and Mg^{2+}) which are also the predominant species in the ice core. Main sources are presumably the surrounding rocks, since little stones and dust are even visible in the ice.

The origin of F^- , K^+ (factor 4 and 5) and NO_3^- (no distinct factor) is not yet clear. The F- record shows very low concentrations with some few high peaks which might

originate from volcanic emissions. K^+ and NO_3^- might have several sources, e.g. marine and land-based.

Tab. 1: Factor analysis of 10 variables: The highest loadings and their corresponding source are indicated.

Factor	1	2	3	4	5
Source	Sea salt	Mineral dust	Ocean	?	?
Sodium	0.80	0.42	-0.20	-0.20	-0.09
Ammonium	0.87	0.03	-0.17	-0.01	-0.22
Potassium	0.26	0.40	-0.10	-0.14	-0.85
Magnesium	0.32	0.79	-0.19	-0.28	-0.13
Calcium	0.09	0.93	-0.19	-0.10	-0.13
Fluoride	0.15	0.20	-0.17	-0.94	-0.11
MSA	0.23	0.18	-0.90	-0.13	-0.05
Chloride	0.92	0.14	-0.17	-0.11	-0.05
Sulfate	0.12	0.93	-0.07	-0.06	-0.22
Nitrate	0.55	0.22	-0.58	-0.17	-0.14
Variance (%)	28	28	14	11	9

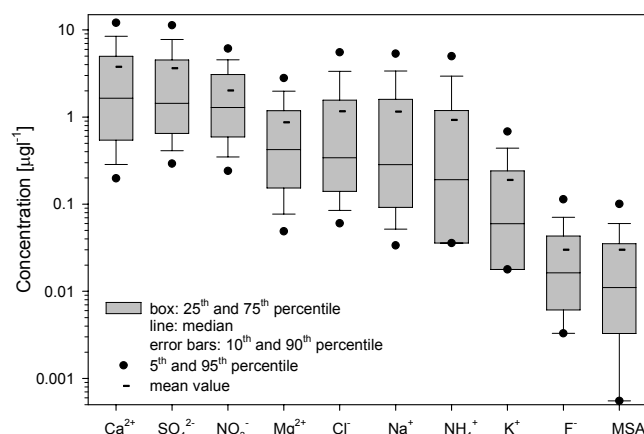


Fig. 1: Statistical distribution of various ionic species from the Mercedario ice core (sorted by decreasing median values, each ionic species contains 3512 data points).

REFERENCES

- [1] M. Schwikowski et al., Ann. Rep. Lab. for Radio- & Environ. Chemistry, Uni Bern & PSI (2005), p. 36.
- [2] A. Döschner et al., Geophys. Res. Lett. **23**, 2741 (1996).
- [3] A. F. Bouwman et al., Global Biogeochem. Cycles, **11**, 561-587 (1997).
- [4] R. Escribano et al., Deep-Sea Research II, **51**, 2389-2411 (2004).
- [5] V. Montecino et al., Deep-Sea Research II, **51**, 2413-2426 (2004).
- [6] B. J. Huebert et al., J. Geophys. Res., **103**, 16493-16509 (1998).

TRACE ELEMENT CONCENTRATIONS IN THE MERCEDARIO ICE CORE

L. Tobler, M. Schwikowski (PSI), A. Ciric, T. Kellerhals (Univ. Bern & PSI)

Trace element concentrations were determined with the *Continuous Ice Melting (CIM) Inductively Coupled Plasma Sector Field Mass Spectrometry (CIM-ICP-SF-MS)* in the ice core from the La Ollada glacier on Cerro Mercedario, Argentina. Most of the elements show much higher concentrations than in an ice core from the Illimani (Bolivia) site. The highest concentration ratios between the two sites are found for soil-derived elements.

INTRODUCTION

Glaciers from high-altitude mountains in the Andes have been used as paleo-climatic archives to reconstruct past atmospheric conditions and anthropogenic influences in the Southern Hemisphere. Highly resolved records of chemical and isotopic tracers are needed to get these informations. The ice core drilled at the La Ollada glacier on Cerro Mercedario (31°58.S, 70°07.W, 6100 m a.s.l.) in the Central Argentinean Andes [1] has been analyzed for major ions by ion chromatography (IC), $\delta^{18}\text{O}$ and δD using isotope mass spectrometry [2]. In addition CIM-ICP-SF-MS analysis is applied to obtain a highly resolved record of trace elements. Result from a depth between 25 m and 50 m weq of the Mercedario ice core are reported, which can help to improve the understanding of biogeochemical cycles and air pollution history.

EXPERIMENTAL

For the CIM-ICP-SF-MS analyses, ice bars of about 70 cm length are placed on a heated melting head (55°C) inside a freezer. The melt water of the inner, uncontaminated part of the ice core is drained through the inner outlet, acidified to ~ 0.25 mol HNO_3 shortly behind, and taken up by a self-aspiring nebulizer of the APEX sample introduction system (Elemental Scientific Inc., Omaha, USA). The generated dry aerosol of the APEX is then transported to the ICP-SF-MS (Element1, Finnigan MAT, Bremen, Germany) [3].

RESULTS

All elements analyzed show lognormal distributions. The median concentrations are given in Table 1 and are compared to the median values from the Illimani ice core in Bolivia [3]. All elements show higher median concentrations in the Mercedario ice core with the exception of the elements Ba, Na and Sr. The lower ratio for sodium and probably also for the earth alkali elements Sr and Ba might be explained by the influence of the nearby saline lakes and salt crusts (called salars) at the Illimani site.

The highest ratios are found for the elements, which show also very high correlations (correlation coefficients $r > 0.93$) among each other. As one example the correlation of Al and Rb is presented in Figure 1. All these elements can be attributed to soil-derived material, which reflects the high input of dust and soil particles at the Mercedario site. However, the different concentration ratios of soil-derived elements indicate that the soil composition differs strongly between the two sites.

Due to the exceptional high amount of small stones and visible dust particles in this ice core, the method encounters sometimes the problem of clogging of the drain system during analysis, which can be very cumbersome.

Element	Mercedario	Mercedario	Element	Mercedario	Mercedario
	Median	Illimani		Median	Illimani
	pg/g	ratio median		pg/g	ratio median
Rb	189.6	5.03	Eu	1.04	1.89
Cs	44.6	4.90	Bi	0.90	1.87
Tl	2.13	4.52	Ca	26322	1.87
Zr	51.5	4.19	Mn	1461	1.83
Sc	8.2	3.71	Sm	4.7	1.79
Al	35789	3.58	Pr	5.6	1.75
Yb	1.8	3.18	La	19.6	1.74
Th	6.1	2.11	Nd	21.0	1.67
V	48.5	2.07	Mg	8509	1.61
Pb	66.2	2.01	Ce	42.3	1.49
U	2.41	2.01	Ba	171	0.95
Fe	16615	1.91	Na	5822	0.77
Sb	4.6	1.91	Sr	92.7	0.64

Tab. 1: Median elemental concentrations of the Mercedario ice core in comparison to the Illimani ice cores [3].

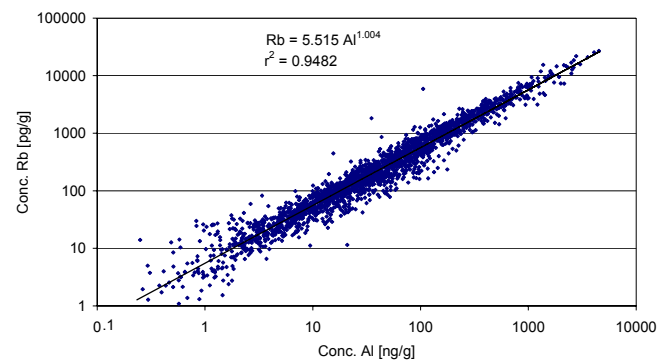


Fig. 1: Correlation between Al and Rb ($n=2293$, $r = 0.974$, $p < 0.001$) concentrations in the Mercedario ice core.

REFERENCES

- [1] M. Schwikowski et al., Ann. Rep. Lab. for Radio- & Environ. Chemistry, Uni Bern & PSI (2005), p. 36.
- [2] A. Ciric et al., Ann. Rep. Lab. for Radio- & Environ. Chemistry, Uni Bern & PSI (2007), p. 37.
- [3] T. Kellerhals, PhD thesis, University of Bern (2008).

SEASONALITY AND TENTATIVE DATING OF THE PIO XI ICE CORE RECORD, SOUTHERN PATAGONIAN ICE FIELD

M. Schläppi (Univ. Bern & PSI), G. Casassa, A. Rivera (CECS), M. Schwikowski (PSI)

Major ion concentrations and the stable isotope ratio $\delta^{18}\text{O}$ were determined in the 50.6 m long ice core from Pio XI. Both $\delta^{18}\text{O}$ and Cl^- show seasonal cycles, suggesting a high accumulation rate of 5.5 m weq y^{-1} .

INTRODUCTION

Ice core records from polar and tropical regions have largely contributed to the understanding of past climate variability. However, little climatic and environmental information is available from the Southern Hemisphere. Although ice cores exist from tropical and subtropical regions, there is a gap between 30°S and 65°S (Antarctic Peninsula). Possible candidates to fill this gap are the Patagonian Ice Fields. In 2006 a 50.6 m (33.2 m weq) ice core was drilled in the accumulation area of Pio XI glacier. Topic of this study is the investigation of this ice core.

RESULTS

$\delta^{18}\text{O}$ values were determined with isotope ratio mass spectrometry. The $\delta^{18}\text{O}$ record is characterized by high fluctuations between -23.6‰ and -14.8‰ (Fig.1). We assume that these fluctuations reflect six years with maximum values in summer and minimum values in winter. This is indicating a very high accumulation rate of about 5.5 m weq y^{-1} which is in good agreement with instrumental data from coastal stations northwest of Pio XI [1] and also with algal biovolume and *Nothofagus* pollen amount in Pio XI ice core [2].

This high accumulation rate suggests that snow is entirely preserved in contrast to San Valentin from the Northern Patagonian ice field where wind erosion leads to redistribution of snow and low accumulation rates of $0.18 \text{ m weq y}^{-1}$ [3].

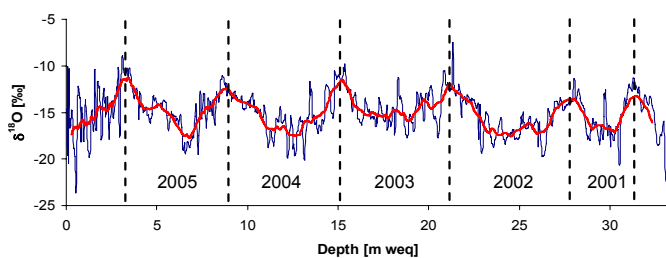


Fig. 1: Pio XI $\delta^{18}\text{O}$ record (blue) with 31 point moving average (red) and tentative dating.

Major ion concentrations, analyzed with ion chromatography, show a clear oceanic signal [4]. Previous studies at Antarctic Peninsula revealed that various ionic species (e.g. chloride) have a seasonal cycle at marine sites with a maximum in summer, determined by sea ice extensions [5]. In contrast, in Pio XI core chloride concentrations above 20 m weq show seasonal variations with a maximum in autumn but also high short time fluctuations in a range of days (Fig. 2). The maximum in chloride concentration around 10.9 m weq as well as the signal loss below 20 m weq is attributed to strong melting

effects. It seems that the seasonal variations are mainly controlled by higher wind speed during austral autumn and spring leading to enhanced sea spray formation compared to winter and summer conditions (Fig. 3).

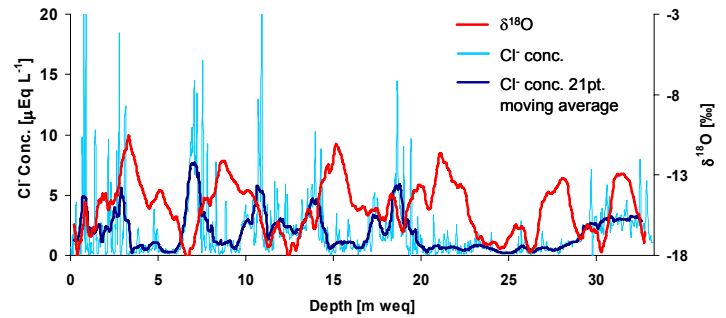


Fig. 2: Pio XI $\delta^{18}\text{O}$ record and chloride concentrations.

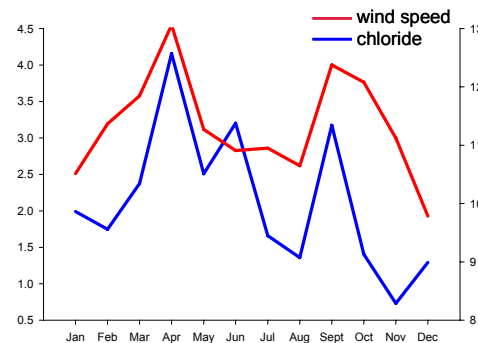


Fig. 3: Mean monthly wind speeds from August 2006 to August 2003 at 850 mbar (red) [NCEP datasets] and mean monthly chloride concentration (blue).

Further work will focus on obtaining benchmark data on concentrations of various trace elements and carbonaceous particles from this unique site in the Southern Hemisphere.

REFERENCES

- [1] J.F. Carrasco et al., in: *The Patagonian Ice Fields*, Kluwer Academic, 29-41 (2002).
- [2] P. Santibañez, personal communication (2008).
- [3] F. Vimeux et al., *J. Geophys. Res.* **113**, D16118 (2008).
- [4] M. Schläppi et al., *Ann. Rep. Lab. for Radio- & Environ. Chemistry, Uni Bern & PSI* (2008) p. 39.
- [5] A.J. Aristarrain and R.J. Delmas, *Atmos. Environ.* **36**, 765-772 (2002).

BIOLOGICAL ANALYSES OF THE PIO XI ICE CORE, SOUTHERN PATAGONIA ICEFIELD

P. Santibáñez, G. Casassa (CECS), M. Schläppi, M. Schwikowski (PSI)

Studies of microorganisms that live on temperate glaciers and pollen provide a novel method for ice core dating. The biological content of a 50 m long ice core of Cordón Mariano Moreno, Southern Patagonia Icefield, was analysed. Microalgae and pollen concentrations show the occurrence of 6 spring-summer peaks, suggesting that the ice at the bottom of the core is six years old, which is in agreement with major ion and stable isotope results.

INTRODUCTION

The use of biological content for dating and for estimating glacier mass balance in ice cores has been applied before at Yala glacier (Nepalese Himalayas), Tyndall Glacier (Southern Patagonia Icefield), Sofiyskiy Glacier (Russian Altai), and in the glaciers of Mocho-Choshuenco and Osorno volcanoes (Andes of the Chilean lake district). These investigations together with other studies of algal communities conclude that snow algae and pollen are useful seasonal and annual markers for ice core dating and assessment of past annual mass balance at low-mid latitudes and low altitudes, where abundant water can be present within temperate glaciers [1]. Here we present the analyses of microalgae biovolume and pollen concentration detected in the ice core from Pio XI Glacier, Patagonia.

RESULTS

The biological method is described earlier [2]. The results of microalgae and pollen concentrations show 5 unequivocal maxima which should correspond to spring-summer, labeled as *Sp-S Signal 1, 2, 4, 5 and 6* in Fig. 1. In addition, one more maximum, labelled as *Sp-S Signal 3*, appears weakly in the microalgal record, and can be identified clearly in the $\delta^{18}\text{O}$ record (Fig. 1. d). *Sp-S Signal 2, 4, 5* correspond well with the $\delta^{18}\text{O}$ peaks (Fig 1), but *Sp-S Signal 1* and *3* occur slightly before (at shallower depths) than the δO^{18} peaks. Possibly this indicates some degree of isotope percolation at these levels.

At depth, pollen concentration and algal biovolume peaks are at the same level, except for the *Sp-S Signal 3* peak where no pollen is preserved. In principle the pollen is expected to occur in the spring, before the algal bloom. The fact that pollen and algae are found at the same level might be due to surface melting of the spring layer. Additionally, flowering timing of genus *Nothofagus* varies for different species, and can occur between August and December [3].

The absence of pollen peaks in spring-summer signals interpreted from microalgae and $\delta^{18}\text{O}$ peaks do not necessarily represent periods without pollen dispersal, because of spatial and/or temporal variability of pollen on the glacier surface and the small sample volume used in this analysis (20-25 mL).

Algal biovolume peaks are on the order of $10^2 \mu\text{m}^3 \text{mL}^{-1}$, which is 2 and 3 orders of magnitude lower than the values found at other places glacier sites (such as in the southern Chilean Andes, the Himalayas and the Altai). This may be explained by the cold conditions at the Pio XI high altitude site where surface water content is lower than at more temperate locations.

Algal biovolume peaks disappear below 27 m w.e., perhaps due to the abundant water presence in the core. At this

depth the drill got stuck for the first time and a water soaked layer appeared close to the firm-ice transition [4]. As there is water, bacteria could be active and decomposing microalgae.

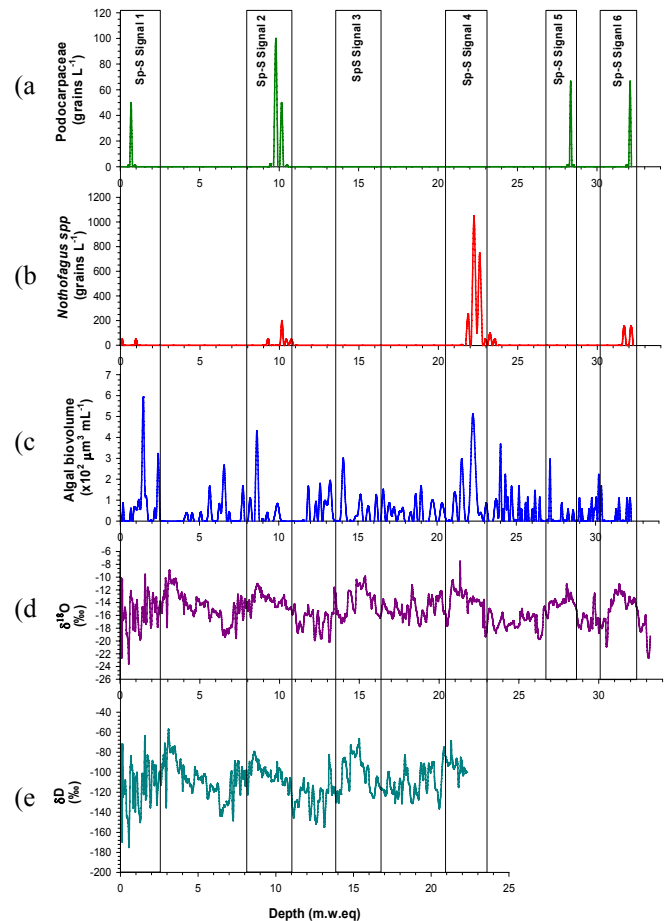


Fig. 1: (a) Profiles of the Pio XI core: (a) Podocarpaceae pollen concentration; (b) *Nothofagus* spp. pollen concentration; (c) Algal biovolume; (d) $\delta^{18}\text{O}$ record; (e) δD record. *Sp-S* (summer-spring) Signal indicate core levels with algal and pollen maxima, which are assumed to correspond to algal growth periods (summer) and pollen flowering periods (spring-summer).

REFERENCES

- [1] N. Takeuchi & S. Kohshima, *Arct. Antarct. Alp. Res.* **36** (1), 92-99 (2004).
- [2] P. Santibáñez et al., *A Ann. Rep. Lab. for Radio- & Environ. Chemistry, Uni Bern & PSI* 2007, p. 40.
- [3] P. Hechenleitner et al., *Plantas amenazadas del Centro-Sur de Chile*. Santiago, Universidad Austral de Chile y Real Jardín Botánico de Edimburgo (2005).
- [4] M. Schwikowski, *Ann. Rep. Lab. for Radio- & Environ. Chemistry, Uni Bern & PSI* (2006), p. 40.

TESTING OF A MELTING HEAD FOR TRACE ELEMENT ANALYSIS IN FIRN

M. Schläppli (Univ. Bern & PSI), P. Monbaron, L. Tobler, M. Schwikowski (PSI)

In order to determine trace elements in firn with Inductively Coupled Plasma Sector Field Mass Spectrometry (ICP-SFMS) a new melting head was tested.

INTRODUCTION

Determination of major ions and trace elements in ice cores provide basic information for interpretation of past environmental and climatic signals. Our current set-up of continuous ice melting ICP-SFMS is optimized to analyze trace elements in ice from the part of the glacier below the firn-ice transition [1]. When applying this set-up to firn sections, melt water is immediately soaked up by the porous firn due to capillary forces. This leads to contamination and smearing of the signals. For effective decontamination a new firn melting head was designed which is a modified version of the one described in [2]. The accuracy and reproducibility was tested on firn samples from the Jungfrauoch.

METHOD AND DESIGN OF THE MELTING HEAD

The new part of the melting head is the aluminium plate with 0.1 mm slits. (Fig.1). These slits generate capillary forces larger than the ones of firn, dragging melt water into the melting head. This avoids a flow of possible contaminated surface melt water into the core center. In contrast to the firn melter described in [2], slits do not extend into the area of the inner circle.

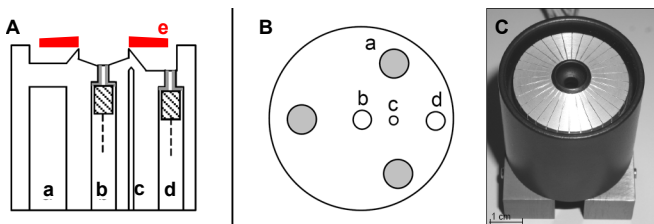


Fig. 1: Lateral (A) and back (B) view of the melting head: (a) heating cartridges, (b) drain of the inner flow (c) thermocouple (d) drain of the outer flow. (e) aluminium disc C) Photo of firn melting head (adapted from [3]).

The performance of the firn melting head was tested by melting and analyzing firn cores from the Jungfrauoch. Several parallel ice bars of 2.2 cm * 2.2 cm cross section and a length of about 70 cm were cut out of a firn core. These firn bars were decontaminated by scraping off the topmost firn layers with a knife. The firn bar was placed onto the melting head which was heated to 45°C. The produced melt water of the inner part was acidified and afterwards nebulized. The aerosol was dried and finally analyzed in the ICP-SFMS.

RESULTS

In order to investigate potential smearing effects, firn bars from the same core section were melted top-down and bottom-up. Most elements e.g. ^{27}Al showed largely different concentration profiles in the four firn bars out of the same firn core (Fig. 2). Two main main problems were identified: smearing and contamination by the firn melter.

The capillary forces of the slits in the aluminium plate were not strong enough to avoid soaking (Fig. 3 A) and subsequent smearing over several centimeters. The melting head showed deposits on the surface of the aluminium plate after melting. In addition, little damage of the PFA coating was detected (Fig. 3 B), probably causing contamination.

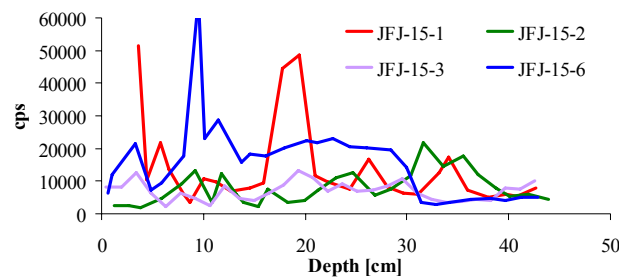


Fig. 2: ^{27}Al record of four parallel firn bars from Jungfrauoch melted with the firn melter.

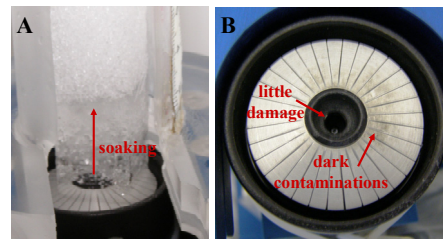


Fig. 3: A) Photo of a firn bar during melting, B) firn melting head after usage.

Interestingly the results of reproducibility test with the ice melting head are consistent for most elements e.g. ^{27}Al (Fig.4). For this reason further work will concentrate on using the ice melting head. Tests on accuracy and reproducibility will be done.

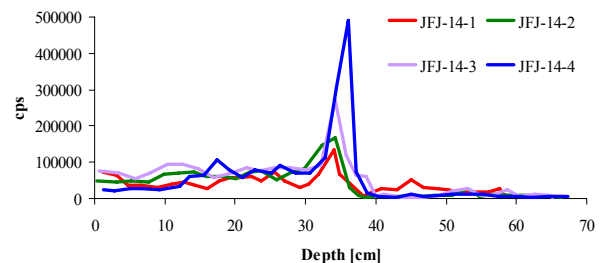


Fig. 4: ^{27}Al record of four parallel firn bars from Jungfrauoch using the ice melting head.

REFERENCES

- [1] T. Kellerhals, PhD thesis University of Bern (2008).
- [2] R. Röthlisberger et al., Environ. Sci. Technol. **34**, 338-342 (2000).
- [3] S. Knüsel, PhD thesis, University of Bern (2003).

A THERMAL DRILL FOR ICE CORING ON HIGH-ELEVATION GLACIERS

M. Schwikowski (PSI), D. Stampfli, F. Stampfli (FS INVENTOR)

A new thermal drill for ice core recovery from mid- and low-latitude, high-elevation glaciers, which can be used in combination with the existing electromechanical drill FELICS, was developed and tested.

Non-polar ice cores have now been obtained from all continents except Australia, almost exclusively by small teams from one or two institutions, and with a modest amount of funding compared to polar ice coring projects. However, many areas remain from which no ice cores have been retrieved yet. This is especially true for temperate glaciers, where the ice reaches the melting point during summer. Such glaciers exist in high precipitation regions of the Canadian and Chilean west coasts, the Himalayas/Tibetan Plateau, as well as in New Zealand, Scandinavia, and elsewhere. It is commonly believed that temperate glaciers are of limited use as paleo climate archives because meltwater formed during summer percolates through the summer snow and erases or homogenizes the chemical or stable isotope information contained therein. Yet useful information may be preserved because the formation of impermeable ice layers at the end of the summer prevents infiltration. Due to global warming many of the cold glaciers will turn into temperate glaciers in the future.

Due to the remoteness and high altitude of most mid- and low-latitude glaciers, the drilling equipment must be custom designed to meet narrow specifications. Particularly for glaciers located above 5500 m, i.e. above the range of helicopter operation, a lightweight and modular drill design is required to allow for transportation by either porters or pack animals. The drill must be easy and fast to assemble and operate under extreme conditions, in order to limit the exposure of scientists to dangerous high altitude environments. Most of the drilling devices used under these conditions are electromechanical (EM) drill systems designed primarily for dry hole drilling. However, EM drilling is constrained to glaciers with temperatures well below the ice melting point, since pressure induced melting during drilling can cause refreezing of meltwater on the drill which then easily gets stuck in the borehole. Another disadvantage of EM drilling is its susceptibility to ice core fracture. Especially in the deepest part just above bedrock, which is under highest shear stress, small pieces ("chips") of ice are often produced instead of good quality ice cores. Fractured ice cores cannot be used for the analysis of most trace species, since the standard decontamination techniques cannot be applied.

Thermal drills (TD) using ethanol/water mixtures as antifreeze drilling fluid provide good ice core quality, where shear stress is high or where the ice is warmer. Because ice conditions at mid- and low-latitude glaciers vary from "warm" ice (just below freezing point), to "cold" ice, a multi-faceted drilling technology is ideal for retrieving the best possible core quality. However, only one system has been designed so far that can quickly be switched from electro-mechanical drilling to a thermal-alcohol drilling, and still be transported by porters [1].

The main goal of this project was the development of a TD for ice core drilling on high-elevation glaciers which can be used in combination with the existing electromechanical drill FELICS [2]. This required a modification of the control unit and the power supply, since thermal drilling consumes more power. The TD itself consists of two barrels. The upper barrel contains two pumps and two containers, for ethanol and for the ethanol/meltwater mix, respectively. The lower one is the core barrel bearing the melting ring and the core catchers (Fig. 1). The new TD was tested on the Jungfrauoch. Good quality ice cores with a diameter of 75 mm and a length of 70 cm could be drilled with a speed of 2 m/h. After this successful test the TD will be used for ice core drilling on Lomonosovfonna in Svalbard in April 2009.

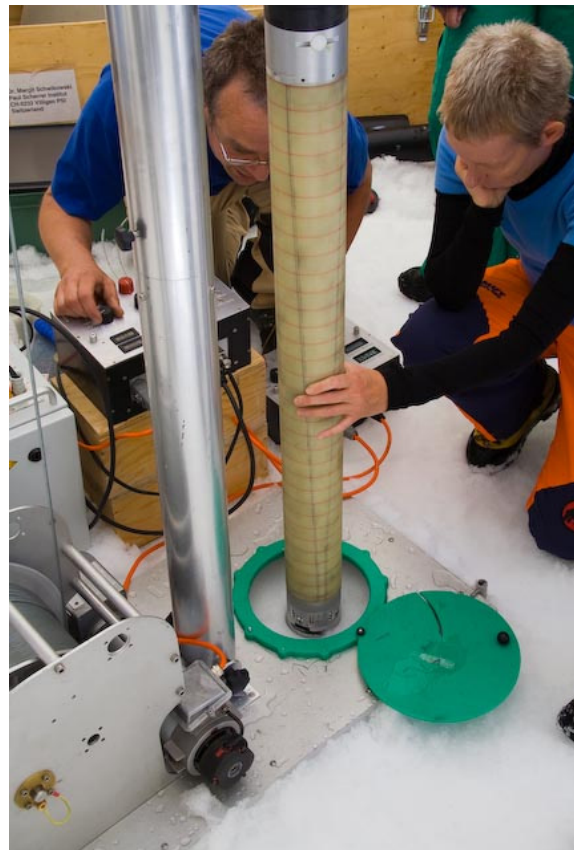


Fig. 1: The core barrel of the new TD during test on the Jungfrauoch (photo J. Cunningham).

REFERENCES

- [1] Zagorodnov et al., *J. Glaciology* **46**, 167 (2000).
- [2] P. Ginot et al., *Mem. Natl. Inst. Polar Res. Spec. Issue* **56**, 38 (2002).

ACKNOWLEDGEMENT

This project was supported by the PSI FoKo.

ACCUMULATION RATES DETERMINED FROM RADIOACTIVE DISEQUILIBRIUM BETWEEN ^{210}Po AND ^{210}Pb

H.W. Gäggeler (Univ. Bern & PSI), L. Tobler (PSI), E. Vogel (Univ. Bern)

^{210}Po reaches secular equilibrium with ^{210}Pb within roughly one year. Since fresh precipitation is nearly free of ^{210}Po , the in-growth of ^{210}Po into ^{210}Pb can be used for dating purposes over this time period. A typical example is the determination of the annual snow accumulation rate at sites where other means (e.g. via. $\delta^{18}\text{O}$) does not apply.

GENERAL

^{210}Pb is widely used for nuclear dating over roughly one century. Another new application of the ^{210}Pb decay series could be the determination of accumulation rates on glaciers at sites where this value can not be determined straightforward (e.g. at remote sites such as in Patagonia or in New Zealand or alpine locations with irregular deposition throughout the year). In such cases quite often no seasonal signature is reflected in the isotopic data (e.g. $\delta^{18}\text{O}$) or in chemical signatures (e.g. NH_4^+). We tested therefore the idea that the in-growth of ^{210}Po into ^{210}Pb may be used for an approximate estimate. ^{210}Po has a half-life of 138.4 d and is nearly absent in fresh snow.

Using the Bateman equations the in-growth of ^{210}Po formed from the decay of ^{210}Pb via the intermediate – though short-lived – nuclide ^{210}Bi can be calculated as a function of time.

EXPERIMENTAL

To test this approach, a snow/firn core of 5.5 m length was drilled on 25 March 2007 on the Aletsch glacier close to the exit of Jungfraujoch at about 3500 m asl. After melting an aliquot of the sample was analysed immediately after the field campaign for ^{210}Po by spontaneous deposition on Ag foils followed by α -spectrometry. After storing the residual samples for nearly one year a second ^{210}Po deposition was performed with the residual sample, in order to determine the ^{210}Pb activity after having reached secular equilibrium (equal activities of all members of the decay chain).

RESULTS

Figure 1 and 2 depict ^{210}Po and ^{210}Pb measurements as well as the in-growth of ^{210}Po (Fig. 1) and the deduced age (Fig. 2). The average ^{210}Pb activity for most of the samples between about 10 and 50 mBq/kg is typical for winter snow at this altitude in the European Alps. The lowermost value of 450 mBq/kg is rather high and represents a summer value. The average ^{210}Pb activity in precipitation from the Swiss plateau is 150 mBq/L [2]. Hence, the age at a depth of about 5.5 m agrees well with the higher activity concentration of ^{210}Pb (Fig. 1) from the summer precipitation in 2006. The constant age for the uppermost meter (Fig. 2) reflects a single prominent snowfall.

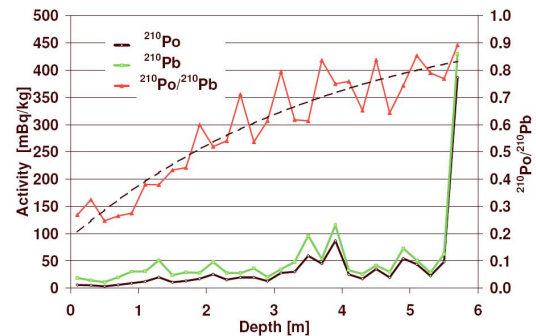


Fig. 1:

Activity concentrations of ^{210}Po and its progeny, ^{210}Pb , in a snow core from Jungfraujoch, Switzerland, as a function of depth (left side). The red triangles depict the in-growth towards a secular equilibrium (right side).

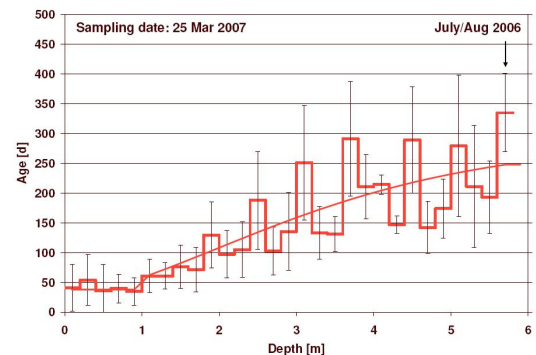


Fig. 2:

Deduced dating of the snow core from the data depicted in Fig. 1.

REFERENCES

- [1] H.W. Gäggeler et al., J. Glaciol., **29**, 165 (1983).
- [2] H.W. Gäggeler et al., BAG/SUER Annual Report 2007 (unpublished).

URANIUM CONCENTRATION IN SURFACE SAMPLES ALONG THE ALETSCHE GLACIER

H.W. Gäggeler (Univ. Bern & PSI), E. Vogel (Univ. Bern), L. Tobler (PSI), H. Boss (Matten/Interlaken)

Surface samples collected along the Jungfrau firn and the Aletsch glacier were analysed for their uranium concentration. The measured values show a trend towards increasing concentrations from the Mönchsloch down the glacier until about 2750 m asl followed by a decrease.

INTRODUCTION

Ice from cold glaciers contains valuable atmospheric information that can be used to e.g. study past air pollution or to get insight into the climate history. Still open is the question whether ice from temperate glaciers archive any valuable information.

We have therefore performed a sampling campaign along the Aletsch glacier starting close to the Mönchsloch and ending in the vicinity of the lake of Märjelen (see Table 1) between August 20 and 22, 2008. A handheld drill device was used to retrieve shallow surface samples from the firn/ice surface. The surface of the drill barrel was covered by a Teflon layer in order to keep contamination minimal. The length of individual samples was usually 20 to 30 cm, rather short, due to technical problems with the drill head.

Tab. 1: Drill sites, sample amounts and measured concentrations.

Sample	Coordinates	Altitude [m asl]	Amount [g]	U conc. [ppt]
P1	643355/155715	3630	585.4	5.6
P2	642112/155036	3445	664.7	2.5
P3	642717/153828	3160	619.1	111.0
P4	643492/152890	2925	523.3	81.7
P5	645005/150898	2751	515.0	279.3
P6	644928/150124	2640	512.8	115.6
P7	645700/150046	2720	568.0	141.6
P8	646505/150379	2720	596.4	136.7
P9	646198/149610	2723	471.3	69.1
P10	647853/147728	2515	572.6	42.8
P11	648558/146565	2485	550.8	37.9

RESULTS AND DISCUSSION

The samples were melted and an aliquot of 200 µl, diluted to 2 ml with 3% HCl, was analysed by HR-ICP-MS. Measured blanks yielded very low values of about 0.1 ppt.

The results are summarized in Tab. 1 and depicted in Fig. 1. The uppermost two samples are from fresh snow collected between Jungfrauoch and Mönchsloch. The values of 5.6 and 2.5 ppt, respectively, are in good agreement with data from Mont Blanc samples [1] with an average value of about 5 ppt for the second half of the 20th century.

To our surprise the concentrations increase downwards the glacier to about 150 ppt and then start to decrease below the equilibrium line of the glacier in August 2009. Obviously, firn accumulates uranium in the course of the year, despite percolating meltwater during spring and summer. As soon as solid ice was reached, starting at the time of the field campaign slightly above the Konkordia place (P6) the concentrations start to decrease, reaching values of about 40 ppt at the end of the sampling trajectory.

The future plan is to also measure sulfate, ²²⁶Ra and ²¹⁰Pb in order to get insight into the entire decay chain of ²³⁸U as well as to study whether nuclear dating is possible on a temperate glacier. Previous attempts on an Austrian glacier yielded encouraging results [2]. Sulfate is known to correlate well with ²¹⁰Pb which should enable a normalization of seasonal variability.

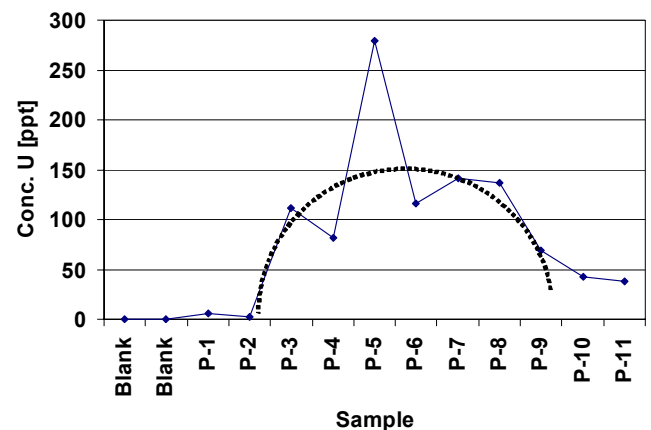


Fig. 1: Uranium concentrations for surface samples along the Aletsch glacier. The positions of the sites P-1 to P-11 are summarized in table 1. The dashed line is to guide the eye through the experimental data.

REFERENCES

- [1] C. Barbante et al., Environ. Sci. Technol. **35**, 4026 (2001).
- [2] H.R. von Gunten et al., Z. für Gletscherkunde und Glazialgeol., **37** (1) 37 (1982).

SEPARATION OF ^7Be FROM THE COOLING WATER OF THE SINQ

D. Schumann, M. Ayranov, F. Heinrich, A. Kalt, D. Viol, R. Erne, O. Morath (PSI)

As a first test experiment, a filter bypass was installed at the cooling system of the SINQ facility in order to separate considerable amounts of the scientifically interesting radioisotope ^7Be . First measurements show that an activity in the range of TBq can be achieved by this method.

SCIENTIFIC BACKGROUND

^7Be as well as ^{10}Be are key radionuclides for investigations of several astrophysical processes and phenomena.

One of the "hot topics" is the half-life of ^{10}Be , where the literature values differ from 1.34 to 1.51 My [1,2]. Additional measurements are, therefore, urgently needed. One possibility is the use of LSC for the determination of the activity and ICP-MS for measuring the number of atoms. The calibration of the ICP-MS requires at least 2 mass points in known amounts, and since Be has only one stable isotope (^9Be), ^7Be can serve as the second marker.

Another application of ^7Be is the study of key reactions concerning the solar neutrino flux, in particular the reaction $^7\text{Be}(p,\gamma)^8\text{B}$ [3]. Highly-active ^7Be targets in the range of several 100 GBq are required for such studies.

PRODUCTION AND SEPARATION OF ^7Be

^7Be is produced in considerable amounts in the cooling water (D_2O) of the SINQ facility at PSI by spallation reactions on ^{16}O with the generated fast neutrons. By-products can be nearly neglected, so that this cooling water establishes an ideal source for highly active ^7Be -samples.

A filtration device shown in Fig.1. was installed as a bypass for the cooling water into the cooling circle of SINQ for 6 weeks. The apparatus contains 1 litre of the mixed-bed ion exchanger LEWATIT (grain size 400 μm), which absorbs cations and anions as well.

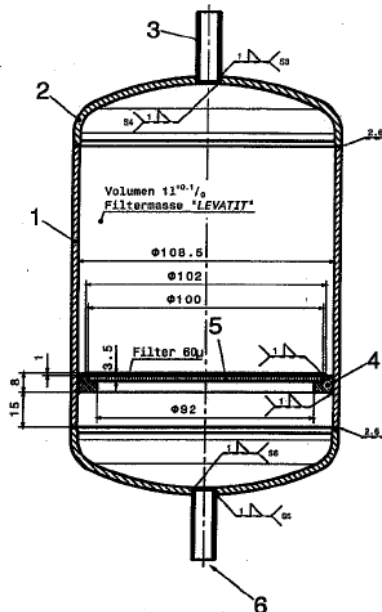


Fig. 1: Drawing of the adsorption device

- 1,2 - stainless steel vessel
- 3 - inlet
- 4 - ring for filter fixing
- 5 - filter
- 6 - outlet

DOSE RATE MEASUREMENTS

After end of beam at the SINQ shutdown on 22.12.08, filtering had been proceeded till 5th of January 2009. The dose measurement at this time and the corresponding activity (calculated by use of the dose rate constant 0.008 mSv/GBq in 1 m distance) can be seen in Tab.1. The differences in the activity calculation are caused by the relative inaccurate distance measurement and the general background. Therefore, only an approximate value for the activity of ^7Be of around 1 TBq can be estimated at the moment.

Tab. 1: Dose rate measurement of the collection device

Date	Distance [cm]	Dose rate [mSv]	Activity [GBq]
5.1.09	surface	1500	-
8.1.09	10	420	525
7.1.09	30	100	1125
7.1.09	100	30	3700

FIRST RESULT UND FURTHER TREATMENT

This first test experiment demonstrated that ^7Be amounts in the range of TBq can be gained by this relatively simple ion exchange technique, which corresponds to $\sim 5 \cdot 10^{18}$ atoms (10 μg). Both kinds of experiments, described above, should be possible with this available amount.

Next step of the experiment is the elution from the ion exchanger, which can be done by use of diluted HCl following the procedure described in [4]. Due to the high dose rate, this procedure has to be carried out in a shielded hotcell, and automated and/or remote controlled systems have to be developed for a safe handling.

Since this separation procedure can be performed every year (preferable at the end of the irradiation period, when sufficient ^7Be has been accumulated), extended collaborative work with the nuclear astrophysics community seems to be prospective. However, a routine production will require also the development of a shielded collection device and a high-sophisticated transportation system.

REFERENCES

- [1] R. Middleton et al., Nucl.Instr.Methods B **82** p. 399-403 (1993).
- [2] D. Fink et al., NIM B **172** p. 838-846 (2000).
- [3] L.T. Baby et al., Phys. Rev. Lett. **90**, 022501 (2003).
- [4] D. Schumann et al., Radiochim. Acta **96** (2008) 31.

PREPARATION OF A ^{26}Al STANDARD FOR AMS-MEASUREMENTS

D. Schumann, J. Neuhausen (PSI), A. Wallner (University of Vienna), P. Kubik (ETHZ)

A ^{26}Al source of $\sim 9\text{Bq}$ was chemically separated from proton-irradiated copper samples. The material was certified by γ -measurement and can serve as AMS standard.

INTRODUCTION

Accelerator Mass Spectrometry as - in most cases - a relative measurement technique requires the availability of the respective standard material. Therefore, it is surprising, that up to now no standard reference material for ^{26}Al can be commercially purchased. Moreover, results of a first international inter-laboratory comparison show deviations of the measured values of up to 10% [1,2]. Obviously, certified material is rare, not available for every laboratory, the quantity of the provided material is not sufficient for distributing to all interested places and the preparation of the final samples is not carried out in consistent procedures. Therefore, it seems to be necessary to prepare a sufficient amount of ^{26}Al standard material, which can be provided to all interested laboratories world-wide. One of the possibilities for gaining ^{26}Al is accelerator waste [3].

CHEMICAL SEPARATION

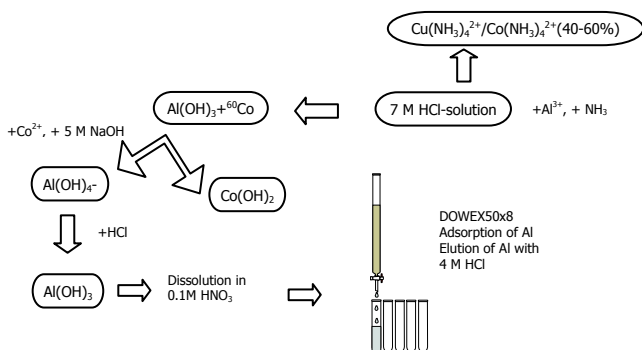


Fig. 1: Separation scheme for the isolation of ^{26}Al from a copper beam dump sample (Figure taken from [4])

Samples from a proton-irradiated copper beam dump were used for the isolation of ^{26}Al . The copper was dissolved in 7 M HNO_3 . After evaporation to dryness, the residue was dissolved in acid, 4 mg of aluminium carrier were added and $\text{Al}(\text{OH})_3$ was precipitated with NH_3 solution. The details of the final separation and purification steps are depicted in Fig.2 and are described in [3].

RESULTS

The obtained ^{26}Al sample was diluted to 25 ml 1M HCl. 5 ml of this sample were sent to PTB Braunschweig in order to get a certified γ -measurement. The value yielded $0.448 \pm 0.014 \text{ Bq/g}$. 4 ml of the solution were filled tightly in a suitable vessel and are used as γ -calibration source for further ^{26}Al samples in a well detector.

6 AMS samples each were prepared for comparison by mixing aliquots of the stock solution with a certified ^{26}Al standard solution for ICP-MS. In Tab.1 the results of the measurements performed at VERA (Vienna) and ETHZ (Zurich) are shown. For the calculation of the theoretical value for the isotopic ratio from the γ -measurement the value $7.16 \cdot 10^5 \text{ y}$ was used [4]. All AMS measurements were normalized to that half-live value.

Tab. 1: Measured isotopic ratios for the ^{26}Al AMS standard

No.	I[10 ⁻¹] ETHZ	δ	I[10 ⁻¹] VERA	δ	I[10 ⁻¹] γ	Date
1	-	-	9.99	-1.2	10.12	19.4.07
2	-	-	10.2	+0.8	10.12	19.4.07
3	1099	+8.6	-	-	1012	26.9.07
4	1097	+8.4	-	-	1012	26.9.07
5	11.42	+12.8	10.8	+6.7	10.12	18.2.08
6	11.21	+10.8	10.7	+5.7	10.12	18.2.08

The data in Table 1 show that ETHZ overestimates the value from the γ -measurement with about 8-9% which was expected already from earlier measurements.

Unfortunately, the samples prepared about one year after the preparation of the standard solution show higher values also at VERA. Probably, this is caused by a partial evaporation of the stock solution. For a proper adjustment of the final standard material, a comparing measurement with the certified γ calibration source has to be performed as well as additional AMS measurements at both facilities.

The discrepancies in the AMS measurements indicate clearly the need for a unified and certified standard material. From the material available now from the described beam dump, appr. 240 g Al_2O_3 (respective 130 g Al) can be provided, based on an isotope ratio of about 10^{-10} . This amount will be sufficient for $\sim 260\,000$ AMS standard measurements. To guarantee reliable results, more efforts have to be undertaken concerning the accurate standard preparation, including a final certification.

REFERENCES

- [1] S. Merchel et al. NIM B 223-224 (2004) 393.
- [2] S. Merchel et al. NIM B 229 (2005) 217.
- [3] D. Schumann, J. Neuhausen, J.Phys.G: Nucl.Part.Phys. 35 (2008)014064.
- [4] Thomas, J.H., Rau, R.L., Skelton, R.T., Kavanagh; R.W., Phys. Rev. C, 30, (1984), 385.

CONSECUTIVE SEPARATION OF ^{26}Al , ^{59}Ni , ^{53}Mn , ^{44}Ti AND ^{60}Fe FROM PROTON IRRADIATED COPPER BEAM DUMP

M. Ayranov, M. Sigrist, D. Schumann (PSI)

A chemical separation procedure was developed for consecutive separation of ^{26}Al , ^{59}Ni , ^{53}Mn , ^{44}Ti and ^{60}Fe from gram scale amounts of a proton irradiated copper beam dump. Activities for setting up the developed procedure for hot cell remote controlled operation are ongoing.

INTRODUCTION

The BMA station for pions cancer therapy was operated at PSI from 1980 to 1992. For this period the copper beam dump of the facility received a total dose of approximately 0.16 Ah of 590 MeV protons. After dismantling in 1993, it was cut and samples were taken for analytical purposes. The sampling collected 500 grams of high active copper chips that can be used for separation of exotic radionuclides [1]. The overall gamma analyses showed main nuclides present to be ^{60}Co , ^{54}Mn , ^{22}Na , ^{65}Zn and long lived ^{44}Ti with a daughter nuclide ^{44}Sc [2]. Further analyses by LSC and AMS demonstrated that significant amounts of ^{55}Fe , ^{63}Ni , ^{26}Al , ^{53}Mn , ^{59}Ni and ^{60}Fe are present in the copper beam dump. The analytical results estimate that about 100 MBq ^{44}Ti , 500 MBq ^{53}Mn , 7 kBq ^{26}Al , 8 MBq ^{59}Ni and 5 kBq ^{60}Fe are available in the collected copper chips [3].

Due to the high activity of ^{60}Co , approx. 4 GBq in total, the separation should be implemented using appropriate shielding, e.g. in a hot cell. The purpose of this work is to develop a simple, selective, efficient and easy to accommodate for remote manipulation procedure for the separation of ^{26}Al , ^{59}Ni , ^{53}Mn , ^{44}Ti and ^{60}Fe from gram amounts of the copper beam dump.

EXPERIMENTAL

The separation procedure, a combination of precipitation and ion exchange, is presented in Figure 1. Copper as the main matrix element interferes with the separation of all elements of interest. For this reason, after the copper dissolution in 7 M HNO_3 the solution is conditioned to 1 M HNO_3 and Cu(II) is precipitated by saturation with H_2S . At these conditions the copper precipitates selectively, while the exotic radionuclides remain in the solution. Further the solution is transferred in 12 M HCl and passed on Dowex 1x8 anion exchange column. Al and Ni are not retained and are washed out of the column with 12 M HCl . The remaining ions are eluted consequently in the following way, Mn – 10 M HCl , Ti – 8 M HCl , Co – 5 M HCl , Cu – 2.5 M HCl and finally Fe with 0.5 M HCl [4]. Further Al is separated from Ni on Dowex 50x4 cation exchange column. The Ni is purified with Eichrom Ni resin based on the traditional dimethylglyoxime precipitation chemistry [5].

RESULTS AND DISCUSSION

The proposed separation procedure is easy for remote controlled implementation in a hot cell. The ion exchange separation of Ni, Al, Mg, Ti and Fe is complete and high decontamination factors for copper and cobalt were achieved.

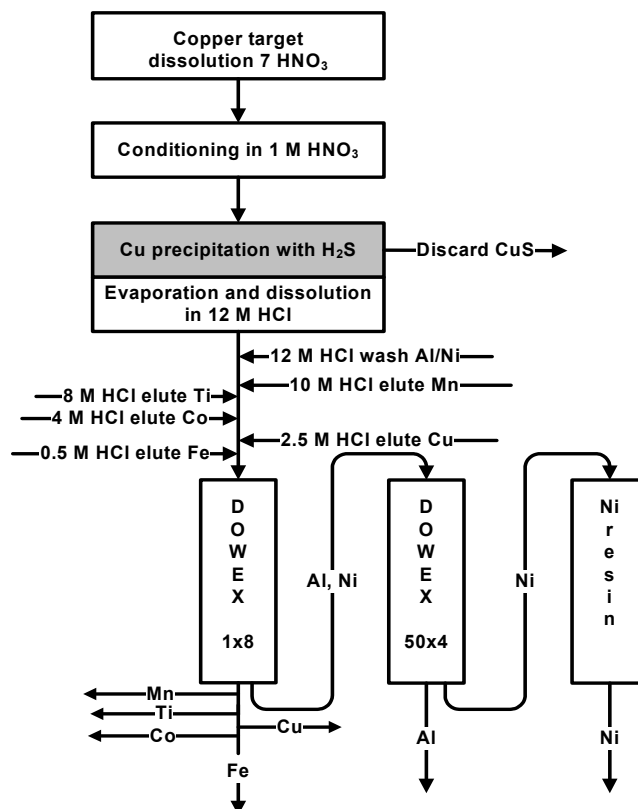


Fig. 1: The flowchart of the exotic radionuclides separation procedure.

A setup in a hot cell of a remotely controlled system for consecutive separation exotic radionuclides from gram amounts of copper beam dump is ongoing.

REFERENCES

- [1] D. Schumann et al., Ann. Rep. Lab. for Radio- & Environ. Chemistry, Uni Bern & PSI (2006), p. 40.
- [2] D. Schumann et al., Radiochim. Acta, accepted (2008).
- [3] D. Schumann et al., Ann. Rep. Lab. for Radio- & Environ. Chemistry, Uni Bern & PSI (2006), p. 38.
- [4] G. Svehla ed., Comprehensive Analytical Chemistry, Vol XIV, Wilson and Wilson's, (1982).
- [5] http://eichrom.com/products/info/ni_resin.cfm.

EXTRACTION OF POLONIUM OUT OF LEAD-BISMUTH EUTECTIC

PART I - GAS BLANKET EFFECTS

S. Heinitz, D. Schumann, J. Neuhausen (PSI), S. Keller (Univ. Bern)

A liquid-liquid phase extraction technique of polonium out of lead bismuth eutectic was studied under variation of various conditions. To achieve this goal, an appropriate extraction device was developed and several systematic experiments with variation of crucial factors like gas blankets, temperature and phase ratio were performed.

INTRODUCTION

Handling and managing the waste of lead bismuth eutectic (LBE) reactor coolant requires severe safety precautions. Due to neutron capture of Bi during operating time, the hazardous element Polonium is formed in considerable large amounts. To avoid Po release by evaporation or sputtering effects from LBE and minimize contamination in case of reactor leakage, a liquid-liquid extraction technique using molten alkaline hydroxides was proposed [1]. The aim of this study is to determine polonium removal efficiency as a function of the main process variables.

EXPERIMENTAL

LBE samples were irradiated at the SINQ spallation source and diluted, homogenized and cut in 1 g samples to be used for experimentation. NaOH and KOH were crushed and mixed to give a eutectic mixture ($T_m = 185\text{ °C}$) and placed into the extraction device shown in figure 1.

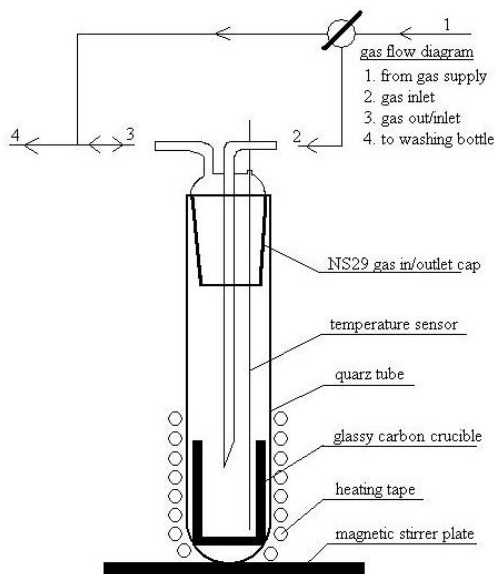


Fig. 1: Extraction device setup used for experimentation.

After heating up and water removal from the hydroxide melt, a certain temperature was adjusted. LBE samples were added and the extraction started in a desired gas blanket and hydroxide to LBE ratio μ . First, different gases were used to determine the extraction behavior under different oxidation potentials. The temperature was set to 250 °C . The extraction was stopped by solidification of both liquids after 30 min of extraction time. The initial and final Po concentrations in LBE and in the hydroxide phase were determined via liquid scintillation counting with dissolving each sample in acidic conditions.

RESULTS AND DISCUSSION

As it can be seen from figure 2, the extraction ratio of Po is highly dependent on the oxidizing potential of the cover gas present at extraction. Compared to inert gases as N_2 and He, experiments under air and O_2 show significantly lower Po extraction rates. A strong reduction of Po removal efficiency in the presence of oxygen was also reported by [1]. Either an oxide barrier between both liquids or a different extraction mechanism is believed to cause this fact.

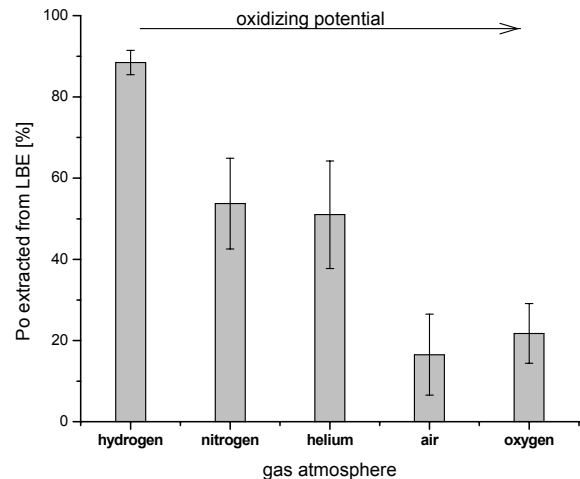


Fig 2: Extraction ratio of Po using different gas blankets performed at 250 °C , 30 min of extraction time and $\mu = 2$.

For hydrogen as a reducing agent, the effect on the extraction ratio is opposite. The reducing ability is increasing the Po transfer rate to the hydroxide phase yielding higher extraction efficiency. As the chemical extraction process still remains unclear, no proved explanation can be given here. Hydrogen is the favourable gas blanket to be used in future Po extraction devices that may be developed to a technically mature state.

REFERENCE

- [1] E.I. Yefimov, D.V. Pankratov, S.V. Ignatiev, *Removal and containment of high-level radioactive polonium from liquid lead-bismuth coolant*. Mat. Res. Soc. Symp. Proc., (1998). **506**: p. 679 - 686.

EXTRACTION OF POLONIUM OUT OF LEAD-BISMUTH EUTECTIC

PART II – WATER AND TEMPERATURE DEPENDENCE

S. Heinitz, D. Schumann, J. Neuhausen (PSI), S. Keller (Univ. Bern)

Various extraction experiments were done under different temperatures and thermodynamic constants were deduced.

INTRODUCTION

For a thermodynamic description of the polonium extraction process, the removal efficiency has to be measured under variation of the extraction temperature. Therefore, several experiments were performed at a range between 185 – 400 °C. The influence of drying of the hydroxide mixture before the experiments was also studied.

EXPERIMENTAL

As described earlier in part I, the hydroxide mixture was heated to 500°C before experimentation to remove water from the extraction system because the highly hygroscopic alkali hydroxides contain a notable amount of water [1]. Afterwards, it was cooled to the desired temperature for the extraction experiment. To determine water influence, another set of extraction runs were performed without preheating. All experiments were done at nitrogen atmosphere at a (Na,K)OH to LBE ratio $\mu = 2$ and 30 min extraction time. The temperature was raised from 185 °C to 400°C in 25°C steps.

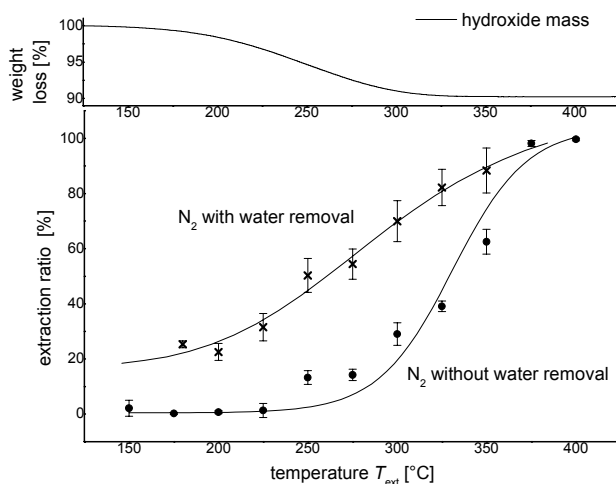


Fig. 1: Influence of water content on the extraction coefficient as function of temperature. The upper graph denotes the water release from hydroxide as function of temperature.

RESULTS AND DISCUSSION

The result of the thermo gravimetric analysis is shown together with both extraction experiment sets in figure 1. Extraction runs without removing water (denoted by ●) exhibit significantly less Po extraction than runs free from water (denoted by x) at temperatures $T_{\text{ext}} \leq 350$ °C.

As it can be seen from the upper graph, water removal is complete at temperatures above 350 °C. The hydroxide

mixture loses about 10% of its weight by water evaporation. At lower temperatures a certain amount of water still remains within the extraction system and does negative influence polonium removal. This may be explained by the influence of water on the polonium uptake mechanism.

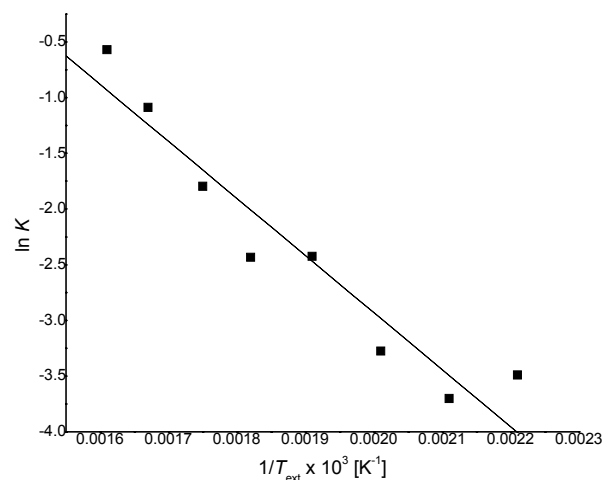


Fig 2: Linear regression of data for computing parameters fitting Gibbs equation; $R^2 = 0,917$.

Figure 1 also denotes increasing polonium removal with rising temperature, which was also found in earlier works [2]. Applying Gibbs law to the dataset obtained without the negative water influence, thermodynamic constants may be derived for the enthalpy and entropy of the extraction under nitrogen. A linear fit of $1/T_{\text{ext}}$ against the logarithmic distribution constant K is given in figure 2 and leads to:

$$\Delta H_{\text{ext}}^{\circ} = -(42,6 \pm 5,2) \text{ kJ/mol}$$

$$\Delta S_{\text{ext}}^{\circ} = 60,8 \pm 9,9 \text{ J/(mol*K)}$$

No data is available in literature concerning the thermodynamic extraction constants of Po out of liquid LBE. These values can, however, be extrapolated from data of polonium's chemical homologues as Te, Se and S.

REFERENCES

- [1] Hevesy, G.v., *Über Alkalihydroxide*. Zeitschrift der physikalischen Chemie, 1919. **73**: p. 676.
- [2] E.J. Wheelwright, T. R. Myers, *Purification of polonium-210 by pyrochemical extraction*. Sep. science and technology, (1980). **15**(4): p. 987 - 997.

EXTRACTION OF POLONIUM OUT OF LEAD-BISMUTH EUTECTIC

PART III – PHASE RATIO AND EXTRACTION TIME

S. Heinitz, D. Schumann, J. Neuhausen (PSI), S. Keller (Univ. Bern)

We analyzed the extraction performance of polonium out of irradiated lead bismuth eutectic regarding the hydroxide / metal mass ratio and the time both liquids are in contact.

INTRODUCTION

If polonium should be extracted from reactor coolant regarding the earlier described method, it is of inherent importance to minimize the quantity of hydroxide melt to decrease its waste disposal efforts and costs. Moreover, the optimum phase ratio at a certain temperature should be known to reach the best removal efficiency.

EXPERIMENTAL

The hydroxide to LBE mass ratio μ was varied in the range of 10^{-1} to 10^1 under a constant temperature of 250 °C. Therefore, specimens of 0,5 to 5 grams of (Na,K)OH and LBE were used for the extraction process with water removal (as described in earlier parts I and II). To examine the efficiency difference of different gas blankets, these experiments were performed under H₂ and N₂.

To qualitatively determine the rate of the extraction process, three separate runs were performed with variation of the extraction time at 350 °C under N₂.

RESULTS AND DISCUSSION

For both gas blankets the mean extraction ratios and standard deviations were calculated and are plotted in figure 1. What can be clearly seen is the difference of hydroxide mass needed to extract same amount of Po under H₂ or N₂, which confirms the observation stated earlier. Calculations show a 9 – 10 times higher efficiency in polonium removal or lower need of hydroxide mass for H₂ at 250 °C.

As expected, polonium removal gets worse with decreasing volume of the extractant. This can, however, be overcome by raising the temperature. Workers in [1] have shown that more than 99 % of polonium can be extracted at a ratio of $\mu \leq 0,5$ at 500 °C / N₂ (for NaOH and pure Bi). For a hydrogen gas blanket μ would become even less. It seems likely that the efficiency is not dependent on polonium concentration in LBE.

Table 1 shows the result for the kinetic experiments. Extraction ratios between 80 to 90 percent were found for given extraction conditions, indicating no significant Po distribution change even after one minute both phases were in contact. The rate of Po extraction at 350 °C is very fast; equilibrium is reached within only one minute. This observation was described earlier in [2], indicating no unusual kinetic limitation on polonium transfer. Future experiments will be done in a region of lower temperatures to quantitatively determine reaction rates as a function of temperature.

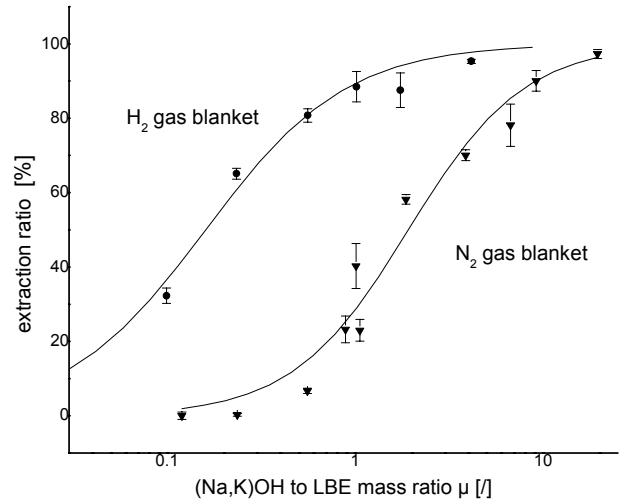


Fig. 1: Dependence of polonium extraction from hydroxide to LBE mass ratio for hydrogen and nitrogen gas blankets; temperature of extraction 250 °C; extraction time 30 min.

Extraction time	Mean extraction ratio
1 min	87 ± 3 %
5 min	85 ± 3 %
30 min	88 ± 8 %

Tab. 1: Po extraction ratios for different extraction times; set temperature 350 °C.

REFERENCES

- [1] W.W. Schulz, G.F. Schiefelbein, *Pyrochemical extraction of polonium from irradiated bismuth metal*. Ind. Eng. Chem. Process Design Develop., (1969). **8**(4): p. 508 - 515.
- [2] F. Gromov et al., *Liquid lead-bismuth target as intense neutron source in accelerator-driven systems for actinides transmutation and plutonium utilization*. in *International conference on future nuclear systems*. (1997). Yokohama, Japan.

SURFACE ENRICHMENT OF POLONIUM IN SOLIDIFIED LEAD BISMUTH ALLOY: FIRST KINETIC STUDIES

F. v. Rohr, J. Neuhausen, D. Schumann, S. Horn, S. Chiriki (PSI)

A surface segregation of ^{210}Po was observed in samples of eutectic lead-bismuth alloy that were neutron irradiated in SINQ. This effect may have an influence on the handling and storage of used spallation targets. We report here first results on the kinetics of the polonium migration process that leads to the surface enrichment.

INTRODUCTION

Liquid eutectic lead-bismuth alloy (LBE) is planned to be used as target material in future high power spallation targets for neutron production. In 2006, PSI performed the first test experiment to demonstrate the feasibility of such a target system in the MW range, MEGAPIE. One of the most significant problems when using LBE as target material is the production of significant amounts of the highly radiotoxic ^{210}Po by neutron capture on ^{209}Bi . A thorough knowledge of its behaviour within the target system is a prerequisite for the safe operation of the target system and its disposal. Previous studies performed in our laboratory indicated that the polonium distribution in solidified LBE is not homogeneous [1]. This effect may be important in the context of target handling after irradiation and final disposal. We studied the migration of polonium to the surface of solidified LBE samples by means of α -spectroscopy. First results are shown in this report.

EXPERIMENTAL

Polonium containing LBE samples were produced by irradiation of pieces of LBE in SINQ using the NAA rabbit system. Typical samples had a mass of ≈ 8 g and were irradiated for 1h without Cd-shielding. The samples were stored for a minimum of 1 month to ensure the decay of ^{210}Bi . The distribution of ^{210}Po within these samples was studied by an etching procedure described in [1], using liquid scintillation counting for the determination of ^{210}Po activity. LBE samples that were molten in a H_2 -stream at 600°C for 30-60 minutes showed a homogeneous polonium distribution after solidification. To study the variation of the surface α -activity with time, these samples were put into an α -measuring chamber directly after homogenization. The chamber was evacuated to $\approx 10^{-2}$ mbar and spectra were recorded successively for periods up to 12 days using a batch routine. Counting time was 1 h for each spectrum.

RESULTS

The change of the recorded α -spectra with time is illustrated in Fig. [1]. The spectra show a drastic increase of the α -counts measured in the range between 4.9 and 5.3 MeV, indicating an enrichment of ^{210}Po in a near-surface layer of the LBE samples, ranging approximately 2μ below the surface. Fig. 2 shows the increase of the α -counts in this energy range, compared to the counts measured at starting time, as a function of time. A fit of this function, using a simplified model for diffusion out of a spherical sample [2], gives a diffusion coefficient in the order of 10^{-11} cm^2s^{-1} . The nature of the diffusion process is still unclear. The enrichment of polonium in the grain boundaries of various p-group metals such as lead and bismuth has been observed

[3], suggesting a grain boundary diffusion mechanism. However, fast impurity diffusion processes that do not involve grain boundaries were also observed in lead [4]. In the eutectic alloy, the situation is still more complex due to the presence of crystallites of two distinct phases. Dedicated experiments to study the diffusion mechanism of polonium in LBE are under way.

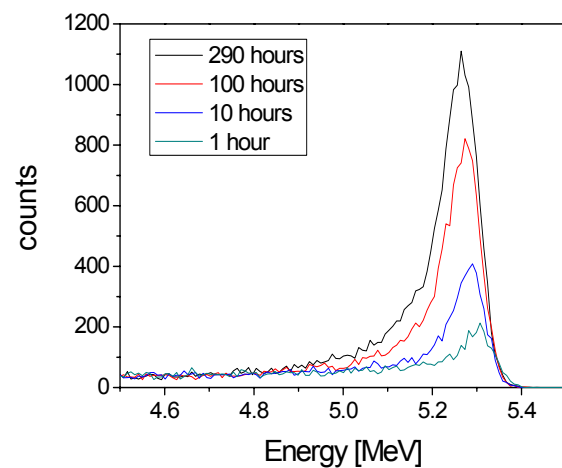


Fig. 1: Variation of α -spectra recorded from a solidified and homogenized ^{210}Po -containing LBE sample with time.

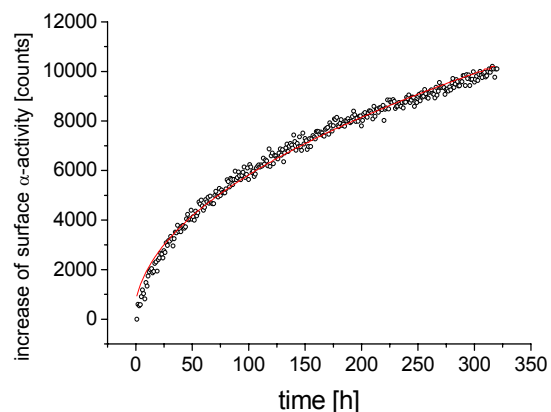


Fig. 2: Increase of surface activity as a function of time.

REFERENCES

- [1] F. V. Rohr et al., Ann. Rep. Lab. for Radio- & Environ. Chemistry, Uni Bern & PSI (2006).
- [2] J. Crank, The Mathematics of Diffusion, Clarendon Press, Oxford, (1992).
- [3] G. Tammann et al., Z. Anorg. Allg. Chem. 205, 145 (1932).
- [4] J. Kärger et al., Diffusion in condensed Matter, Vieweg, Braunschweig, (1998)

DETERMINATION OF THE RADIONUCLIDE INVENTORY OF SELECTED SAMPLES FROM SINQ TARGET 3

D. Schumann, J. Neuhausen (PSI), V. Alfimov, H.-A. Synal (ETHZ), G. Korschinek, G. Rugel, Th. Festermann (TUM)

Zircaloy, steel and an aluminium alloy, stemming from construction components of the SINQ target 3 were investigated concerning their radionuclide inventory. The values are compared with the declaration limits and limited activity concentrations given by Swiss authorities for decommissioning and disposal of radioactive waste.

INTRODUCTION

Swiss authorities (NAGRA) require the determination of the radionuclide inventory of activated components from accelerator complexes for decommissioning and disposal. The so-called "Deklarationslimit" (DL) defines all radionuclides which have to be declared, whereas "Zulässige Aktivitätskonzentration" (ZAK) gives an upper limit for the allowed concentration of a radionuclide in a package. Activation of the targets from the Spallation Neutron Source (SINQ) at PSI concerns not only the "real" target material lead, but also structure materials like the beam window, screws and protection hulls.

SAMPLE TAKING AND MEASUREMENT

In Fig.1, the sample taken positions for the 3 samples taken from the SINQ target 3 are shown. The target had been operated from June 1998 till December 1999 and consumed a total beam dose of 6.77 Ah.

Most of the γ -emitting radionuclides could be measured without destruction of the material (exception: ^{108m}Ag). ^{55}Fe and ^{63}Ni were measured by liquid scintillation counting (LSC), for ^{59}Ni and ^{36}Cl accelerator mass spectrometry (AMS) was used. The chemical separation procedures, necessary for the determination of these mentioned radionuclides are described in [1].

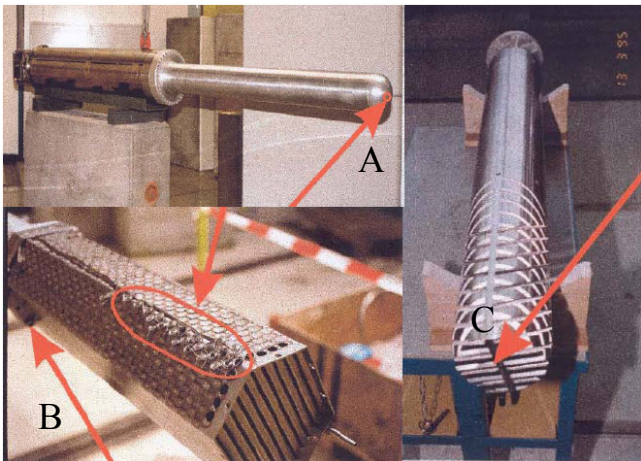


Fig. 1: Sample taking: A - beam entrance window, AlMg3; B - Zircaloy screw; C - protection hull steel 316L; Photo taken from [2]

RESULTS

The results from the measurements are collected in Table 1. For comparison, the DL and ZAK values are also shown. Empty cells mean: the radionuclide is not present or is below the detection limits.

The results clearly show, that in all three samples nearly all of the determined radionuclides have to be declared for a disposal. Additionally, the value for ^{22}Na within the beam window is in the same range as the ZAK value. Therefore, a somewhat longer cooling time (half-life of ^{22}Na : 2.6 y) should be taken into consideration.

Measurements of the "real" target component, the lead, are currently ongoing. First results, mainly on γ -emitting radionuclides, are presented in [3].

Tab. 1: Measured radionuclide inventory of selected components of SINQ target 3 in [Bq/g].

Nuclide	Zirkaloy	steel 316L	AlMg3	DL	ZAK
Na-22	$6.20 \cdot 10^3$	-	$2.88 \cdot 10^7$	$3.0 \cdot 10^3$	$4.5 \cdot 10^7$
Cl-36	$3.80 \cdot 10^1$	$7.58 \cdot 10^1$	$1.55 \cdot 10^1$	$1.0 \cdot 10^1$	$9.6 \cdot 10^5$
Mn-53	$4.23 \cdot 10^1$	7.99	-	$3.0 \cdot 10^2$	$5.3 \cdot 10^7$
Ti-44	-	-	$1.47 \cdot 10^4$	$1.0 \cdot 10^3$	$>10^{10}$
Mn-54	$6.50 \cdot 10^3$	$5.20 \cdot 10^4$	$1.63 \cdot 10^5$	-	-
Fe-55	$1.10 \cdot 10^6$	$2.55 \cdot 10^7$	-	$7.0 \cdot 10^4$	$>10^{10}$
Co-57	$2.00 \cdot 10^3$	$1.48 \cdot 10^4$	$8.10 \cdot 10^3$	-	-
Ni-59	$1.66 \cdot 10^3$	-	-	$2.0 \cdot 10^2$	$3.3 \cdot 10^7$
Co-60	$1.14 \cdot 10^5$	$1.51 \cdot 10^7$	$2.75 \cdot 10^5$	$1.0 \cdot 10^2$	$>10^{10}$
Fe-60	$1.14 \cdot 10^2$	$1.14 \cdot 10^1$	-	0.3	$2.8 \cdot 10^4$
Ni-63	$1.40 \cdot 10^6$	$2.33 \cdot 10^6$	-	$5.0 \cdot 10^4$	$3.1 \cdot 10^9$
Zn-65	$1.20 \cdot 10^3$	-	$2.39 \cdot 10^4$	$3.0 \cdot 10^3$	$>10^{10}$
Nb-94	$2.00 \cdot 10^2$	-	-		
Rh-101	$1.50 \cdot 10^3$	-	-		
Rh-102m	$3.50 \cdot 10^3$	-	-		
Ru-103	$6.00 \cdot 10^2$	-	-		
Rh-106	$9.00 \cdot 10^2$	-	-		
Ag-108m	-	-	$5.20 \cdot 10^1$		
Cd-109	$2.08 \cdot 10^4$	-	-		
Sb-125	$7.24 \cdot 10^5$	-	-		

REFERENCES

- [1] D. Schumann, J. Neuhausen, R. Weinreich, F. Atchison, P. Kubik, H.-A. Synal, G. Korschinek, Th. Faestermann, G. Rugel, NIM B 2007 264 (2007) 83.
- [2] D. Kiselev, D. Schumann, S. Teichmann, M. Wohlmuther, Berechnung des Radionuklidinventars von 3 Proben aus dem SINQ-Target 3; PSI-TM-85-08-03, (2008).
- [3] D. Schumann, J. Neuhausen, S. Horn, S. Lüthi, Y. Dai (PSI Villigen), P.W. Kubik, H.A. Synal, V. Alfimov, Ann. Rep. Lab. for Radio- & Environ. Chemistry, Uni Bern & PSI (2007) p. 45.

CHARACTERIZATION OF THE ENGINEERING MODEL OF THE LOW ENERGY ELECTRON DETECTOR LEED

St. Scherrer, W. Hajdas, K. Egli, N. Schlumpf, B. Schmitt, A. Bergamaschi (PSI), A. Mohammadzadeh (ESA)

The engineering/demonstration model of the low energy electron detector LEED was constructed as a spin-off of the PSI MYTHEN device. The instrument shall find its application area both in space as well as at lower X-ray energy range of the SLS or XFEL facilities. We report on first tests with the X-rays and electrons aimed to characterize it.

LEED AND MYTHEN OBJECTIVES

Low Energy Electron Detector LEED is a miniature particle monitor for measurements in space. It is based on the MYTHEN Si-microstrip system made at Paul Scherrer Institut PSI for X-ray detection at the Synchrotron Light Source SLS. It was designed in collaboration with the European Space Agency ESA in order to provide a new instrument covering an unexplored energy range of space electrons below few tens of keV. Such electrons can shed a new light on the acceleration and trapping processes and on the dynamics of radiation belts. Measurements of electrons in wide range of energies can provide a link between hot plasma and trapped higher energy particles. LEED development is also beneficial for PSI new facilities like XFEL with its requirements for very high count rates or integration mode and for low energy areas of the SLS.

ENGINEERING/DEMONSTRATION MODEL

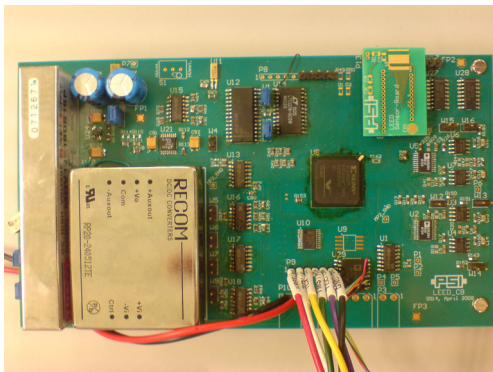


Fig. 1: LEED Engineering/demonstration model.

LEED is based on the MYTHEN instrument that utilizes an ASIC coupled with a microstrip SI-detector. The ASIC works for 128 channels and provides signal amplification, energy discrimination and 24 bits long counters. Engineering model EM of LEED (see Fig. 1) was constructed in order to study the properties of the instrument. In particular the low energy threshold, response differences between individual channels as well as linearity and energy range were scrutinized. First measurements were performed with Si-sensor of 300 μm thickness and 50 μm strip widths. Two different sensors as well as various polarization voltages and ASIC gain settings were used during the study. The EM was exposed to several sources of X-ray and γ -ray radiation ranging from 8 keV K_{α} X-rays from Cu up to 122 keV from ^{57}Co source. Results of the discriminator threshold scan are shown for source energies up to 44 keV in Fig. 2. It allowed determining of the noise level of the LEED at about 4. keV. One can also see rise of the curve indicating charge distribution between strips. The linearity of the instrument was tested using groups of 10

channels. As LEED should cover energies up to 200 keV the ASIC was tested at low gain settings. The data in Fig. 3 confirms LEED capability of wide energy range response.

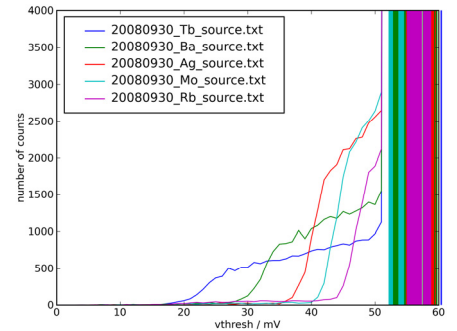


Fig. 2: Discriminator threshold scans at standard gain settings of LEED ASIC done for various X-ray sources.

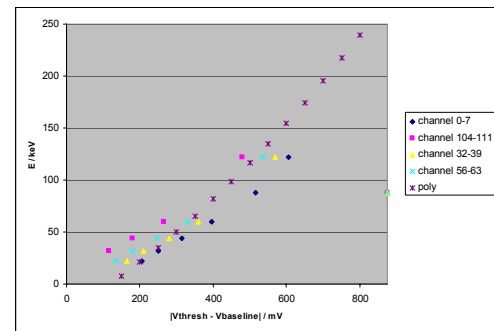


Fig. 3: Energy – voltage response linearity data.

FIRST DATA WITH ELECTRON SOURCES

The energy-calibrated LEED was exposed to the electrons from the ^{90}Sr source. First results are shown in Fig. 4. Further tests with electron monochromator are currently under preparation. In parallel the Monte Carlo simulation to verify the results are also planned.

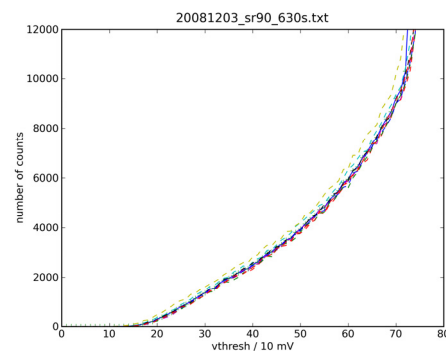


Fig. 4: Integral spectrum of electrons from ^{90}Sr source.

ENERGY CALIBRATION OF THE PROTON IRRADIATION FACILITY AT THE PROSCAN PROJECT OF THE PAUL SCHERRER INSTITUTE

W. Hajdas, U. Grossner, K. Egli, R. Brun (PSI), R. Harboe-Sorensen (ESA-ESTEC)

The new Proton Irradiation Facility for components tests and device characterization was installed in the PROSCAN experimental area. The facility is open for wide range of users from space community, industry, research institutes and universities. We report on the facility characterization with respect to the beam quality aspects. It includes energy calibration, spectral measurements, beam profile tests and background determination.

NEW PIF FACILITY AT PSI

New Proton Irradiation Facility for space- and particle-physics communities was installed at PSI within the PROSCAN Project [1]. Beam energies between a few MeV up to 250 MeV with intensities up to 10 nA and uniform profiles cover up to tens cm² sized targets. Proton fluxes between 10³ /cm²/s and few 10⁸ /cm²/s with beam profiles with FWHM between 10 cm and few mm are routinely available. The facility is easily accessible and characterized by user friendly setup (see Fig. 1) and operating procedure. This report describes energy calibration procedure performed to characterize the PIF facility.

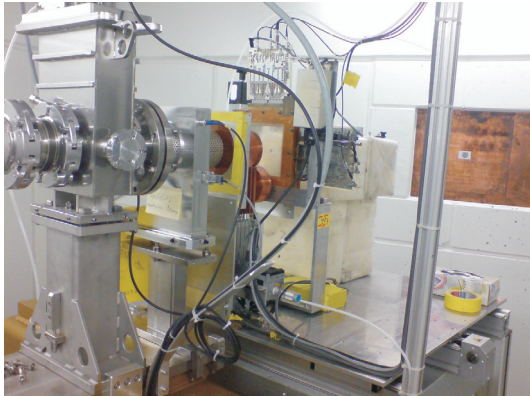


Fig. 1: View to the experimental area looking downstream with the last beam profile monitors, ionization chambers, degraders and XY-table and the beam dump at the end.

ENERGY CALIBRATION

To calibrate the energies delivered by the cyclotron, measurements of the Water Equivalent Range (WER) have been performed using a water phantom setup.

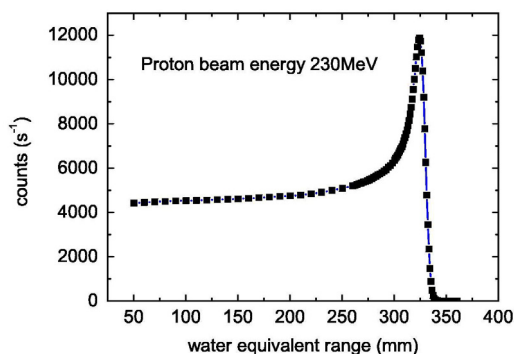


Fig. 2: Bragg curve for the proton range measurements in water for a proton beam energy of 230 MeV. Six initial energies were calibrated this way.

Here, the range of the impinging protons is measured by a flat, air-filled ionization chamber moving along the beam direction through a water filled tank. A typical Bragg curve from such a measurement at the proton beam energy of 230 MeV is shown in Figure 2. Using the WER of 80 % of the incoming protons (R80), the actual beam energies have been estimated using the calibrated PROSCAN energy from the cyclotron degrader and including corrections for the PIF dosimetry equipment at the beamline. For an incoming proton beam with the energy of 74.3 MeV, the extrapolated range energy has been determined to 75.7 MeV. In Figure 3, the respective values are compared to the ones listed in the ICRU Report 49 [2], the proton range-energy tables by J. F. Janni [3], and values as obtained by a standard SRIM simulation [4]. It should be noted that the energy differences between the three reference data sets are larger for higher energies and almost negligible for lower energies. In the range between 235 MeV and 74.3 MeV, the proton beam energy is set using the global degrader placed directly at the cyclotron exit. For energies lower than 74.3 MeV, the local degrader with Copper plates are used.

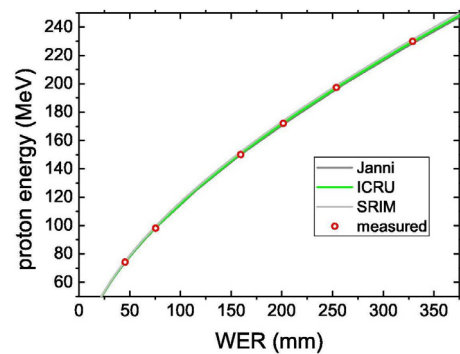


Fig. 3: Proton energy versus water equivalent range as measured and according to three reference data sets.

Tab. 1: Main parameters of the new PIF facility.

Initial energies	230, 200, 150, 100, 70 MeV
Energies / local degrader	Ca. 10 to 230 MeV
Intensity (E > 200 MeV)	2 nA
Intensity (E < 100 MeV)	10 nA
Max. flux / prim. energy	2-5·10 ⁸ p/cm ² /s (wide beam)
Beam profile /wide beam	Gaussian, FWHM ≈ 7-10 cm
DUT frame	25 x 25 cm ² (ECIF standard)

REFERENCES

- [1] <http://p-therapie.web.psi.ch/e/proscan.html>.
- [2] ICRU Report 49, {Stopping Powers and Ranges for Protons and Alpha Particles, (1992).
- [3] J.F. Janni, Atomic Data and Nuclear Data Tables, {27, 147, (1982).
- [4] J.F. Ziegler, The Stopping and Range of Ions in Matter {<http://srim.org>}, (2008).

SPACE WEATHER OBSERVATIONS WITH SREM RADIATION MONITORS

D. Marinov, W. Hajdas, N. Schlumpf (PSI), L. Desorgher (SpaceIT), H. Evans, P. Nieminen (ESA-ESTEC)

The Standard Radiation Environment Monitor is a product of the collaboration between PSI, ESA and Oerlikon-Space. Five SREM devices are already flying on satellites providing continuous data about radiation environment in the interplanetary space and Earth magnetosphere. We report on measurements and propagation features of Solar Energetic Particles as well as present first data from SREM onboard of the ESA Galileo Giove-B mission.

SREM – DETECTOR FOR DOSIMETRY IN SPACE

The ESA Standard Radiation Environment Monitor (SREM) is a particle detector developed with the main purpose of permanent monitoring of the space radiation environment and providing alerts of radiation related hazards to the spacecraft. Four SREM instruments are launched onboard of ESA satellites including its new GPS mission GIOVE-B. SREM offers fair spectral and directional sensitivity thus allowing for precise quantitative studies of the radiation environment in the Solar system.

SPACE WEATHER AND SREM

Space weather is an environmental concept that refers to the dynamic conditions in the space contiguous to Earth, interplanetary, and interstellar space. Wide variety of physical phenomena influences space weather. This includes Solar events like Coronal Mass Ejections (CME) and Solar flares, Galactic Cosmic Rays (GCR), spectral hardening and intensity variations in the Van Allen radiation belts, geomagnetic storms, ionospheric disturbances, geomagnetically induced currents at Earth's surface, etc. [1]. Space weather has impact on several areas generally related to the spacecraft operation and functioning of the ground-based communication systems. Geomagnetic storms, due to increased solar activity can potentially blind sensors aboard spacecraft, or interfere with on-board electronics. An understanding of space environmental conditions is also important in designing shielding and life support systems for manned spacecrafts. In addition, there is justified concern that geomagnetic storms may expose conventional aircraft flying at high latitudes to increased amounts of radiation.

SREM was developed by the Paul Scherrer Institute (PSI) and was manufactured by Contraves Space AG under a contract with the European Space Agency (ESA). Ten SREM units have been produced. Four of them are in operation onboard of PROBA-I, INTEGRAL, ROSETTA and GIOVE-B satellites. Two additional units are scheduled for launch onboard of HERSCHEL and PLANCK satellites in 2009. SREM is capable of measuring fluxes of highly energetic charged particles coming within $\pm 20^\circ$ of its pointing direction and exhibits fair spectral resolution. Multiple, individually calibrated radiation monitors provide the unique possibility of mapping the radiation environment and comparing in-flight data for the same time periods in different regions of the magnetosphere. In addition, verification of the space radiation models (i.e. AP-8 [2]).

SOLAR ENERGETIC PARTICLES

With SREM detectors at different locations in the Solar System one can study spectral and spatial properties of Solar Energetic Particles SEP. Fig. 1 presents

measurements of such events performed with 3 instruments. Clear differences seen in the occurrence and intensities allow for accurate characterization of these events

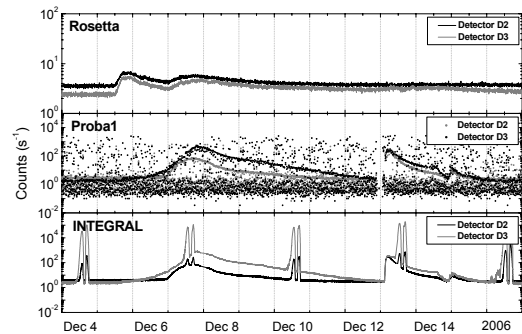


Fig. 1: SREM total counts from ROSETTA, PROBA-I and INTEGRAL during several solar particle events starting on 5 December 2006.

FIRST DATA FROM GIOVE-B

The second Galileo In-Orbit Validation Element (GIOVE-B) part of the future ESA Galileo positioning system was launched on 27 April 2008 aboard Soyuz-FG/Fregate rocket launcher from Baikonur, Kazakhstan. GIOVE-B is a 530 kg spacecraft and is positioned at Middle Earth Orbit (MEO) of 22 300 km.

The path of GIOVE-B crosses the outer electron radiation belt. Example of the data is presented in Fig. 2. It shows the total counts of SREM detectors D1, D2 and D3 during GIOVE-B single passage through the outer electron radiation belt. The readings are interpreted so that D3 represents electron fluxes for energies higher than 0.5 MeV, D1 - higher than 2.0 MeV and D2 – higher than 2.8 MeV.

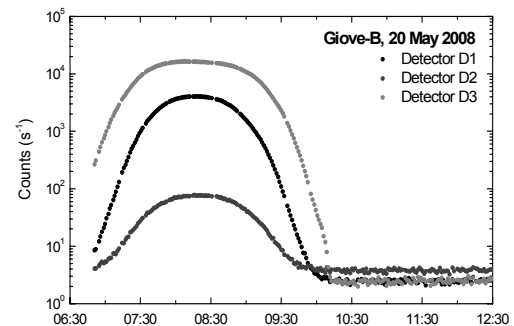


Fig. 2: Giove-B single passage through the outer e-belt.

REFERENCES

- [1] D.N. Baker, "What is space weather?", *Adv. Space Res.* Vol. **22**, No. 1, (1998), pp. 7–16.
- [2] J. Vette, "The AE-8 trapped electron environment," *NSSDC/WDC-A-R&S*, (1991)

DIRECT MEASUREMENTS OF SMALL RADIOCARBON SAMPLES AFTER OXIDATION IN QUARTZ TUBES

S. Fahrni, M. Ruff, H.W. Gägger (Univ. Bern & PSI), S. Szidat (Univ. Bern), L. Wacker, I. Hajdas (ETHZ)

Small ^{14}C samples gain importance in environmental research and for dating purposes. However, throughput of such samples is limited by the preparation of graphite targets for accelerator mass spectrometry (AMS) measurements. In our approach, oxidation of samples with copper oxide in quartz tubes was applied to form CO_2 which was measured directly with the gas ion source of the small AMS facility MICADAS.

INTRODUCTION

Sample combustion by means of copper oxide oxidation in quartz tubes and subsequent graphitisation is a common procedure in many ^{14}C and AMS laboratories and is well-established [1]. However, since there is a strong demand for measurements of small samples ($<100\ \mu\text{g C}$), for example in environmental science [2] and dating of ice cores [3], it is appropriate to adapt the sample preparation to these sample sizes. Because the conversion of CO_2 to graphite contributes to contaminations and is moreover time consuming, we suggest an oxidation of small ^{14}C samples in quartz ampoules by means of copper oxide, followed by a direct measurement of the combustion gases with a gas ion source. To prove the feasibility of the suggested method, the influence of gaseous combustion byproducts and other gases on AMS measurements was investigated and reference materials were analysed accordingly.

EXPERIMENTAL

For the sample preparation, quartz tubes closed at one end were used (4.0 mm O.D., 3.5 mm I.D., l: 15 cm). About 0.1 g copper oxide were filled into the quartz tubes which were then heated up to $950\ ^\circ\text{C}$ in a muffle furnace for 2 h. Sample material was weighed on a microgram balance and filled into the quartz tubes. The tubes were then plugged into a gastight Ultra-Torr port and evacuated to about 1 mbar with an oil-free turbo scroll pump for 5 minutes each. After evacuation, the tubes were sealed with a propylene/oxygen flame. For combustion, the ampoules were heated up to $950\ ^\circ\text{C}$ for 2 h.

We used NIST OX-2, IAEA C5 and C7 as reference materials and coal as a blank material. They were weighed, filled into tubes and processed following the described method. For the drying of combustion gases in the cracker system, we used drying shells which were prepared in our lab and consisted of CaSO_4 pressed into short pieces of aluminium tubing. After drying, the sample was flushed into a gas tight syringe with helium as a carrier gas [4]. Finally a mixture of 5% CO_2 in He was fed into the gas ion source with a flow of $36\ \mu\text{l}/\text{min}$ for the measurement.

RESULTS

Tests with artificial gas mixtures have shown a strong effect of H_2O on the ionisation efficiency of CO_2 . A water content of 15% in the sample reduced the C^- current to about one third (Figure 1). The removal of water is therefore crucial for high C^- currents and has to be performed prior to every measurement. Other combustion byproducts do not need to be removed.

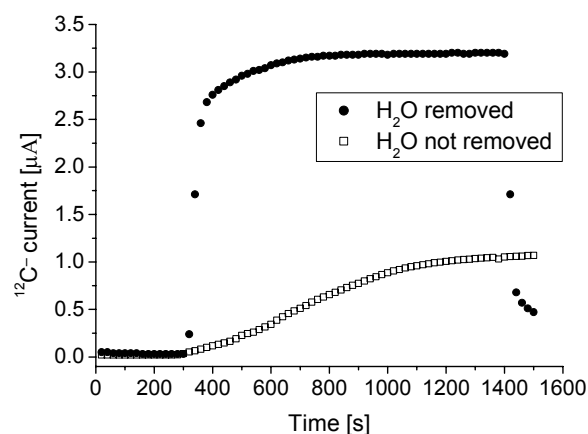


Fig. 1: $^{12}\text{C}^-$ courses of small samples with and without water removal.

Reference materials with 14 to $38\ \mu\text{g C}$ were prepared and measured under stable conditions and with high C^- currents after water removal. Results are summarised in Table 1. 68% of the ^{14}C values lie within the 1σ interval and 95% within the 2σ interval, which demonstrates a good agreement with normal distribution. Moreover, the $\delta^{13}\text{C}$ data gives evidence that no significant isotopic fractionation took place. The presented method has also been shown to be suitable for ^{14}C measurements of aqueous samples when water is gently evaporated prior to sample combustion. Blank values with coal were determined to $0.95\ \text{pmC}$ ($38'000$ years).

Tab. 1: Weighted averages and averaged uncertainties of IAEA C5 and C7 and NIST OX-2 reference materials.

C5	average	$22.35 \pm 0.35\ \text{pmC}$
(n=6)	nominal	$23.05 \pm 0.02\ \text{pmC}$
C7	average	$49.03 \pm 0.47\ \text{pmC}$
(n=8)	nominal	$49.53 \pm 0.12\ \text{pmC}$
OX-2	average	$134.14 \pm 1.00\ \text{pmC}$
(n=8)	nominal	$134.07\ \text{pmC}$

REFERENCES

- [1] I. Hajdas et al., Nucl. Instr. and Meth. B **223-224**, 267-271 (2004).
- [2] S. Szidat, et al., Radiocarbon **46**, 475-484 (2004).
- [3] T. M. Jenk, et al., Nucl. Instr. and Meth. Phys. B **259**, 518-525 (2007).
- [4] M. Ruff et al., Radiocarbon **49**, 307-314 (2007).

A PREPARATIVE 2D-CHROMATOGRAPHY METHOD FOR COMPOUND-SPECIFIC RADIOCARBON MEASUREMENTS OF AEROSOL COMPONENTS

S. Fahrni, H.W. Gäggeler, M. Ruff (Univ. Bern & PSI), S. Szidat (Univ. Bern), L. Wacker (ETHZ)

Compound-specific radiocarbon measurements offer a unique tool for the assessment of the sources of environmental pollutants. Previously, a HPLC method for the separation of oxalic acid from carbonaceous aerosols has been developed. In practice, high matrix contents in aqueous aerosol extracts led to an overloading of the HPLC column. In order to overcome this problem, the separation method was refined: a high capacity anion chromatography column was used which can deal with the high loading. The new procedure was tested with certified oxalic acid ^{14}C reference materials.

INTRODUCTION

Oxalic acid and other small dicarboxylic acids in carbonaceous aerosols have received much attention recently. Biogenic and fossil emissions as well as wood burning are thought to contribute precursors for a secondary formation of dicarboxylic acids [1]. Nevertheless, sources of those compounds in aerosols are subject to speculations. In order to give further insight into sources and formation processes of dicarboxylic acids, a compound-specific radiocarbon measurement is the method of choice. In our approach, the separation of compounds is achieved through liquid chromatography and the radiocarbon measurement is conducted with accelerator mass spectrometry (AMS). Since the carbon amounts needed for such ^{14}C measurements are in the low microgram level, very high amounts of aerosols on air filters are necessary. A developed HPLC method was applied to concentrated aerosol extracts which revealed a heavy overloading of the column by inevitable matrix components. Since a good separation of the compound of interest from other organic compounds is a prerequisite for radiocarbon determination, matrix problems have to be overcome. In order to solve this problem, a pre-separation is needed.

EXPERIMENTAL

An anion chromatography column (IonPac AS 11HC, Dionex) was used in a 30 min hydroxide gradient run to remove neutral components and to separate oxalate roughly from other inorganic and organic anions as for example humic-like substances. The ion chromatography was therefore operated in a manner that allows the recovery of the eluted analyte by fraction collection.

Tests with artificial solutions of certified oxalic acid ^{14}C reference materials (IAEA C7 and NIST OX-2 [2]) containing sulphate, malonic, maleic, malic and succinic acid and humic acid were performed to simulate real samples and possible contaminations (Figure 1).

50 μl of the artificial mixtures were injected into the ion chromatography manually in order to obtain high yields. Fractions of the peaks were collected in PFA vials and dried at 40°C under a stream of nitrogen. The dried eluate was then redissolved in 25 μl water, injected into the HPLC and separated on an Acclaim OA column with an isocratic run (eluent: aqueous HCl, 5mM, pH 2.3) within 15min. Fractions were collected and dried again. The oxalic acid fractions were redissolved in H_2O and put into baked out quartz tubes for subsequent drying and combustion for gaseous ^{14}C measurements [2].

RESULTS

The top of Figure 1 shows the ion chromatography run upon injection of an artificial mixture of humic acid, malonic, maleic, malic and succinic acid with sulphate and oxalic acid reference materials (Step 1). Given a high loading of 1000 ppm sulphate, the separation is still good. HPLC is used to assure the purity of oxalic acid in a second separation step and for further separation in real samples (Step 2). ^{14}C measurements of the processed samples with the gas ion source of MICADAS [3] confirm a good agreement of the measured values with nominal values. This indicates a complete separation of oxalic acid from other compounds. The over-all yield of the presented procedure is about 50%. Depending on the amounts present in aerosol samples, also other dicarboxylic acid fractions can be collected and measured with AMS.

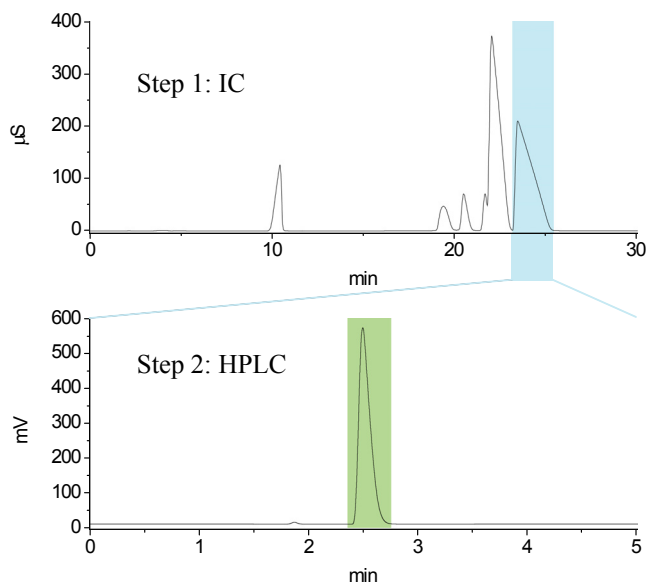


Fig. 1: Top: IC run with humic acid, different dicarboxylic acids, sulphate and oxalic acid ^{14}C reference material (blue).

Below: HPLC chromatogram of the fraction collected with IC. The green fraction was collected for a subsequent ^{14}C measurement.

REFERENCES

- [1] M. Legrand et al., J. Geophys. Res. **112**, D23S07 (2007).
- [2] S. Fahrni et al., this report p. 47.
- [3] M. Ruff et al., Radiocarbon **49**, 307–314 (2007).

SEPARATION OF ORGANIC AND ELEMENTAL CARBON FOR ^{14}C ANALYSIS

N. Perron, A. Prévôt, U. Baltensperger (PSI LAC), S. Szidat, S. Fahrni, M. Ruff (Univ. Bern & PSI)

A three-step thermal method to separate EC and OC for ^{14}C analysis was investigated by running a Sunset EC/OC analyzer under pure oxygen. Results from Göteborg samples are comparable with those measured with a former method, except for the winter EC, where the higher ^{14}C values suggest a better recovery of the biomass-burning EC.

MOTIVATIONS

Carbonaceous aerosol is traditionally divided into two sub-fractions: the non-refractory, very weakly light-absorbing organic carbon (OC) and the refractory, highly polymerised and light-absorbing elemental carbon (EC). Whereas OC mainly stems from non-fossil sources such as biogenic production or biomass-burning, EC predominantly originates from fossil, ^{14}C -depleted sources [1]. Consequently, any relevant ^{14}C -based source apportionment of carbonaceous aerosol requires the physical separation of OC and EC, even if no real sharp boundary separates them, but rather a continuous increase of thermochemical refractiveness and specific optical absorption [2]. The thermal separation method Theodore [3] used so far does not allow assessing two major artefacts linked to the sample heating, which are OC charring to EC and EC/OC co-volatilisation. Using a thermo-optical device enables to monitor EC production or removal during analysis and to investigate the best condition to separate and recover OC and EC with high yields.

METHODS

Filter samples from three different conditions (rural winter, urban winter and urban summer) were water-extracted so as to reduce their charring potentials. They were analysed with a thermo-optical device (*RT 3080, Sunset Laboratory Inc.*) using a three-step thermal method under pure O_2 (Fig. 1).

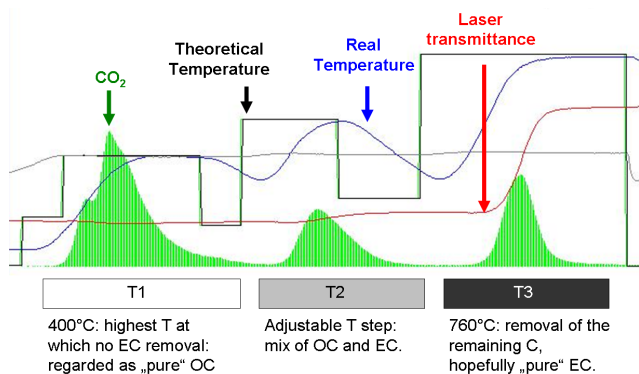


Fig. 1: Three-step thermogramme for an ambient aerosol analysed with a thermo-optical device under pure O_2 .

Filter attenuation during analysis was calculated from the laser transmittance in order to assess the EC production and removal and used to calculate the yield and OC content of EC in the T3 step. T2 was investigated so as to find the best compromise between a high EC recovery and a low OC content in the last step and values of 530°C and 550°C were chosen for the winter and summer samples, respectively.

RESULTS AND DISCUSSION

Fig. 2 shows that the attenuation increase due to charring is strongly reduced by using pure oxygen and water-extracted filters [3]. For all these samples, we regarded charring as negligible.

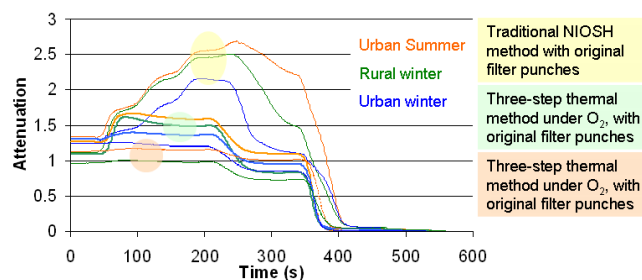


Fig. 2: Attenuation variation for three types of samples under different analysing conditions.

The CO_2 emitted at each thermal step was quantitatively recovered for ^{14}C analysis. The results for the T1 and T3 fractions were compared with those from the Theodore method (Fig. 3).

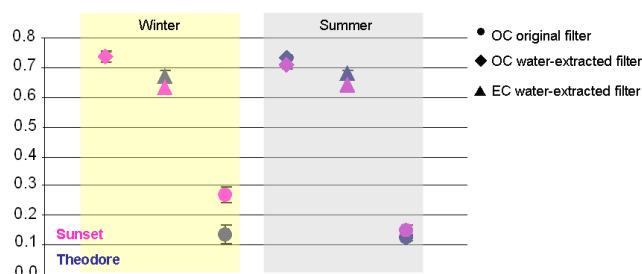


Fig. 3: ^{14}C values (as fractions of modern carbon) for winter and summer samples from Göteborg.

The agreement is good, except for EC in winter where the Sunset method shows a higher ^{14}C value. This suggests that the mainly winter-emitted, biomass-burning EC, which is less refractory than fossil EC, is better recovered with this method.

REFERENCES

- [1] S. Szidat et al., (2006): *J. Geophys. Res.* 111, D07206, doi:10.1029/2005JD006590.
- [2] U. Pöschl, (2005): *Angew. Chem. Int. Ed.* 2005, 44, 7520 – 7540.
- [3] S. Szidat et al., (2004): *Nucl. Instrum. Methods Phys. Res., Sect. B*, 223-224, 829-836.
- [4] S. Szidat et al., (2008): *Atmos. Chem. Phys. Discuss.*, 8, S7986–S7987.

OPTIMISATION OF GRAPHITISATION PROCEDURE AT AGE-1

M. Němec (Univ. Bern), L. Wacker (ETHZ)

The Automated Graphitisation Equipment (AGE-1) was developed at ETH Zurich to produce solid targets for ^{14}C measurement with accelerator mass spectrometry (AMS). AGE-1 was designed to use the CO_2 reduction by H_2 to graphite on the iron catalyst. For such a system, the optimisation of the reaction conditions was necessary.

INTRODUCTION

Graphitisation of samples is required for high-precision AMS ^{14}C measurement. AGE-1 was designed as a compact system for routine sample preparation [1]. It uses a column with zeolite absorber to trap the CO_2 produced from sample combustion in elemental analyzer; CO_2 is then thermally released to the reactor. The procedure is described in Fig. 1.

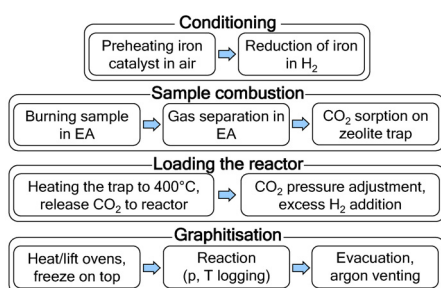


Fig. 1: AGE-1: Sample preparation procedure [1].

The main goal of optimisation procedure was to find conditions for the fastest reaction completion and the smallest isotopic fractionation without formation of molecular fragments or hydrocarbons. The tuned parameters were reaction temperature, H_2/CO_2 ratio, reaction time, preconditioning of iron catalyst and the suitable timing for each step of the whole procedure.

EXPERIMENTAL

Each of the 4.4 mL reactors consists of two vertically mounted vials, a heated reaction vial at the bottom and a cooled water trap vial on top (Fig. 2). The upper part of the reactor is cooled during the reaction by Peltier cooler to temperatures $< -10^\circ\text{C}$ and the bottom vial can be heated by an electric oven up to 700°C . The pressures and temperatures during a reaction are logged as function of time. For the optimisation, about 3 mg of the pure iron catalyst (Alfa Aesar iron -325 mesh) and 400 mbar of blank CO_2 (3.0 purity) were used.

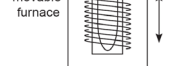


Fig. 2: AGE-1 reactor scheme.

RESULTS AND DISCUSSION

CO_2 was graphitised using different parameters; the temperature range 545 to 620°C and H_2/CO_2 ratio 1.9 to 2.5 were tested. Resulting graphite samples were measured by AMS with the MICADAS system [2] to determine the smallest isotopic changes ($\delta^{13}\text{C}$) at minimum of molecular

fragment formation (^{13}CH current) and reaction time (Fig. 3). The catalyst preconditioning routine was tuned with respect to final reaction time and pressure profile over time.

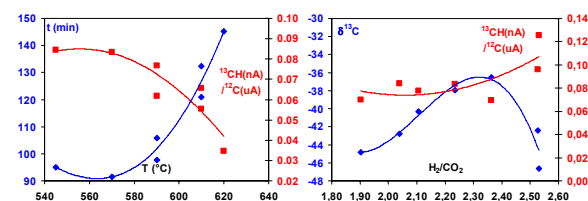


Fig. 3: Trends of fractionation ($\delta^{13}\text{C}$) and normalized ^{13}CH molecular current on temperature and H_2/CO_2 ratio.

It was found that the catalyst oxidation with air at the beginning of the conditioning step significantly reduces the reaction time. Finally, 580°C and 2.3 H_2/CO_2 together with the 150 s catalyst preheating were used and reaction time was reduced from >3 hours to <2 hours. That allowed additional heating for 20 minutes to minimize isotopic fractionation. Now the whole procedure, including sample combustions and sample transfers to all 7 reactors, takes only approx. 4.5 hours. A pressure-time record of the graphitisation procedure is shown on the Fig. 4.

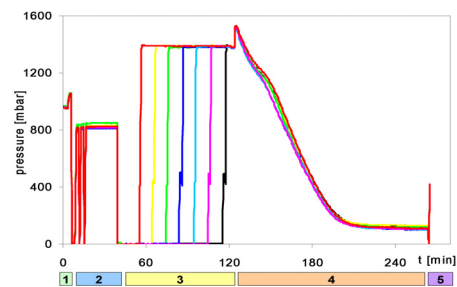


Fig. 4: Pressure record of the optimised (580°C , 2.3 H_2/CO_2 ratio) graphitisation procedure: 1-iron preheating with air, 2-iron cleaning with H_2 , 3-loading reactors, 4-reaction, 5-argon flushing.

ACKNOWLEDGEMENT

We are very grateful to the Paul Scherrer Institut and University of Bern for financial support.

REFERENCES

- [1] L. Wacker et al., Nucl. Instr. Meth. Phys. Res. B, submitted.
- [2] H.-A. Synal et al., Nucl. Instr. Meth. Phys. Res. B, **259**, 7-13 (2007).

ONLINE RADIOCARBON MEASUREMENTS OF MICRO-SCALE SAMPLES USING ELEMENTAL ANALYSER AND AMS

*M. Ruff, S. Fahrni, H.W. Gäggeler (Univ. Bern & PSI), S. Szidat (Univ. Bern),
H.-A. Synal (ETHZ & PSI), L. Wacker, M. Suter (ETHZ)*

An online measurement system was installed at the MICADAS in Zurich, using an elemental analyser (EA) as combustion unit, to make direct radiocarbon (^{14}C) measurements of samples containing carbon in the range of 5-80 μg possible with minimum effort.

INTRODUCTION

The gas ion source of the small 200 kV accelerator mass spectrometer (MICADAS) at ETH Zurich [1] has become a routinely used sample introduction system for radiocarbon measurements of small samples (<80 μg carbon). Most of the >500 samples measured within the last two years have been handled with our ampoule cracker system. This method is very useful for small samples containing carbon in the range of 1-40 μg . However, this method requires a relatively large effort to combust the samples and to transfer them to glass tubes for the measurement. Online sample combustion with direct AMS measurement provides a more efficient and cost-effective solution. Such systems can completely be automated. Due to the small sample masses, precision is limited at the moment to approximately 1% [1]. However, there is an increasing potential for samples which do not have to be measured very precisely, but in a large number e.g. in the field of biomedical or environmental research.

INSTRUMENTAL SETUP

An elemental analyser serves as combustion unit. The sample material is stored in small tin capsules and burned in an enriched oxygen atmosphere at temperatures of about 1000 °C. Combustion gases are separated chromatographically and the sample CO_2 leaves the analyser in an 80 ml/min He stream. For enrichment, the CO_2 is trapped on an external column filled with X13 zeolite material. To avoid unnecessary dead volumes in the system, the column was constructed to be as small as possible. The column in use has dimensions of 11 mm x 3.2 mm ID containing just 61 mg of the zeolite. By heating the column from room temperature to about 450 °C, the CO_2 is released and flushed with a very low helium flow into the syringe of the gas inlet system of the MICADAS gas ion source. The system was validated and is now ready for measurements.

RESULTS

For the external column, a trapping and releasing recovery of 95-100% was observed for CO_2 amounts containing up to 80 μg carbon. Recoveries for samples containing >80 μg carbon resulted in slightly decreased values of 90-95%, which is the consequence of a starting breakthrough of the small trap. But the good desorption properties of a small trapping system are essential to avoid cross-contamination effects between samples. Systematic tests with succeeding standard and blank samples resulted in a sample cross-contamination effect of <0.4%.

The method is limited by a constant blank contribution which is caused by the tin capsules used for sample storage. Ten different materials, capsules and foils have been tested. Lowest carbon contaminations were found in 25 μl tin capsules of about 35 mg mass, containing $0.33 \pm 0.17 \mu\text{g}$ carbon ($65 \pm 6 \text{ pmC}$). This contribution can be corrected using a model of constant contamination. As the effect of this contamination is increasing exponentially with smaller sample sizes, the online method cannot be used for samples <10 μg carbon.

The method was validated measuring a number of certified IAEA C5 and C7 reference materials. Five samples in the range of 14-26 μg carbon for the C5 standard (nominal value: 23.05°pmC) and seven samples in the range of 15-36 μg carbon for the C7 standard (49.54 pmC) were determined to average values of $22.64 \pm 0.31 \text{ pmC}$ and $49.07 \pm 0.38 \text{ pmC}$, respectively. The calculated mean of means is not significantly different from the nominal value (t-test) for both standard materials.

Tab. 1: Validation data with different materials compared to solid graphite samples with the value of the reduced χ^2 test over all results.

Material	Weight $\mu\text{g C}$	$^{12}\text{C}^+$ μA	^{14}C age gas MICADAS	^{14}C age solid TANDEM
Bone	22	1.0	9208 ± 240	9205 ± 75
Bone	27	1.1	8451 ± 205	8565 ± 90
Charcoal	18	0.9	501 ± 152	715 ± 50
Charcoal	20	1.0	876 ± 135	1105 ± 50
Textile	11	1.0	1777 ± 181	1525 ± 45
Textile	23	1.1	520 ± 119	435 ± 40
Tooth	21	1.0	2095 ± 146	2070 ± 55
red χ^2			0.99 (n=7)	

Additionally, seven samples of different materials previously analysed as 2 mg graphite samples at the 6 MV EN Tandem accelerator, were measured with the online gas analysing system. The results are given in Table 1. These results were in perfect statistical agreement with the previous analysed results.

REFERENCES

- [1] M. Ruff et al., Radiocarbon, **49**(2), 307 (2007).
- [2] T. Schulze-König et al., submitted to NIMB.

COMPOUND-SPECIFIC RADIOCARBON DATING OF VARIOUS SOIL COMPONENTS

S. Schmoker, H.W. Gäggeler (Univ. Bern & PSI), S. Szidat, H. Veit (Univ. Bern), L. Wacker, I. Hajdas (ETHZ)

The age determination of soil layers by radiocarbon dating methods depends strongly on the composition of the analysed material and its origin. Hence the applied pretreatment method to isolate organic material from soil samples plays an important role. We compared humic acid, cellulose and glucose extracts from soil and wood samples from an alluvial fan near Interlaken.

INTRODUCTION

For investigations of the dynamics of alpine rivers, soil samples were taken from the alluvial fan of the Lüscher river in the region of Interlaken [1]. For stratigraphical purposes the ages of these soil samples were determined by radiocarbon dating methods. For some of the samples the obtained ages were much older than the samples from proximate layers. These complications were the motivation to investigate the radiocarbon age of different soil components. The goal was to use different pretreatment methods for isolation of soil components which were chemically stable and have not been transported vertically since the time of their deposition in the soil.

EXPERIMENTAL

Three different pretreatment methods were applied to isolate humic acids, cellulose and glucose from the soil samples.

The isolation of the humic acids was performed by dissolution of the carbonates using 10% HCl, extraction of the humic acids with 10% NaOH and precipitation of the humic acids by acidification of the extract to a pH 2 [2]. Cellulose was isolated from wood pieces in a bleaching process with sodium chlorite and HCl with precedent toluol/ethanol (2:1) and ethanol soxhlet extraction [3] (Fig. 1).

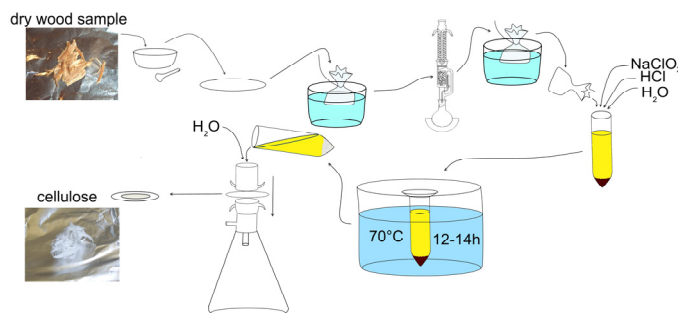


Fig. 1: Bleaching procedure of wood material from the soil samples.

In order to isolate glucose, wood particles and soil materials were hydrolysed in 37% HCl solution for 4 hours at 55° C. The purification of the glucose from the hydrolysate was performed by preparative thin-layer chromatography [4]. The isolated material was then graphitised at the AGE-1 graphitisation device [5] and measured at the small AMS-facility MICADAS at ETH Zürich.

RESULTS

The radiocarbon measurements of cellulose and humic acid extracted from the two peat samples P2 and P3 gave similar

results (Fig.2). For the sediment sample IN-10.25, the much older age (6450±130 BP) compared to the neighbouring wood sample IN-10.24 (2160±20 BP) from the previous investigation [1] could not be reproduced with our pretreatment methods. The discrepancy between humic acid and cellulose calls for further investigation.

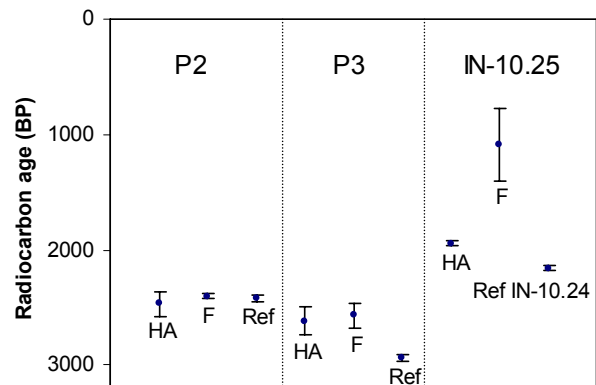


Fig. 2: Radiocarbon ages of the humic acids (HA), cellulose (F) and the previous measurements from other radiocarbon dating laboratories (Ref) for the peat samples P2, P3 and the sediment sample IN-10.25 [1].

However the purity of the isolated cellulose and humic acid is limited because of their high-molecular structures and thus not well defined chemical properties. For the cellulose, this limitation was avoided by hydrolysing the cellulose to glucose. Due to a contamination with eluent in the chromatographic purification step, the results for glucose could not be considered in this comparison. Nevertheless, the experiments pointed out that oligosaccharides can be isolated from soil samples with our technique, even if wood pieces are not macroscopically identifiable.

OUTLOOK

The above mentioned problems of glucose purification might be solved by applying a preparative HPLC method [6]. This combination of acid hydrolysis with a subsequent HPLC purification step seems to be a suitable pretreatment method for any cellulose containing materials.

REFERENCES

- [1] L. Schulte et al., *Geomorphology*, accepted (2008).
- [2] I. Hajdas, PhD Thesis ETH Zürich (1993).
- [3] S.W. Leavitt and S.R. Dancer, *Anal. Chem.* **65**, 87-89 (1993).
- [4] E. Seo et al., *Biosci. Biotechnol. Biochem.* **68**, 1146-1148 (2004).
- [5] M. Nemeč et al., this Annual Report, p. 50.
- [6] S. Fahrni et al., this Annual Report, p. 48.

FOSSIL AND NON-FOSSIL SOURCES OF ORGANIC CARBON (OC) AND ELEMENTAL CARBON (EC) IN GÖTEBORG, SWEDEN

S. Szidat, M. Ruff (Univ. Bern), N. Perron (PSI LAC), L. Wacker, H.-A. Synal (ETHZ), M. Hallquist, A.S. Shannigrahi (Univ. Göteborg), K.E. Yttri, C. Dye (NILU), D. Simpson (NMI)

Sources of carbonaceous particulate matter from an urban and a rural site at Göteborg were apportioned by ^{14}C measurements of OC and EC. Whereas the urban site was largely influenced by fossil sources during winter, the rural site was more dominated by wood-burning emissions. During summer, biogenic SOA was the largest source.

INTRODUCTION

Airborne particulate matter (PM) influences the global radiation balance and causes respiratory and cardiopulmonary diseases. Carbonaceous aerosols (total carbon, TC) are a major fraction of PM. They are distinguished into optically absorptive and highly polyaromatic elemental carbon (EC) and the low-molecular-weight fraction organic carbon (OC). In spite of the importance of the carbonaceous aerosol, detailed apportionment and quantification of its sources is still difficult due to the large number of sources and the vast number of organic compounds associated with the aerosol. Radiocarbon (^{14}C , $T_{1/2} = 5730$ a) measurements of the carbonaceous aerosol offer the unique opportunity of a direct distinction of fossil and non-fossil sources. Due to its age, ^{14}C has completely disintegrated in fossil substances, whereas modern plant material is on the contemporary radiocarbon level.

METHODS

In February/March 2005 and June/July 2006, aerosol samples were collected on quartz fibre filters for subsequent analysis of its carbonaceous content during the Göte-2005 campaign in the area of Göteborg, Sweden [1]. Sampling during winter was conducted simultaneously at the urban site Femman and the rural EMEP site Råö (SE14), which is located 35 km south of Göteborg. During summer, sampling was conducted at the urban site only.

OC and EC were separated from the filters with a step-wise oxidation as described elsewhere [1, 2]. ^{14}C measurements were performed at the ETH accelerator mass spectrometry (AMS) facility using the gas ion source of the 200 kV mini-radiocarbon dating system MICADAS [3]. Levoglucosan was determined with HPLC-HRMS-TOF [4]. EC was distinguished into fossil ($\text{EC}_{\text{fossil}}$) and wood-burning (EC_{wood}) emissions. OC was separated into fossil ($\text{OC}_{\text{fossil}}$) and non-fossil ($\text{OC}_{\text{nonfossil}}$) sources, of which the second fraction comprises biogenic (OC_{bio}) and wood-burning (OC_{wood}) emissions. In order to differentiate between the latter two sources, OC_{wood} is estimated using two independent techniques, namely EC_{wood} and levoglucosan measurements using average emission ratios for residential wood burning in fireplaces [1].

RESULTS AND DISCUSSION

Source apportionment of the carbonaceous aerosol is summarized in Fig. 1. During the winter campaign, the urban impact was more pronounced for the urban site compared to the rural site, as seen from the higher carbonaceous aerosol concentration and a higher EC/TC

ratio. Furthermore, the contribution of fossil sources was relatively larger at the urban site as shown by the EC fraction, which originated nearly exclusively from fossil sources. The rural characteristics of the Råö site gave rise to relative importance of wood burning, which was indicated by the elevated contributions of OC_{wood} and EC_{wood} .

The presence of OC_{bio} during winter is consistent with model calculations suggesting that biogenic SOA can be formed in Scandinavia in the cold season [5]. For summer, OC_{bio} was even the dominating source.

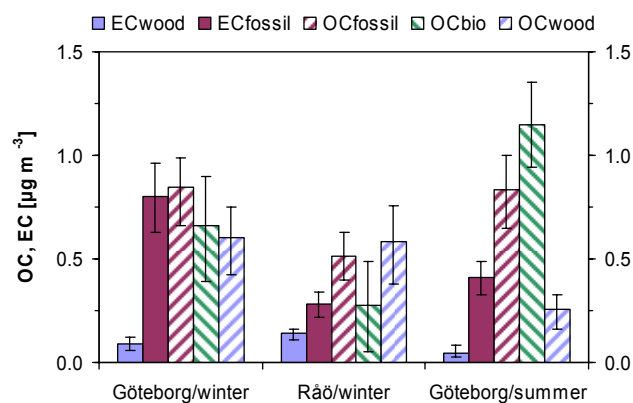


Fig. 1: Average concentrations of different carbonaceous particle fractions for the three campaigns [1]. Uncertainty bars represent 10th and 90th percentiles.

ACKNOWLEDGEMENT

This work was partly supported by the European Network of Excellence ACCENT, the Swedish Foundation for Strategic Environmental Research MISTRA, the Norwegian SORGA project, the EU Program No.036833-2 (EUCAARI), and the EMEP network.

REFERENCES

- [1] S. Szidat et al., Atmos. Chem. Phys. Discuss., **8**, 16255 (2008).
- [2] S. Szidat et al., Radiocarbon, **46**, 475 (2004).
- [3] M. Ruff et al., Radiocarbon, **49**, 307 (2007).
- [4] C. Dye and K.E. Yttri, Anal. Chem., **77**, 1853 (2005).
- [5] D. Simpson et al., J. Geophys. Res., **112**, D23S14, 2007.

LIST OF PUBLICATIONS

HEAVY ELEMENTS

R. Eichler, N.V. Aksenov, A.V. Belozerov, G.A. Bozhikov, V.I. Chepigin, R. Dressler, S.N. Dmitriev, H.W. Gäggeler, V.A. Gorshkov, F. Haenssler, M.G. Itkis, V.Y. Lebedev, A. Laube, O.N. Malyshev, Yu.Ts. Oganessian, O.V. Petruschkin, D. Piguet, P. Rasmussen, A. Serov, S.V. Shishkin, A.V. Shutov, A.I. Svirikhin, E.E. Tereshatov, G.K. Vostokin, M. Wegrzecki, A.V. Yeregin

Thermochemical and physical properties of element 112
Angew. Chem. Int. Ed., **47**(17), 3262-3266 (2008).

R. Eichler, N.V. Aksenov, A.V. Belozerov, G.A. Bozhikov, V.I. Chepigin, R. Dressler, S.N. Dmitriev, H.W. Gäggeler, V.A. Gorshkov, F. Haenssler, M.G. Itkis, V.Y. Lebedev, A. Laube, O.N. Malyshev, Yu.Ts. Oganessian, O.V. Petruschkin, D. Piguet, P. Rasmussen, A. Serov, S.V. Shishkin, A.V. Shutov, A.I. Svirikhin, E.E. Tereshatov, G.K. Vostokin, M. Wegrzecki, A.V. Yeregin

Thermochemische und physikalische Eigenschaften von Element 112
Angew. Chem. **120**(17), 3306-3310 (2008).

J.M. Gates, M.A. Garcia, K.E. Gregorich, Ch.E. Düllmann, I. Dragojević, J. Dvorak, R. Eichler, C.M. Folden, W. Loveland, S.L. Nelson, G.K. Pang, L. Stavsetra, R. Sudowe, A. Türler, H. Nitsche

Synthesis of rutherfordium isotopes in the $^{238}\text{U}(^{26}\text{Mg}, xn)^{264-x}\text{Rf}$ reaction and study of their decay properties
Phys. Rev. C **77**, 034603 (2008).

S.L. Nelson, C.M. Folden III, K.E. Gregorich, I. Dragojevich, Ch.E. Düllmann, R. Eichler, M.A. Garcia, J.M. Gates, R. Sudowe, H. Nitsche

Comparison of complementary reactions for the production of $^{261,262}\text{Bh}$
Phys. Rev. C **78**, 024606 (2008).

SURFACE CHEMISTRY

J. Abbatt, T. Bartels-Rausch, M. Ullerstam, T. Ye

Uptake of acetone, ethanol and benzene to snow and ice: Effects of surface area and temperature
Env. Res. Let. **3**(4), 045008 (2008).

T. Bartels-Rausch, T. Huthwelker, M. Jöri, H.W. Gäggeler, M. Ammann

Interaction of gaseous elemental mercury with snow surfaces: Laboratory investigation
Env. Res. Let. **3**(4), 045009 (2008).

M. Kerbrat, B. Pinzer, T. Huthwelker, H.W. Gäggeler, M. Ammann, M. Schneebeli

Measuring the specific surface area of snow with x-ray tomography and gas adsorption: Comparison and implications for surface smoothness
Atmos. Chem. Phys. **8**(5), 1261-1275 (2008).

M. Ndour, B. D'Anna, C. George, O. Ka, Y. Balkanski, J. Kleffmann, K. Stemmler, M. Ammann

Photoenhanced uptake of NO_2 on mineral dust: Laboratory experiments and model simulations
Geophys. Res. Let. **35**(5), L058/2 (2008).

K. Stemmler, A. Vlasenko, C. Guimbaud, M. Ammann

The effect of fatty acid surfactants on the uptake of nitric acid to deliquesced NaCl aerosol
Atmos. Chem. Phys. **8**(17), 5127-5141 (2008).

O. Vesna, S. Sjogren, E. Weingartner, V. Samburova, M. Kalberer, H.W. Gäggeler, M. Ammann

Changes of fatty acid aerosol hygroscopicity induced by ozonolysis under humid conditions
Atmos. Chem. Phys. **8**(16), 4683-4690 (2008).

ANALYTICAL CHEMISTRY

E. Dietze, A. Kleber, M. Schwikowski

Response of regional climate and glacier ice proxies to El Niño-Southern Oscillation (ENSO) in the subtropical Andes
Clim. Past. Discuss. **4**, 173-211 (2008).

S. Kaspari, R. Hooke, P.A. Mayewski, S. Kang, S. Hou, D. Qin

Snow accumulation rate on Mt. Everest: synchronicity with sites across the Tibetan Plateau on 50-100 year timescales
J. Glaciol., **45**(185), 343-352 (2008).

F. Vimeux, P. Ginot, M. Schwikowski, M. Vuille, G. Hoffmann, L.G. Thompson, U. Schotterer

Some aspects of the climate variability during the last 1,000 years from Andean ice cores: a review of recent results
Palaeogeography, Palaeoclimatology, Palaeoecology, doi:10.1016/j.palaeo.2008.03.054 (2008) in press.

RADWASTE ANALYTICS

S. Chiriki, J. Fachinger, R. Mormann

Decommissioning and safety issues of liquidmercury waste generated from high power spallation sources with particle accelerators

11th International Conference on Radiation Shielding (ICRS-11) of American Nuclear Society, Pine Mountain, Georgia, USA.

J. Neuhausen, S. Horn, B. Eichler, D. Schumann, T. Stora, M. Eller

Mercury purification in the Megawatt Liquid Metal Spallation Target of EURISOL-DS

Proceedings of the Eighth International Topical Meeting on Nuclear Applications and Utilization of Accelerators (AccApp'07), Pocatello, Idaho, July 29- August 2, 2007, American Nuclear Society, LaGrange Park, Illinois, USA.

D. Schumann, J. Neuhausen, S. Horn, P.W. Kubik, I. Günther-Leopold

Radiochemical separation and analytical determination of ¹⁰Be from proton-irradiated graphite targets

Radiochim. Acta **96** (31) (2008).

D. Schumann, J. Neuhausen

Accelerator waste as a source for exotic radionuclides

J. Phys. G: Nucl. Part. Phys. **35** 014046 (2008).

E. E. Tereshatov, H. Bruchertseifer, G.A. Bozhikov, N.V. Aksenov, G.Ya. Starodub, G.K. Vostokin, A.G. Belov,

S.V. Shishkin, S.N. Dmitriev, H.W. Gäggeler, R. Eichler, D. Schumann

Cation-exchange separation of group V elements: Model experiments on isolation and chemical identification of Db

Radiochemistry **50** (3), 290-293 (2008).

PROTON IRRADIATION FACILITY

E. Bellm, M.E. Bandstra, S.E. Boggs, W. Hajdas, K. Hurley, D.M. Smith, C. Wigger

RHESSI Spectral Fits of Swift GRBs

GAMMA-RAY BURSTS 2007: Proceedings of the Santa Fe Conference. AIP Conference Proceedings, Volume 1000, p. 154-157 (2008).

H.D.R. Evans, P. Bühler, W. Hajdas, E.J. Daly, P. Nieminen, A. Mohammadzadeh

Results from the ESA SREM monitors and comparison with existing radiation belt models

Advances in Space Research, **42**, Issue (9), p. 1527-1537 (2008).

U. Grossner, W. Hajdas, K. Egli, R. Brun, R. Harboe-Sorensen

Proton Irradiation Facility at the PROSCAN project of the Paul Scherrer Institute

Proceedings of the 8th European Workshop on Radiation Effects on Components and Systems RADECS2008, PD4 (256).

- N. Homazava, A. Shkabko, D. Logvinovich, U. Krähenbühl, A. Ulrich
Element-specific in situ corrosion behaviour of Zr-Cu-Ni-Al-Nb bulk metallic glass in acidic media studied using a novel microcapillary flow injection inductively coupled plasma mass spectrometry technique
Intermetallics **16**, 1066-1072 (2008).
- W. Hsu, A. Zhang, R. Bartoschewitz, Y. Guan, T. Ushikubo, U. Krähenbühl, R. Niedergesaess, R. Pepelnik, U. Reus, T. Kurtz, P. Kurtz
Petrography, mineralogy and geochemistry of Lunar meteorite Sayh al Uhaymir 300
Meteoritics Planet. Sci. **43**, 1363-1381 (2008).
- V.A. Lanz, M.R. Alfarra, U. Baltensperger, B. Buchmann, C. Hueglin, S. Szidat, M.N. Wehrli, L. Wacker, S. Weimer, A. Caseiro, H. Puxbaum, A.S.H. Prévôt
Source attribution of submicron organic aerosols during wintertime inversions by advanced factor analysis of aerosol mass spectra
Environ. Sci. Technol. **42**, 214-220, doi:10.1021/es0707207 (2008).
- I. Leya, M. Schönbächler, U. Wiechert, U. Krähenbühl, A.N. Halliday
Titanium isotopes and the radial heterogeneity of the solar system
Earth Planet Science Letters **226**, 233-244 (2008).
- J. Mohn, S. Szidat, J. Fellner, H. Rechberger, R. Quartier, B. Buchmann, L. Emmenegger
Determination of biogenic and fossil CO₂ emitted by waste incineration based on ¹⁴CO₂ and mass balances
Bioresour. Technol. **99**, 6471-6479, doi:10.1016/j.biortech.2007.11.042 (2008).
- J. Sandradewi, A.S.H. Prévôt, S. Szidat, N. Perron, M.R. Alfarra, V.A. Lanz, E. Weingartner, U. Baltensperger
Using aerosol light absorption measurements for the quantitative determination of wood burning and traffic emission contributions to particulate matter
Environ. Sci. Technol. **42**, 3316-3323, doi:10.1021/es702253m (2008).
- R.P.W. Struis, C. Ludwig, T. Barrelet, U. Krähenbühl, H. Rennenberg
Studying sulphur functional groups in Norway spruce year rings using S L-edge total electron yield spectroscopy
Science of the Total Environment **403**, 196-206 (2008).
- W. Tinner, C. Bigler, F.S. Hu, S. Gedye, I. Gregory-Eaves, R.T. Jones, P. Kaltenrieder, U. Krähenbühl
Boreal ecosystem responses to climatic variation in southeastern Alaska during the past seven centuries
Ecology **89**, 729-743 (2008).
- M. Viana, T.A.J. Kuhlbusch, X. Querol, A. Alastuey, R.M. Harrison, P.K. Hopke, W. Winiwarter, M. Vallius, S. Szidat, A.S.H. Prévôt, C. Hueglin, H. Bloemen, P. Wählin, R. Vecchi, A.I. Miranda, A. Kasper-Giebl, W. Maenhaut, R. Hitzenberger
Source apportionment of particulate matter in Europe: A review of methods and results
J. Aerosol Sci. **39**, 827-849, doi:10.1016/j.jaerosci.2008.05.007 (2008).

TECHNICAL REPORTS

- Y. Dai, J. Neuhausen, D. Schumann
Specimen extraction plan for MEGAPIE PIE
MEGAPIE-Report MPR-11-DY34-001-V2, 2008.
- D. Kiselev, D. Schumann, S. Teichmann, M. Wohlmuther
Berechnung des Radionuklidinventars von 3 Proben aus dem SINQ-Target 3
TM-85-08-03, PSI 25.6.2008.

REPORTS

H.W. Gäggeler, S. Szidat, E. Vogel, L. Tobler

²¹⁰Pb Messungen in Niederschlagsproben

BAG (Federal Office of Public Health) report "Umweltradioaktivität und Strahlendosen in der Schweiz 2007", Bern 2008.

W. Hajdas

Demo electronics preliminary test plan

POLAR Progress Meeting, ISDC, Versoix, 11 February 2008.

W. Hajdas

POLAR Engineeringmodel – concept of electronics

POLAR Progress Meeting, ISDC, Versoix, 11 February 2008.

W. Hajdas

Demo electronics test flow

POLAR Progress Meeting, DPNC, Geneva, 11 March 2008.

W. Hajdas

POLAR Demo electronics status

POLAR Progress Meeting, DPNC, Geneva, 4 April 2008.

W. Hajdas

POLAR engineering model and demonstration model status

POLAR Progress Meeting, ISDC, Versoix, 9 July 2008.

W. Hajdas

ProtonIrradiation facility Annual Report 2007

European SpaceAgency Internal Document.

K. Hurley, J. Goldsten, S. Golenetskii, R. Aptekar, E. Mazets, V. Pal'Shin, D. Frederiks, T. Cline, E. Bellm, D.M. Smith, R.P. Lin, J. McTiernan, R. Schwartz, C. Wigger, W. Hajdas, A. Zehnder, A. von Kienlin, G. Lichti, A. Rau, E. Del Monte, I. Donnarumma, Y. Evangelista, M. Feroci, I. Lapshov, F. Lazzarotto, L. Pacciani, M. Galli, M. Marisaldi
IPN triangulation and energy spectrum of GRB080916C.

GRB Coordinates Network, Circular Service, 8251, 1 (2008).

K. Hurley, T. Cline, J. Goldsten, W. Boynton, C. Fellows, K. Harshman, C. Shinohara, R. Starr, I.G. Mitrofanov, D. Golovin, M.L. Litvak, A.B. Sanin, S. Golenetskii, R. Aptekar, E. Mazets, V. Pal'Shin, D. Frederiks, D.M. Smith, R.P. Lin, J. McTiernan, R. Schwartz, C. Wigger, W. Hajdas, A. Zehnder, K. Yamaoka, M. Ohno, Y. Fukazawa, T. Takahashi, M. Tashiro, Y. Terada, T. Murakami, K. Makishima
IPN localization of GRB 080211.

GRB Coordinates Network, Circular Service, 7295, 1 (2008).

CONTRIBUTIONS TO CONFERENCES, WORKSHOPS AND SEMINARS

HEAVY ELEMENTS

R. Dressler, D. Schumann, R. Eichler, S.V. Shishkin

Experiments with the descendants of ²⁸⁸115 revisited from the spectroscopic point of view

7-th International Conference on Nuclear and Radiochemistry (NRC7), Budapest, Hungary, 24-29 September, 2008.

R. Eichler

Adsorptionsuntersuchungen mit den Superschweren Elementen 112 und 114

Seminar für Kern- und Radiochemie am Institut für Kernchemie der Universität Mainz, Germany, 7 January 2008.

R. Eichler for a PSI-University of Bern-FLNR-LLNL-ITE collaboration
Chemical investigation of element 114 – status report
 7-th International Conference on Nuclear and Radiochemistry (NRC7), Budapest, Hungary, 24-29 September, 2008.

R. Eichler
Chemical investigation of SHE 112&114
 International Symposium on Heavy Ion Physics (ISHIP 08), GSI Darmstadt, Germany, 17-20 November 2008.

H.W. Gäggeler
Chemical studies with single atoms of superheavy elements
 Technical University Prague, Czech Republic, 3 March 2008.

H.W. Gäggeler
How chemists have reached the island of superheavy elements
 Symp. on the occasion of the 75th birthday of Y.T. Oganessian, Dubna, Russia, 24 May 2008.

H.W. Gäggeler
Happy landing on the island of superheavy elements
 CERN, Geneva, Switzerland, 19 August 2008.

A. Serov
On the adsorption interaction of ^{211}At , ^{212}Pb , and $^{200-202}\text{Tl}$ with metal surfaces
 7-th International Conference on Nuclear and Radiochemistry (NRC7), Budapest, Hungary, 24-29 September, 2008.

A. Serov
Adsorption interaction of lighter homologues of superheavy elements with various surfaces
 Seminar of the Laboratory of Radiochemistry and Environmental Chemistry, University of Berne and Paul Scherrer Institut, 12 December 2008.

SURFACE CHEMISTRY

M. Ammann
Effects of fatty acids on HNO_3 uptake to deliquesced NaCl particles
 American Chemical Society National Meeting, New Orleans, USA, 6-11 April 2008.

M. Ammann
Phase transfer properties, ozonolysis and photochemistry of organic films of atmospheric relevance
 Seminar, Brookhaven National Laboratory, Long Island, NY, USA, 11 April 2008.

M. Ammann
Tracing phase transfer at the interface between chemistry and climate
 Seminar, Department of Chemistry of Biochemistry, University of Bern, Bern, Switzerland, 24 April 2008.

M. Ammann
Photosensitized uptake of nitrogen dioxide and ozone to humic acid containing ice and aerosol surfaces
 IGAC International Conference, Annecy, France, 7-12 September 2008.

M. Ammann, A. Křepelová, T. Huthwelker, J. T. Newberg, H. Bluhm
The effect of strong acids on the ice - air interface probed by photoelectron spectroscopy
 IGAC International Conference, Annecy, France, 7-12 September 2008.

M. Ammann
Can a XFEL shed light on atmospheric particles?
 PSI XFEL Science Workshop, EPFL, Lausanne, Switzerland, 10 October 2008.

M. Ammann
Mechanisms and kinetics of heterogeneous reactions of nitrogen oxides with tropospheric aerosol particles
 Seminar, Institut of Hydrochemistry, TU München, Germany, 6 November 2008.

- T. Bartels-Rausch, M. Ammann, J. Kleffmann, Y. Elshorbany, M. Brigante, B. D'Anna, C. George
Sun, soil, snow and HONO
Invited Eurochamp HONO Workshop, Bergische Universität Wuppertal, Wuppertal, Germany, 1-3 March 2008.
- T. Bartels-Rausch, M. Jöri, T. Huthwelker, H.W. Gäggeler, M. Ammann
Interaction of gaseous, elemental mercury with snow surfaces: Laboratory investigations
AICI-HiT Workshop "Ice and Halogens: Laboratory Studies to Improve the Modelling of Field Data", British Antarctic Survey, Cambridge, UK, 16-18 June 2008.
- T. Bartels-Rausch, M. Ammann
A new dye to probe the acidity at the water/air and ice/air interface
Faraday Discussion 141: Water – From Interfaces to the Bulk, Heriot-Watt University, Edinburgh, United Kingdom, 27-29 August 2008.
- T. Bartels-Rausch
From russia with love: Thermo-chromatography in atmospheric science
Seminar of the Laboratory of Radiochemistry and Environmental Chemistry, University of Berne and Paul Scherrer Institut, 17 October 2008.
- T. Bartels-Rausch
Matlab in the lab: Use of matlab in atmospheric and climate science
Matlab Information Day, Paul Scherrer Institut, 22 October 2008.
- T. Bartels-Rausch, M. Ammann
A new dye to probe the acidity at the water/air and ice/air interface
Atmospheric Chemical Mechanisms, University of California, Davis, USA, 10-12 December 2008.
- T. Bartels-Rausch, T. Huthwelker, I. Zimmermann, M. Ammann
Interaction of peroxyinitric acid with ice surfaces
Annual Meeting of the American Geophysical Union, San Francisco, USA, 15-19 December 2008.
- M. Kerbrat, T. Bartels-Rausch, T. Huthwelker, M. Ammann
Recent results on the uptake of HNO_2 and HNO_4 on ice surfaces from laboratory studies
Annual Meeting of the EU FP6 project SCOUT-O3, Alfred-Wegener-Institut für Polar- und Meeresforschung (AWI), Potsdam, Germany, 21-23 April 2008.
- A. Křepelová, M. Ammann, J.T. Newberg, H. Bluhm, T. Huthwelker
Influence of HNO_3 on ice surface melting studied by X-ray photoelectron spectroscopy
Seminar of the Laboratory of Radiochemistry and Environmental Chemistry, University of Berne and Paul Scherrer Institut, 9 May 2008.
- A. Křepelová, M. Ammann, J.T. Newberg, H. Bluhm, T. Huthwelker
Influence of nitric acid on ice surface melting studied by X-ray photoelectron spectroscopy
AICI-HiT-SPARC Workshop, British Antarctic Survey, Cambridge, United Kingdom, 16-18 June 2008.
- A. Křepelová, M. Ammann, J.T. Newberg, H. Bluhm, T. Huthwelker
Impact of HNO_3 and HCl on ice surface melting
Faraday Discussion 141: From Interfaces to the Bulk, Heriot-Watt University, Edinburgh, UK, 27-29 August 2008.
- A. Křepelová, V. Zelenay, M. Ammann, T. Huthwelker, J.T. Newberg, H. Bluhm, G. Tzvetkov, J. Raabe
Environmental studies using XAS
Workshop on X-ray absorption spectroscopy and advanced XAS techniques, Paul Scherrer Institut, Villigen, Switzerland, 6-10 October 2008.
- A. Rouvière, M. Ammann
Heterogeneous reactions of ozone on inorganic aerosol particles. Influence of fatty acid coating.
Seminar of the Laboratory of Radiochemistry and Environmental Chemistry, University of Berne and Paul Scherrer Institut, 4 April 2008.

A. Rouvière, M. Ammann

Effect of fatty acid coating on ozone uptake to deliquesced iodide particles

European Geophysical Union - General Assembly 2007, Vienna, Austria, 13-18 April 2008.

A. Rouvière, M. Ammann

Etude de l'interaction de l'ozone avec des particules d'iodure de potassium - influence des acides gras

Conférence annuelle de cinétique et de photochimie, Strasbourg, France, 9 June 2008.

A. Schlierf

Photochemical aging of organic aerosol

EUCAARI Workshop, Mainz, Germany, 26 February 2008.

A. Schlierf

Photochemical altering of organic aerosol

Seminar, Institute for Atmospheric and Climate Science, ETH Zürich, Switzerland, 12 March 2008.

A. Schlierf

Photochemical aging of organic aerosol

Seminar of the Laboratory of Radiochemistry and Environmental Chemistry, University of Berne and Paul Scherrer Institut, 9 May 2008.

O. Vesna, M. Kalberer, M. Ammann

Formation of hydrogen peroxide in the ozonolysis of mixed oleic acid - NaCl aerosol particles under humid conditions

American Chemical Society National Meeting, New Orleans, USA, 6-11 April 2008.

V. Zelenay, A. Křepelová, M. Ammann, M.G.C. Vernooij, M. Birrer, G. Tzvetkov, J. Raabe, T. Huthwelker

X-ray microspectroscopy of aerosol particles

Seminar Institute for Atmosphere and Climate, ETH, Zürich, Switzerland, 14 March 2008.

V. Zelenay, A. Křepelová, M. Ammann, M.G.C. Vernooij, M. Birrer, R. Chirico, G. Tritscher, G. Tzvetkov, J. Raabe, T. Huthwelker

X-ray microspectroscopy of aerosol particles

Seminar PSI/Uni Bern, PSI, Villigen, Switzerland, 9 May 2008.

V. Zelenay, A. Křepelová, M. Ammann, M.G.C. Vernooij, M. Birrer, R. Chirico, G. Tritscher, G. Tzvetkov, J. Raabe, T. Huthwelker

Water uptake experiments with combustion particles using X-ray microspectroscopy

XRM, ETH, Zürich, Switzerland, 21-25 July 2008.

V. Zelenay, A. Křepelová, T. Huthwelker, M. Birrer, G. Tzvetkov, J. Raabe, M. Ammann

Development of an environmental cell to study phase changes in aerosol particles using X-ray microspectroscopy

9th International Conference on X-Ray Microscopy, ETH Zürich, Switzerland, 21-25 July 2008.

V. Zelenay, A. Křepelová, M. Birrer, M.G.C. Vernooij, M. Ammann, G. Tzvetkov, J. Raabe, T. Huthwelker

X-ray microspectroscopy of aerosol particles

Seminar ETH, Zürich, Zürich, Switzerland, 15 August 2008.

V. Zelenay, A. Křepelová, M. Birrer, M.G.C. Vernooij, M. Ammann, G. Tzvetkov, J. Raabe, T. Huthwelker

A new device for the study of water uptake and release in aerosol particles using x-ray microspectroscopy

European Aerosol Conference, Thessaloniki, Greece, 25-29 August 2008.

V. Zelenay, A. Křepelová, M. Ammann, M. Birrer, M.G.C. Vernooij, G. Tzvetkov, J. Raabe, T. Huthwelker

Water uptake on aerosol particles studied by X-ray microspectroscopy

XAS workshop, PSI, Villigen, Switzerland, 7-8 October 2008.

V. Zelenay, A. Křepelová, M. Ammann, M.G.C. Vernooij, M. Birrer, R. Chirico, G. Tritscher, G. Tzvetkov, J. Raabe, T. Huthwelker

Observations on water uptake in soot particles using X-ray microspectroscopy

NEADS Workshop, Zürich, Switzerland, 4 November 2008.

ANALYTICAL CHEMISTRY

A. Ciric

Regionale Klimarekonstruktion mit Eisbohrkernen von Hochgebirgsgletschern
Geographisches Kolloquium, TU Dresden, Germany, 25 June 2008.

A. Ciric, L. Tobler, H.W. Gäggeler, G. Casassa, M. Schwikowski

Source apportionment of trace species and possible ENSO detection in the Mercedario ice core
7th NCCR Climate Summer School, Monte Verità, Switzerland, 31 August-5 September 2008.

A. Ciric

Mercedario ice core records and the regional climate

Seminar of the Laboratory of Radiochemistry and Environmental Chemistry, University of Berne and Paul Scherrer Institut, 14 November 2008.

A. Ciric, L. Tobler, H.W. Gäggeler, G. Casassa, M. Schwikowski

An ice core record from Mercedario (32°S), Central Argentinean Andes

4th EGU Alexander von Humboldt International Conference "The Andes: Challenge for Geosciences",
Santiago, Chile, 24-28 November 2008.

E. Dietze, A. Kleber, P. Ginot, U. Schotterer, M. Schwikowski

Response of regional climate and glacier ice proxies to El Niño-Southern Oscillation (ENSO) in the subtropical Andes
EGU General Assembly, Vienna, Austria, 13-18 April 2008.

A. Eichler, S. Olivier, H. Henderson, A. Laube, J. Beer, T. Papina, M. Schwikowski

Ice core climate and environmental signals over the past 750 years from Belukha glacier (Siberian Altai)

Swiss-Russian Seminar "Reconstruction of past climate variability in Siberia from natural archives",
Barnaul, Russia, 1-7 June 2008.

S. Eyrikh, T. Papina, L. Tobler, M. Schwikowski

Representativeness of ice-core analysis for reconstruction of historic mercury deposition in Altai region

Swiss-Russian Seminar "Reconstruction of past climate variability in Siberia from natural archives",
Barnaul, Russia, 1-7 June 2008.

H.W. Gäggeler

Die naturwissenschaftlichen Grundlagen des Klimawandels: Umweltforschung anhand von Gletschereis
Weiterbildung der PH Bern, Switzerland, 31 May 2008.

H.W. Gäggeler, A. Eichler

Long-term air pollution records retrieved from Alpine ice cores

Workshop "Spawning the Atmosphere Measurements of Jungfraujoeh", Swiss Academy of Sciences, Bern, Switzerland,
25/26 November 2008.

S. Kaspari, P. Mayewski, S. Kang, S. Sneed, S. Hou, R. Hooke, K. Kreutz, D. Introne, M. Handley, K. Maasch, D. Qin

Reduction in northward incursions of the South Asian Monsoon since ~1400 AD inferred from a Mt. Everest ice core

Swiss-Russian Seminar "Reconstruction of past climate variability in Siberia from natural archives",
Barnaul, Russia, 1-7 June 2008.

S. Kaspari, M. Schwikowski, P. Mayewski, S. Kang, S. Hou

Carbonaceous particle concentrations since the pre-industrial era from Asian ice cores

9th Int. Conference on Carbonaceous Particles in the Atmosphere, Berkeley, California, 12-14 August 2008.

S. Kaspari, M. Schwikowski, M. Gysel, P. Mayewski, S. Kang, B. Grigholm

Carbonaceous particle and dust concentrations since the pre-industrial era from Asian ice cores

Third International Training School on Atmospheric Brown Clouds, United Nations Environmental Program,
Kathmandu, Nepal, 4-7 December 2008.

S. Kaspari, M. Schwikowski, M. Gysel, P. Mayewski, S. Kang, B. Grigholm

Carbonaceous particle and dust concentrations since the pre-industrial era from Asian ice cores

American Geophysical Union Fall Meeting, San Francisco, California, USA, 15-19 December 2008.

- T. Kellerhals, S. Brütsch, M. Sigl, S. Knüsel, H.W. Gäggeler, M. Schwikowski
Holocene climatic fluctuations including Medieval Warm Period and Little Ice Age type events in tropical South America deduced from Illimani ice core
 4th EGU Alexander von Humboldt International Conference “The Andes: Challenge for Geosciences”,
 Santiago, Chile, 24-28 November 2008.
- M. Schläppi, T. Jenk, B. Rufibach, A. Rivera, M. Rodríguez, G. Casassa, M. Schwikowski
Results of the ice core from Pio XI, Southern Patagonian ice field
 9th Swiss Global Change Day, Bern, Switzerland, 1 April, 2008.
- M. Schläppi, T. Jenk, B. Rufibach, A. Rivera, M. Rodríguez, G. Casassa, M. Schwikowski
Seasonality of different proxies in Pio XI ice core, Southern Patagonia Ice Field (49° S)
 7th NCCR Climate Summer School, Monte Verità, Switzerland, 31 August-5 September 2008.
- M. Schläppi, T. Jenk, B. Rufibach, P. Santibáñez, A. Rivera, M. Rodríguez, G. Casassa, M. Schwikowski
First ice core record from Pio XI Glacier, Southern Patagonia Ice Field (49°S)
 4th EGU Alexander von Humboldt International Conference “The Andes: Challenge for Geosciences”,
 Santiago, Chile, 24-28 November 2008.
- M. Schwikowski
Ist CO₂ an allem Schuld?
 Ökumenisches Bildungswerk Laufenburg, Laufenburg, Germany, 14 January 2008.
- M. Schwikowski
Klimageschichte aus alpinen Eisbohrkernen
 Vortragsreihe Klima und Atmosphäre im Kernkraftwerk Leibstadt, Leibstadt, Switzerland, 16 January 2008.
- M. Schwikowski
Schnee von gestern - Gletschereis als Klimaarchiv
 KLIMASonntag Paul Scherrer Institut, Villigen, Switzerland, 13 April 2008.
- M. Schwikowski
Chemistry of glacier ice: Frozen archive of past environmental conditions
 Lectures in Radiochemistry: Succession of Prof. Heinz W. Gäggeler, Universität Bern, Bern, Switzerland, 24 April 2008.
- M. Schwikowski
Zeitreise durch das Eis: Hochalpine Gletscher als Klimaarchive
 Senioren-Universität Bern, Bern, Switzerland, 2 May 2008.
- M. Schwikowski
Schnee von gestern - Gletschereis als Klimaarchiv
 SGK Young Generation Frühjahrstreffen 2008 “Basiswissen Klima und Energie“, ETH Zürich, Zürich, Switzerland,
 13 May 2008.
- M. Schwikowski
Ice cores from the Alps: Challenges in reconstructing paleo climate
 Høltedahlfonna-Lomonosovfonna workshop, Norwegian Polar Institute, The Polar Environmental Centre, Tromsø, Norway,
 24-25 September 2008.
- M. Schwikowski
High-alpine glaciers as archives of atmospheric pollution and climate
 POMklim seminar, Norwegian Polar Institute, The Polar Environmental Centre, Tromsø, Norway, 25 September 2008.
- M. Sigl
Radiocarbon dating of Alpine ice cores
 Seminar - Laboratory of Ion Beam Physics ETH Zurich, Switzerland, 5 March 2008.
- M. Sigl
Radiocarbon dating of Alpine ice cores
 Seminar - Laboratory for Radiochemistry and Environmental Chemistry, Villigen, Switzerland 7 March 2008.

M. Sigl, T.M. Jenk, D. Divine, M. Schwikowski
Climate signals from Colle Gnifetti ice core, Swiss Alps
 Millennium European Climate 2nd Milestone Meeting, Cala Millor Mallorca, Spain, 10-16 March 2008.

M. Sigl
Climate signals from Colle Gnifetti ice core, Swiss Alps
 9th Swiss Global Change Day, Bern, Switzerland, 1 April 2008

M. Sigl, T.M. Jenk, T. Kellerhals, M. Ruff, S. Szidat, C. Boutron, C. Barbante, H.-A. Synal, H.W. Gäggeler, M. Schwikowski
Radiocarbon dating of glacier ice on a microgram level – examples from the Alps and the Andes
 EGU General Assembly, Vienna, Austria, 13–18 April 2008.

M. Sigl, T.M. Jenk, T. Kellerhals, M. Ruff, S. Szidat, C. Boutron, C. Barbante, H.-A. Synal, L. Wacker, H.W. Gäggeler, M. Schwikowski
Radiocarbon dating of glacier ice on a microgram level – examples from the Alps and the Andes
 7th NCCR Climate Summer School, Monte Verità, Switzerland, 31 August-05 September 2008.

M. Sigl
Towards radiocarbon dating of ice cores
 MILLENNIUM Young Writers Workshop, Tihany, Hungary, 6-10 October 2008.

L. Tobler, A. Ciric, T. Kellerhals, M. Schwikowski
Anwendung der (Continuous Ice Melting) CIM-ICP-SF-MS zur Bestimmung von Spurenelementen in Eiskernen aus den Südamerikanischen Anden
 21. ICP-MS Anwendertreffen und 8. Symposium über Massenspektrometrische Verfahren der Elementspurenanalyse, Dresden, Germany, 17-19 September 2008.

RADWASTE ANALYTICS

S. Chiriki, N. Prolingheur, R. Moormann
A simplified method for estimation of groundwater contamination surrounding accelerators and high power targets
 11th International Conference on Radiation Shielding (ICRS-11) of American Nuclear Society, Pine Mountain, Georgia, USA, 13-18 April 2008.

S. Chiriki, K. Bongardt, J. Fachinger, M. Herbst, B. Heuel-Fabianek, R. Moormann, R. Nabbi, N. Prolingheur, B. Schlögl
Safety and disposal activities of Hg-target systems
 Joint collaboration meeting `SAFERIB and Safety and Radioprotection task within EURISOL-DS` Lithuanian Academy of Sciences, Vilnius, 05-06 May 2008.

C. Domingo-Pardo, I. Dillmann, T. Faestermann, U. Giesen, J. Goerres, M. Heil, S. Horn, F. Käppeler, S. Köchli, G. Korschinek, J. Lachner, M. Maiti, J. Marganec, J. Neuhausen, R. Nolte, M. Poutivtsev, R. Reifarh, R. Rugel, D. Schumann, E. Uberseder, F. Voss, S. Walter, M. Wiescher
s-process nucleosynthesis in massive stars: new results on ⁶⁰Fe, ⁶²Ni and ⁶⁴Ni
 CGS-13, Köln, Germany, 25-29 August 2008.

D. Kiselev, D. Schumann, S. Teichmann, M. Wohlmuther
Activation of targets and accelerator components at PSI – a comparison of simulation and measurement
 HB08, Nashville, USA, 25-29 August 2008.

R. Moormann, S. Chiriki, K. Bongardt
Safety aspects of high power targets for European spallation sources
 International Conference on the Physics of Reactors “Nuclear Power: A Sustainable Resource” Casino-Kursaal Conference Center, Interlaken, Switzerland, 14-19 September 2008.

J. Neuhausen, R. Dressler, F. v. Rohr, M.M. Marin Marmol, St. Heinitz, S. Lüthi, D. Schumann
Results on nuclear peaction product behavior in LBE
 EUROTRANS Domain 4 Technical Meeting, Forschungszentrum Karlsruhe, Germany, 03 March 2008.

J. Neuhausen

Recent results on the chemistry of liquid mercury and lead-bismuth targets

Seminar of the Laboratory of Radiochemistry and Environmental Chemistry, University of Berne and Paul Scherrer Institut, 4 April 2008.

J. Neuhausen, D. Schumann

PIE-samples for radiochemical analysis

Technical Meeting MEGAPIE target cutting, Paul Scherrer Institut, Villigen, Switzerland, 27 May 2008.

J. Neuhausen

Radiochemistry of activated mercury

EURISOL-DS METEX Preparation Meeting, Paul Scherrer Institut, Villigen, Switzerland, 17 June 2008.

J. Neuhausen, F. v. Rohr, M.M. Marin Marmol, St. Heinitz, S. Lüthi, S. Horn, D. Schumann

Recent results on polonium behavior in eutectic lead-bismuth alloy

NRC7 – Seventh International Conference on Nuclear and Radiochemistry, Budapest, Hungary, 29 August 2008.

J. Neuhausen, D. Schumann, S. Heinitz, F. v. Rohr, S. Horn, S. Lüthi

Nuclear reaction product behavior in lead-bismuth alloy

3rd Conference Heavy Liquid-Metal Coolants in Nuclear Technology, Obninsk, Russia, 15-19 September 2008.

J. Neuhausen, D. Schumann

Radiochemical analysis in MEGAPIE PIE

MEGAPIE-PIE Meeting, Aix-en-Provence, France, 24 September 2008.

J. Neuhausen, D. Schumann

Radiochemical analysis in MEGAPIE PIE

9th MEGAPIE Technical Review Meeting, Aix-en-Provence, France, 26 September 2008.

J. Neuhausen, D. Schumann

Radiochemistry of activated mercury

EURISOL-DS Deliverable Review, Paul Scherrer Institut, Villigen, Switzerland, 10 October 2008.

J. Neuhausen, S. Heinitz, F. v. Rohr, S. Lüthi, S. Horn, D. Schumann

Nuclear reaction product behavior in liquid metal targets

1st International Workshop on Accelerator Radiation Induced Activation, ARIA 2008, Paul Scherrer Institut, Villigen, Switzerland 13-17 October 2008.

J. Neuhausen

Abschätzung der Aktivitätsfreisetzung beim Ausschmelzen der Proben im Megapie-Target

Technisches Meeting zur Konzeption des Ausschmelzens des MEGAPIE Targets, Paul Scherrer Institut, Villigen, Switzerland, 30 October 2008.

R. Reifarh , L.P. Chau, I. Dillman, C. Domingo Pardo, J. Goerres, M. Heil, F. Kaeppler, J. Marganec, O. Meusel,

J. Neuhausen, R. Plag, U. Ratzinger, A. Schempp, D. Schumann, E. Überseder, K. Volk, F. Voss, S. Walter, M. Wiescher

Opportunities for nuclear astrophysics at FRANZ

Workshop "The Origin of the Elements Heavier than Fe", Torino, Italy, 25-27 September 2008.

G. Rugel, I. Dillmann, Th. Faestermann, I. Günther-Leopold, N. Kivel, K. Knie, G. Korschinek, J. Lachner, M. Poutivtsev,

D. Schumann, R. Weinreich, M. Wohlmuther

A new approach to determine the half-life of ^{60}Fe

AMS-11, Rome, Italy 14-19 September 2008.

D. Schumann

Progresses in ERAWAST

EFNUDAT workshop, Dresden-Rossendorf, Germany, 13-15 February 2008.

D. Schumann

ERAWAST - A status report

Seminar - Laboratory for Radiochemistry and Environmental Chemistry, Villigen, Switzerland 7 March 2008.

D. Schumann

Production of long-lived exotic radionuclides for nuclear physics experiments

BRIX meeting, Mol, Belgium, 06-09 April 2008.

D. Schumann

Wässrige Chemie von Transaktiniden

Succession Professorship H.W. Gäggeler, University of Berne, Switzerland, 24/25 April 2008.

D. Schumann, S. Horn, S. Teichmann, M. Wohlmuther, P.W. Kubik, H.-A. Synal, G. Korschinek, K. Knie, G. Rugel

Measurement of long-lived radionuclides in proton-irradiated accelerator components

Jahrestagung der Deutschen Gesellschaft für Kerntechnik, Hamburg, Germany, 26-29 May 2008.

D. Schumann, J. Neuhausen, S. Horn, S. Lüthi, J. Eikenberg, M. Rüthi

Liquid scintillation counting as measuring method for the analytics of accelerator waste

LSC2008, Davos, Switzerland, 26-30 May 2008.

D. Schumann

The ERAWAST initiative - a new approach for isotope production

Annual meeting of the American Nuclear Society, Anaheim, USA, 8-12 June 2008.

D. Schumann, J. Neuhausen, M. Wohlmuther, J. Eikenberg, M. Rüthi, Peter. W. Kubik, H.-A. Synal, V. Alfimov, G. Korschinek, G. Rugel, Th. Faestermann

Radiochemische Charakterisierung eines Kupfer- Beamdumps vom 590-MeV-Ringzyklotron des Paul Scherrer Instituts Villigen

5. Workshop RCA, Dresden-Rossendorf, Germany, 16/17 June 2008.

D. Schumann, J. Neuhausen, J. Eikenberg, M. Rüthi, M. Wohlmuther, P.W. Kubik, H.-A. Synal, V. Alfimov, G. Korschinek, G. Rugel, Th. Faestermann, I. Dillmann, C. Domingo Pardo, F. Käppeler, J. Marganec, F. Voss, S. Walter, M. Heil,

R. Reifarh, J. Goerres⁶, E. Überseder, M. Wiescher

Radionuclides of astrophysical interest from accelerator waste

NRC07, Budapest, Hungary, 25-29 August 2008.

D. Schumann, J. Neuhausen, I. Dillmann, C. Domingo Pardo, F. Käppeler, J. Marganec, F. Voss, S. Walter, M. Heil, R. Reifarh, J. Goerres, E. Überseder, M. Wiescher. M. Pignatari

Preparation of a ⁶⁰Fe target for nuclear astrophysics experiments

INTDS2008, Caen, France, 14-17 September 2008.

D. Schumann, J. Neuhausen

The ERAWASTi Initiative - a new approach for isotope production

ARIA2008 workshop, Villigen, Switzerland, 13-17 October 2008.

D. Schumann

ERAWAST - A status report

SARAF workshop, Jerusalem, Israel, 26-29 October 2008.

D. Schumann

Wässrige Chemie von Transaktiniden

Succession Professorship J.V. Kratz, University of Mainz, Germany, 24/25 November 2008.

PROTON IRRADIATION FACILITY

U. Grossner, W. Hajdas, K. Egli, R. Brun, R. Harboe-Sorensen

New proton irradiation facility at Paul Scherrer Institute

NUCLEAR AND SPACE RADIATION EFFECTS CONFERENCE NSREC 2008

And Radiation Effects Data Workshop, Tucson, Arizona, USA, 14-18 July 2008.

U. Grossner, W. Hajdas, K. Egli, R. Brun, R. Harboe-Sorensen

Proton irradiation facility at the PROSCAN project of the Paul Scherrer Institute

8th European Workshop on Radiation Effects on Components and Systems RADECS2008, Jyväskylä, 10-12 September 2008.

W. Hajdas, C. Eggel, D. Kotlinski, B. Schmitt, St. Scherrer, N. Schlumpf, A. Mohammadzadeh, P. Nieminen
Development of the low energy electron detector
Seminar in the Swiss Space Office, Bern, Switzerland, 12 March 2008.

W. Hajdas

PIF activities: from ground tests to space weather monitoring and biggest cosmic explosions
Seminar in the Physics Institute of the Bern University, Bern, Switzerland, 12 March 2008.

W. Hajdas, St. Scherrer, K. Egli, N. Schlumpf, B. Schmitt, A. Mohammadzadeh, P. Nieminen, C. Eggel, D. Kotlinski
Current status of the low energy electron detector
13th SPINE Meeting, ESA-ESTEC Noordwijk, 28-29 May 2008.

W. Hajdas

POLAR - novel hard X-ray polarimeter for gamma ray bursts
37th COSPAR Scientific Assembly, Montréal, Canada, 13-20 July 2008.

W. Hajdas

Low energy electron detector for space radiation measurements
37th COSPAR Scientific Assembly, Montréal, Canada, 13-20 July 2008.

H. Evans, E.J. Daly, P. Nieminen, W. Hajdas, A. Mohammadzadeh, D. Rodgers, G. Mandorlo, K. Ryden
Use of radiation Monitor data for validation of radiation environment specifications based on the NASA AE8 Models
37th COSPAR Scientific Assembly, Montréal, Canada, 13-20 July 2008.

W. Hajdas

SREM data base and calibration meeting
ESA-ESTEC, Noordwijk, 6-7 October 2008.

W. Hajdas, E. Daly, L. Desorgher, C. Eggel, K. Egli, H. Evans, D. Kotlinski, D. Marinov, A. Mohammadzadeh, P. Nieminen, G. Santin, St. Scherrer, N. Schlumpf, B. Schmitt
Space radiation monitoring activities at PSI
SEENoTC Workshop, IAC Toulouse, France, 13-15 October 2008.

St. Scherrer, W. Hajdas, U. Grossner, N. Schlumpf

Proton radiation test of DC/DC converter with high voltage output
8th European Workshop on Radiation Effects on Components and Systems RADECS2008, Jyväskylä, 10-12 September 2008.

ENVIRONMENTAL RADIONUCLIDES UNIVERSITÄT BERN

A.C. Aiken, C. Wiedinmyer, B. de Foy, D. Salcedo, M. Cubison, I. Ulbrich, P. DeCarlo, J.A. Huffman, K. Docherty, D. Sueper, D.R. Worsnop, A. Trimborn, M. Northway, A.S.H. Prevot, S. Szidat, M.N. Wehrli, E.A. Stone, J.J. Schauer, J. Wang, J. Zheng, E. Fortner, R. Zhang, A. Laskin, J. Gaffney, N. Marley, L. Molina, G. Sosa, J.L. Jimenez
Organic aerosols in Mexico City: urban and biomass burning contributions during MILAGRO / MCMA-2006 at the urban supersite (T0)
American Association for Aerosol Research (AAAR): 27th Annual Conference, Orlando, FL, USA, 20-24 October 2008.

S. Fahrni

Towards compound-specific radiocarbon analysis of carbonaceous aerosols
Seminar Radio- und Umweltchemie, University of Berne, Switzerland, 4 April 2008.

S. Fahrni

Towards compound-specific radiocarbon analysis of carbonaceous aerosols
First Year Graduate Student Symposium, University of Berne, Switzerland, 8 September 2008.

S. Fahrni, H.W. Gäggeler, I. Hajdas, M. Ruff, S. Szidat, L. Wacker

A direct combination of CuO oxidation with a gas ion source for small ¹⁴C samples
11th International Conference on Accelerator Mass Spectrometry, Rome, Italy, 14-19 September 2008.

- N. Perron, L. Besnier, S. Szidat, A.S.H. Prévôt, U. Baltensperger
EC and OC separation for ¹⁴C analysis: a challenge
 Seminar Laboratory of Atmospheric Chemistry, Paul Scherrer Institut, Switzerland, 19 May 2008.
- N. Perron, L. Besnier, S. Szidat, A.S.H. Prévôt, U. Baltensperger
EC and OC separation for ¹⁴C analysis
 Summer School on Organic Aerosols, University of Gothenburg, Sweden, 25 June 2008.
- N. Perron, L. Besnier, A.S.H. Prévôt, S. Szidat, M. Ruff, S. Fahrni, U. Baltensperger
Optimised separation of OC and EC for radiocarbon-based source apportionment of carbonaceous aerosol
 9th International Conference on Carbonaceous Particles in the Atmosphere, Berkeley, CA, USA, 12-14 August 2008.
- N. Perron, S. Szidat, A. S. H. Prévôt, U. Baltensperger
Carbonaceous aerosol: OC and EC separation for radiocarbon-based source apportionment
 Seminar Radio- und Umweltchemie, University of Berne, Switzerland, 17 October 2008.
- N. Perron, S. Szidat, A.S.H. Prévôt, U. Baltensperger
Carbonaceous aerosol: OC and EC separation for radiocarbon-based source apportionment
 Seminar Laboratory of Atmospheric Chemistry, Paul Scherrer Institut, Switzerland, 10 November 2008.
- N. Perron, S. Szidat, A.S.H. Prévôt, M. Ruff, S. Fahrni, U. Baltensperger
Improved separation of OC and EC for radiocarbon-based source apportionment of carbonaceous aerosol
 EUCAARI annual meeting, Helsinki, Finland, 17-21 November 2008.
- A.S.H. Prevot, J. Sandradewi, M.R. Alfarra, S. Szidat, M.N. Wehrli, M. Ruff, S. Weimer, V.A. Lanz, E. Weingartner, N. Perron, A. Caseiro, A. Kasper-Giebl, H. Puxbaum, L. Wacker, U. Baltensperger
A comparison of new and classic methods to estimate the wood smoke contribution to particulate matter for several field campaigns
 European Aerosol Conference, Thessaloniki, Greece, 24-29 August, 2008.
- A.S.H. Prevot, J. Sandradewi, M.R. Alfarra, S. Szidat, M.N. Wehrli, M. Ruff, S. Weimer, V.A. Lanz, E. Weingartner, N. Perron, A. Caseiro, A. Kasper-Giebl, H. Puxbaum, L. Wacker, U. Baltensperger
Comparison of different wood smoke markers in ambient aerosol
 American Association for Aerosol Research (AAAR): 27th Annual Conference, Orlando, FL, USA, 20-24 October 2008.
- M. Ruff, H.W. Gäggeler, M. Suter, H.-A. Synal, S. Szidat, L. Wacker
Fully automated radiocarbon AMS measurements with elemental analyser and gas ion source
 Frühjahrstagung der Deutschen Physikalischen Gesellschaft – Fachverband Massenspektrometrie, Darmstadt, Germany, 10-14 March 2008.
- M. Ruff, H.W. Gäggeler, I. Hajdas, T. Jenk, M. Němec, S. Riedi, M. Sigl, M. Suter, H.-A. Synal, S. Szidat, L. Wacker
Radiocarbon dating of small samples
 5th International Symposium on Radiocarbon and Archaeology, Zürich, Switzerland, 26-28 March 2008.
- M. Ruff, S. Fahrni, H.W. Gäggeler, M. Suter, H.-A. Synal, S. Szidat, L. Wacker
Radiocarbon measurements with the MICADAS gas ion source
 11th International Conference on Accelerator Mass Spectrometry, Rome, Italy, 14-19 September 2008.
- S. Schmoker
Compound-specific radiocarbon dating of various soil components
 Seminar Radio- und Umweltchemie, University of Berne, Switzerland, 12 December 2008.
- M. Suter, G. Bonani, I Hajdas, M. Ruff, T. Schulze-König, H.-A. Synal, S. Szidat, L. Wacker
Recent developments in accelerator mass spectrometry and its impact to archaeology
 5th International Symposium on Radiocarbon and Archaeology, Zürich, Switzerland, 26-28 March 2008.
- S. Szidat
¹⁴C-Analysen von Feinstaubproben
 Fachtagung Immissionsmesstechnik, Dübendorf, Switzerland, 25 January 2008.

S. Szidat, S. Fahrni, U. Baltensperger, M. Ruff, L. Wacker, B. Klatzer, H. Puxbaum, E. Finessi, S. Decesari

Refined ^{14}C source apportionment of organic carbon

9th International Conference on Carbonaceous Particles in the Atmosphere, Berkeley, CA, USA, 12-14 August 2008.

L. Wacker, M. Němec, J. Bourquin

A revolutionary graphitisation system: fully automated, compact and simple

11th International Conference on Accelerator Mass Spectrometry, Rome, Italy, 14-19 September 2008.

PUBLIC RELATIONS

Analytical Chemistry

Printed media

- Die Botschaft
Menschliche Einflüsse unbestreitbar
19 January 2008.
- Argauer Zeitung
In Zukunft recht unbeständig, Leibstadt Vortragsreihe „Klima und Atmosphäre“ im Kernkraftwerk
23 January 2008.
- PSI media release
Temperatur im Altai folgt Sonne mit Verzögerung
19 December 2008.
- Tagesanzeiger
Sonne beeinflusst die Temperatur Sibiriens
23 December 2008.

Demonstration

Tage der Offenen Tür am PSI
Klimasignale im Gletschereis und in Bäumen
25-26 October 2008.

Proton Irradiation Facility

Demonstration

Tage der Offenen Tür am PSI
Radiation detectors for space weather monitoring
25-26 October 2008.

Environmental Radionuclides Universität Bern

- Homepage Department of Chemistry and Biochemistry, Uni Bern
Device of the month: Radiocarbon dating of small samples using on-line combustion
<http://www.dcb-server.unibe.ch/dcbneu/mom/mom0408.html>
April 2008.
- PSI Scientific report 2007
New findings on the sources of fine particles in ambient air in Switzerland
June 2008.
- PSI, Energie-Spiegel Nr.19
Vorsicht Feinstaub
July 2008.
- Senioren-Universität, Uni Bern
Vortrag U. Krähenbühl: Auf Meteoritensuche in kalten und heissen Wüstengebieten (Antarktis und Oman)
2 December 2008.

LECTURES AND COURSES

Prof. Dr. H.W. Gäggeler

Universität Bern, FS2008:

Bachelor

- Instrumentalanalytik II (with others) (3 ECTS)
- Allgemeine Chemie (Einführung Radioaktivität) (with others) (4 ECTS)

Master

- Kolloquium Radio- und Umweltchemie in collaboration with the Paul Scherrer Institut (organized by D. Schumann)

Universität Bern, HS2008:

Bachelor

- Physikalische Chemie IV (with Prof. T. Wandlowski) (3,75 ECTS)
- Praktikum Phys. Chemie II (with others) (4 ECTS)
- Biochemische Methoden I (with others) (3 ECTS)
- Biochemische Methoden (Übungen) (with others)
- Chemistry of Heaviest Elements (with R. Eichler) (1,5 ECTS)

Master

- Nuclear and Radiochemistry (3 ECTS)
- Lab course Nuclear and Radiochemistry (with others) (4 ECTS)
- Lab course Paul Scherrer Institut (with others) (4 ECTS)
- Kolloquium Radio- und Umweltchemie in collaboration with the Paul Scherrer Institut (organized by D. Schumann)

Prof. Dr. U. Krähenbühl

Universität Bern, FS2008:

- Ergänzungen zur analytischen Chemie für Pharmazeuten
- Ergänzungen zur analytischen Chemie für Pharmazeuten (praktische Übungen)

PD Dr. M. Schwikowski

Universität Bern, FS2008:

- Instrumentalanalytik II (with others) (3 ECTS)

Dr. M. Ammann

ETH Zürich, FS 2008:

- Course 'Atmospheric Interface Chemistry'

Dr. R. Eichler

Universität Bern, HS2008:

- Praktikum Phys. Chemie II (with Prof. H.W. Gäggeler) (4 ECTS)
- Lab course Nuclear and Radiochemistry (with Prof. H.W. Gäggeler and S. Szidat) (4 ECTS)
- Lab course Paul Scherrer Institut (with Prof. H.W. Gäggeler and S. Szidat) (4 ECTS)
- Chemistry of Heaviest Elements (with Prof. H.W. Gäggeler) (1,5 ECTS)

Dr. D. Schumann

- Kolloquium Radio- und Umweltchemie in collaboration with Paul Scherrer Institut

Dr. S. Szidat

Universität Bern, HS2008:

- Chemie für Studierende der Veterinärmedizin (with Prof. C. Leumann)
- Praktikum Physikalische Chemie II (with others) (4 ECTS)
- Lab Course Nuclear and Radiochemistry (with Prof. H. W. Gäggeler and R. Eichler) (4 ECTS)

MEMBERS OF SCIENTIFIC COMMITTEES EXTERNAL ACTIVITIES

Dr. Markus Ammann:

- Air-Ice Chemical Interactions (AICI), Member of Steering Committee
- Atmospheric Chemistry and Physics: member of editorial board
- Member of the IUPAC Subcommittee on gas kinetic data evaluation
- PSI internal research commission (FoKo), member

Dr. Robert Eichler:

- PSI internal research commission (FoKo), member

Prof. Dr. Heinz W. Gäggeler:

- Nuklearforum Schweiz, Member of the Executive Board and Member of the Science Board
- Schweizerische Kommission für die hochalpine Forschungsstation Jungfrauoch der SANW (Mitglied)
- Astronomische Kommission der Stiftung Jungfrauoch und Gornergrat (Member)
- Joint IUPAC/IUPAP Working Party (JWP) on the discovery of new elements (Member)
- International Union of Pure and Applied Chemistry (IUPAC) (Fellow)
- Steering Committee of EURISOL (Member)
- Division of Nuclear and Radiochemistry, European Association for Chemical and Molecular Sciences (EuCheMS) (Chairman)
- Oeschger Centre for Climate Change Research, Member of the Scientific Board

Dr. Wojtek Hajdas:

- Official Reviewer for the 8th European Workshop on Radiation Effects on Components and Systems RADECS2008, Jyväskylä, 10-12 September 2008
- Session Chair for the session “dosimetry and facilities” of the 8th European Workshop on Radiation Effects on Components and Systems RADECS2008, Jyväskylä, 10-12 September 2008
- International Technical Committee of the 8th European Workshop on Radiation Effects on Components and Systems RADECS2008, Jyväskylä, 10-12 September 2008
- Organizing Committee for 9th ESA Final Presentation Days and RADECS Thematoc Workshop, 27-29 January, PSI Villigen

Dr. Dorothea Schumann:

- Member of the Nuklearforum Schweiz
- Member of the Schweizerische Gesellschaft der Kernfachleute
- Member of the PSI internal Neutron Source Development Group

PD Dr. Margit Schwikowski:

- Expert of the Matura Examination of Kantonsschule Baden
- Member of the Coordinating Committee of the Pages/IGBP initiative LOTRED SA (Long-Term climate Reconstruction and Diagnosis of (southern) South America)
- Schweizerische Gesellschaft für Schnee, Eis und Permafrost (SEP), board member
- Member of the Oeschger Centre for Climate Change Research

Leonhard Tobler:

- Experte Physik, 42. Nationaler Wettbewerb Schweizer Jugend forscht, April 25, 2008, Freiburg, Schweiz. Betreuung der Arbeit: „Der Nachweis von gesundheitsschädlichen Stoffen in handelsüblichen Fischen mit Hilfe der Neutronenaktivierungsanalyse“

BACHELOR THESIS



Stephan Keller

Anionenbestimmungen von Aerosolfiltern

Dr. S. Szidat / Uni Bern
Prof. Dr. H.W. Gäggeler / PSI & Uni Bern
May 2008

MASTER THESIS



Beat Muther

Chemische Modellstudien für die Elemente 113 und 114

Dr. R. Eichler / PSI
Prof. Dr. H.W. Gäggeler / PSI & Uni Bern
January 2008



Stephan Heinitz

Extraction of polonium from lead-bismuth eutectic

Dr. D. Schumann / PSI
Prof. Dr. H. Morgner / University Leipzig
November 2008



Andreas M. Bernhard

Photo-induced reduction of mercury in ice

PD Dr. M. Schwikowski / PSI & Uni Bern
Dr. M. Ammann / PSI, Dr. T. Bartels-Rausch / PSI
December 2008



Stéphane Schmoker

Isolierung einzelner Bodenkomponenten aus Bodenproben für die Radiokohlenstoffdatierung

Dr. S. Szidat / Uni Bern
Prof. Dr. H.W. Gäggeler / PSI & Uni Bern
December 2008



David Wittwer

Stopping force measurements of ^{48}Ca induced reaction products in Mylar and argon

Dr. R. Eichler / PSI
Prof. Dr. H.W. Gäggeler / PSI & Uni Bern
December 2008

DOCTORAL THESIS



Olga Vesna

*Ozonolysis of unsaturated organic acids in aerosol particles:
products, secondary chemistry and hygroscopicity studies*

Dr. M. Ammann / PSI
Prof. Dr. H.W. Gäggeler / PSI & Uni Bern
February 2008



Kaizhen Li

On the investigation of I-129 in the environment by ICP-MS: possibilities and limitations

Prof. Dr. U. Krähenbühl / Uni Bern
April 2008



Hanna Franberg

Production of exotic, short-lived carbon isotopes at ISOL-type facilities

Dr. M. Ammann / PSI
Prof. Dr. H.W. Gäggeler / PSI & Uni Bern
October 2008



Thomas Kellerhals

Holocene climate fluctuations in tropical South America deduced from an Illimani ice core

PD Dr. M. Schwikowski / PSI & Uni Bern
Prof. Dr. H.W. Gäggeler / PSI & Uni Bern
December 2008



Matthias Ruff

Radiocarbon measurement of micro-scale samples – a carbon dioxide inlet system for AMS

Dr. S. Szidat / Uni Bern
Prof. Dr. H.W. Gäggeler / PSI & Uni Bern
December 2008

AWARD



Sönke Szidat received the *Atmospheric Chemistry and Physics (ACP) Award* for his work on source apportionment of carbonaceous aerosols using radiocarbon (^{14}C) isotope analysis. Granted by the ACP Commission of the Swiss Academy of Sciences, April 2008.

SUMMER STUDENTS

Keller Stephan

The extraction of ^{210}Po from lad-bismuth-eutectic

Universität Bern

July – August 2008

König Andreas

Ice core based reconstruction of past climate conditions and air pollution in the Alps

Universität Bern

July – August 2008

Monbaron Philippe

Testen eines Firnschmelzkopfes für Continuous Ice Melting (CIM) Inductively Coupled Plasma Sector Field Mass Spectrometry (ICP-SFMS)

Universität Bern

July – August 2008

Sigrist Marc

"Separation of Fe, Mn, Ni, Al and Ti from an irradiated beam dump"

Universität Bern

July – August 2008

Weiss Florian

Elektrochemische Herstellung von Seltenerd-Edelmetallverbindungen über den Amalgamprozess

Universität Bern

July – August 2008

Zimmermann Iwan

Synthese von HNO_4 und Untersuchung der Adsorptionseigenschaften an Eisoberflächen

Universität Bern

June – August 2008

Maurus Landolt

3-wöchiges Berufspraktikum zur Analyse von Gletschereis mit Ionenchromatographie und ICP-Massenspektrometrie

Kantonsschule Wettingen

October 2008

VISITING GUESTS AT PSI 2008

3-9 February:

Dmitry Divine, Norwegian Polar Institute, Norway
Discussion of FP6 MILLENNIUM ice group results

6-7 March:

Franz Käppeler, FZ Karlsruhe, Germany
Neutron reactions in massive stars: the origin of Fe-60

16-17 March:

Gunther Korschinek, Georg Rugel, Technische Universität München, Germany
Discussion on ^{60}Fe -half-life

3-4 April:

Paul Schuurmans, SCK Mol, Belgium
Development of a windowless high power spallation target for use in an experimental accelerator driven system

9 May:

Heinz Surbeck, University de Neuchâtel, Switzerland
Natural radionuclides in Swiss groundwater

30 June-03 July:

Daniel Affolter, Gymnasium Alpenstrasse, Biel, Switzerland
Trace analysis of different common salt products

20 August:

Tatyana Papina, Institute for Water and Environmental Problems SB RAS, Barnaul, Russia
Preparation of the ice core drilling project in the Mongolian Altai

27-31 August:

Dmitry Divine, Norwegian Polar Institute, Norway
Discussion of FP6 MILLENNIUM ice group results

4-7 September:

Francisco Cereceda, Universidad Tecnica Federico Santa Maria, Chile
Discussion of future collaboration and joint projects

8-20 October:

Jakub Ripa, University Prague, Czech Republic
Analysis and publishing of the PSI Database with the RMESSI satellite list of GAMME Ray Burst

17 October:

Nadja Homazava, EMPA, Dübendorf, Switzerland
Novel microcapillary FI-ICP-MS technique for in situ time- and element-resolved corrosion investigations

2-9 November:

Yuri Tsyganov Flerov Laboratory for Nuclear Reactions, Dubna, Russia
Discussion of experimental results with element 114 and of the new pureCOLD DAQ-system.

14 November:

Mathias Trachsel, Geographie, University of Bern, Switzerland

Das alpine Klima der letzten 500 Jahre rekonstruiert aus den Sedimenten des Silvapanerseees. Methoden und Ergebnisse; "Die bedeutenden archäologischen Funde vom Schnidejoch (Wildhorngebiet) und ihre Bedeutung für die holozäne Klimageschichte

30 November-7 December:

Sergei V. Shishkin, Vjatcheslav Y. Lebedev, Flerov Laboratory for Nuclear Reactions, Dubna, Russia

Participation at the Ar-40 beam time at PSI Philips cyclotron

7-14 December:

Gospodin A. Bozhikov, Nikolay V. Aksenov, Flerov Laboratory for Nuclear Reactions, Dubna, Russia

Participation at the Ar-40 beam time at PSI Philips cyclotron

2-4 December:

Dr. Matthew Brown, Departement of Chemical Physics, Fritz-Haber-Institut, Berlin, Germany

Heterogeneous reactivity of O₃ and OH with potassium iodide investigated by AFM and synchrotron radiation based XPS and XRD

AUTHOR INDEX

- Alfimov, V., 43
 Ammann, M., 9, 10, 11, 12, 13, 14, 15, 16, 17, 18, 19, 20
 Ayranov, M., 36, 38
 Baltensperger, U., 49
 Bartels-Rausch, T., 17, 18
 Beer, J., 21
 Bergamaschi, A., 44
 Bernhard, A., 18
 Birrer, M., 10, 11, 13, 14, 19
 Bluhm, H., 15, 16
 Boss, H., 35
 Brigante, M., 12, 17
 Brüttsch, S., 10, 22, 26, 27
 Brun, R., 45
 Casassa, G., 30, 31
 Chirico, R., 14
 Chiriki, S., 42
 Ciric, A., 28, 29
 D'Anna, B., 12, 17
 DeCarlo, P., 12
 Desorgher, L., 46
 Dressler, R., 6, 7
 Dye, C., 53
 Egli, K., 44, 45
 Eichler, A., 21, 22, 23
 Eichler, R., 3, 4, 5, 6, 7, 8
 Elshorbany, Y., 17
 Erne, R., 36
 Evans, H., 46
 Fahrni, S., 47, 48, 49, 51
 Festermann, Th., 43
 Gäggeler, H.W., 4, 5, 6, 7, 8, 19, 20, 21, 25, 26, 27, 28, 34, 35, 47, 48, 51, 52
 George, C., 12, 17
 Grigholm, B., 24
 Grossner, U., 45
 Gysel, M., 24
 Hajdas, I., 47, 52
 Hajdas, W., 44, 45, 46
 Hallquist, M., 53
 Harboe-Sorensen, R., 45
 Heinitz, S., 39, 40, 41
 Heinrich, F., 36
 Henderson, K., 21
 Horn, S., 42
 Huthwelker, T., 13, 14, 15, 16, 19, 20
 Jammoul, A., 12
 Jenk, T.M., 25
 Kalt, A., 36
 Kalugin, I., 23
 Kang, S., 24
 Kaspari, S., 24
 Keller, S., 39, 40, 41
 Kellerhals, T., 25, 27, 29
 Kerbrat, M., 19, 20
 Kleffmann, J., 17
 König, A., 26
 Korschinek, G., 43
 Křepelová, A., 13, 14, 15, 16
 Kubik, P., 37
 Laube, A., 21
 Marinov, D., 46
 Mayewski, P., 24,
 Mohamadzadeh, A., 44
 Monbaron, P., 32
 Morath, O., 36
 Němec, M., 50
 Neuhausen, J., 37, 39, 40, 41, 42, 43
 Newberg, J.T., 15, 16
 Nieminen, P., 46
 Olivier, S., 21, 22
 Ovchinnikov, D., 23
 Papina, T., 21, 22, 23
 Perron, N., 49, 53
 Piguet, D., 4, 6
 Pinzer, B., 19, 20
 Prévôt, A., 49
 Raabe, J., 13, 14
 Rivera, A., 30
 Rouvière, A., 9, 10, 11, 12
 Ruff, M., 25, 47, 48, 49, 51, 53
 Rufibach, B., 26
 Rugel, G., 43
 Santibáñez, P., 31
 Scherrer, St., 44
 Schläppi, M., 18, 30, 31, 32
 Schlierf, A., 12
 Schlumpf, N., 44, 46
 Schmitt, B., 44
 Schmoker, S., 52
 Schneebeli, M., 19, 20
 Schumann, D., 36, 37, 38, 39, 40, 41, 42, 43
 Schwikowski, M., 18, 21, 22, 23, 24, 25, 26, 27, 28, 29, 30, 31, 32, 33
 Serov, A., 4, 5, 6, 8
 Shannigrahi, A.S., 53
 Sigl, M., 25, 26, 27
 Sigrist, M., 38
 Simpson, D., 53
 Sosedova, Y., 9, 10
 Stampfli, D., 33
 Stampfli, F., 33,
 Steffensone, J.P., 25
 Suter, M., 51
 Synal, H.-A., 43, 51, 53
 Szidat, S., 25, 47, 48, 49, 51, 52, 53
 Tobler, L., 27, 28, 29, 32, 34, 35
 Tritscher, T., 14
 Tzvetkov, G., 13, 14
 Utyonkov, V.K., 6
 Veit, H., 52
 Vernooij, M.G.C., 14
 Viol, D., 36
 Vogel, E., 34, 35
 V. Rohr, F., 42
 Wacker, L., 25, 47, 48, 50, 51, 52, 53
 Wallner, A., 37
 Wittwer, D., 6, 7
 Yttri, K.E., 53
 Zelenay, V., 13, 14

AFFILIATION INDEX

ATOMKI Debrecen	Institute of Nuclear Research of the Hungarian Academy of Sciences, Debrecen, Bem ter 18/C, H-4026, Hungary
BAS	British Antarctic Survey, High Cross, Madingley Road, Cambridge CB3 0ET, United Kingdom
CEA-Saclay	DSM/DAPNIA/SPhN, Bat. 703, CEA-Saclay, 91191 Gif-sur-Yvette cedex, France
CERN (ISOLDE/CERN)	Organisation (Conseil) Européenne pour la Recherche Nucléaire, CH-1211 Genève 23
CECS	Centro de Estudios Científicos, Valdivia, Chile
CG BadW	Commission for Glaciology, Bavarian Academy of Sciences, Alfons-Goppel Str. 11, D-80539 Munich, Germany
EAWAG Dübendorf	Eidgen. Anstalt für Wasserversorgung, Abwasserreinigung und Gewässerschutz, Überlandstrasse 133, CH-8600 Dübendorf, Switzerland
ETHZ	Eidgen. Technische Hochschule Zentrum, CH-8092 Zürich, Switzerland
FLNR Dubna	Flerov Laboratory of Nuclear Reactions, Joliot Curie 6, 141980 Dubna, Russia
EMPA	Forschungsinstitution im ETH-Bereich, Überlandstrasse 129, CH-8600 Dübendorf, Switzerland
ESA-ESTEC	Space Environments and Effects section, ESTEC/TEC-EES, Keplerlaan 1 - 2200 AG Noordwijk, Netherlands
FS INVENTOR	FS Inventor AG, Muristr. 18, CH-3132 Riggisberg, Switzerland
FZ Jülich	Forschungszentrum Jülich GmbH, Leo-Brandt-Str., D-52428 Jülich, Germany
FZ Karlsruhe	Forschungszentrum Karlsruhe, Hermann-von-Helmholtz-Platz 1, D-76344 Eggenstein-Leopoldshafen, Germany
IF SB RAS	Institute of Forest, Siberian Branch of the Russian Academy of Sciences, Akademgorodok, Krasnoyarsk, 660036, Russia
IGM SB RAS	Institute of Geology and Mineralogy Siberian Branch of the Russian Academy of Sciences, Pr. Ak. Koptuyga 3, RU 630090, Novosibirsk, Russia
ILL, Grenoble	Institut Laue-Langevin, 6, Rue Jules Horowitz, BP 156 - 38042 Grenoble Cedex 9, France
IRCELYON	Institut de recherches sur la catalyse et l'environnement de Lyon, Université Lyon1 and Centre national de la recherche scientifique, 69622 Villeurbanne cedex, France
ITE	Instytut Technologii Elektronowej, al. Lotnikow 32,46, 02-668 Warszawa, Poland
ITP, China	Institute of Tibetan Plateau Research, Chinese Academy of Sciences, Beijing 100085, China
IWEP	Institute for Water and Environmental Problems, Siberian Branch of the Russian Academy of Sciences, 105 Papanintsev Str., RU-Barnaul 656099, Russia
JINR	Joint Institute for Nuclear Research, Joliot-Curie 6, 141980 Dubna, Moscow region, Russia
KUP	Climate and Environmental Physics, Physics Institute, University of Bern, Sidlerstrasse 5, CH-3012 Bern, Switzerland
LAC	Laboratory of Atmospheric Chemistry, Paul Scherrer Institut, CH-5232 Villigen PSI, Switzerland
LBNL	Lawrence Berkeley National Laboratory, Berkeley, CA 94720, USA
LGGE	Laboratoire de Glaciologie et Geophysique de l'Environnement, 38402 Saint Marin d'Hère, Cedex, France
NCCR Climate	NCCR Climate Management Centre, University of Bern, Erlachstrasse 9a, CH-012 Bern, Switzerland

Niels Bohr Inst.	Centre for Ice and Climate, Niels Bohr Institute, Copenhagen University, Juliane Maries Vej 30, DK-2100 København Ø, Denmark
NILU	Norwegian Institute for Air Research, 2027 Kjeller, Norway
NMI	Norwegian Meteorological Institute, 0313 Oslo, Norway
PSI	Paul Scherrer Institut, CH-232 Villigen PSI, Switzerland
SLF	Institut für Schnee- und Lawinenforschung, Flüelastr. 11, CH-7260 Davos, Switzerland
SLS	Swiss Light Source, Paul Scherrer Institut, CH-5232 Villigen PSI, Switzerland
Space IT	SpaceIT GmbH, Sennweg 15, 3012 Bern, Switzerland
Tokyo Institute of Technology	Department of Biological Sciences, Graduate School of Bioscience and Biotechnology, Tokyo Institute of Technology, 2-12-1-W3-43 Ookayama Meguro-ku, Tokyo 152-8551, Japan
TU Dresden	Technische Universität Dresden Institut für Geographie, Helmholtzstr. 10, HÜL O 262, D-01069 Dresden, Germany
TU / TUM	Technische Universität München, Physik Department E 15, James-Franck-Strasse, D-85748 Garching, Germany
UCI	University of California, Chemistry Departement, Irvine, CA 92697, USA
Univ. Bergen	Geofysisk Institutt, (124400) Allegt. 70, 5007 BERGEN, Norway
Univ. Bern	Departement für Chemie und Biochemie, Universität Bern, Freiestr. 3, CH-3012 Bern, Switzerland
Univ. Erlangen	Friedrich-Alexander Universität Erlangen-Nürnberg, Physikalische Chemie II, Egerlandstrasse 3, D-91058 Erlangen, Germany
Univ. Göteborg	University of Gothenburg, PO Box 100, 405 30 Gothenburg, Sweden
Univ. Lyon	IRCELYON - Institut de Recherches sur la Catalyse et l'Environnement de Lyon UMR5256 CNRS-Université LYON 1, Domaine Scientifique de la Doua, Batiment J. Raulin - 4eme Etage, 43 Bd du 11 Novembre 1918, F-69622 Villeurbanne Cedex, France
Univ. Maine	Climate Change Institute and Department of Earth Sciences, University of Maine, Orono ME 04469, USA
Univ. Mainz	Universität Johann Gutenberg, Institut für Kernchemie, D-55128 Mainz, Germany
VAW ETHZ	Versuchsanstalt für Wasserbau Hydrologie und Glaziologie, ETH Zürich, CH-8092 Zürich, Switzerland
Universidad Austral de Chile	Instituto de Botanica, Facultad de Ciencias, Universidad Austral de Chile, Valdivia, Chile.
Univ. Venice	University of Venice, 30123 Venice, Italy
Univ. Vienna	University of Vienna, Dr.-Karl-Lueger-Ring 1, 1010 Wien, Austria
Univ. Wuppertal	Physikalische Chemie/FB C, Bergische Universität Wuppertal, D- 42097 Wuppertal, Germany
ZSR Hannover	Zentrum für Strahlenschutz und Radioökologie, Universität Hannover, Hannover, Germany